AD_____

Award Number: W81XWH-08-1-0179

TITLE: Targeting of Breast Cancer through MT1-MMP/Tetraspanin Complexes

PRINCIPAL INVESTIGATOR: Martin Hemler

CONTRACTING ORGANIZATION: Dana-Farber Cancer Institute
Boston, MA 02115

REPORT DATE: August 2011

TYPE OF REPORT: Final

PREPARED FOR: U.S. Army Medical Research and Materiel Command
Fort Detrick, Maryland 21702-5012

REPORT DOCUMENTATION PAGE

Form Approved
OMB No. 0704-0188

1. REPORT DATE *(DD-MM-YYYY)*	2. REPORT TYPE	3. DATES COVERED *(From - To)*
01-08-2011	Final	1 Aug 2008 - 31 Jul 2011

4. TITLE AND SUBTITLE

Targeting of Breast Cancer through MT1-MMP/Tetraspanin Complexes

5a. CONTRACT NUMBER

5b. GRANT NUMBER
W81XWH-08-1-0179

5c. PROGRAM ELEMENT NUMBER

6. AUTHOR(S)

Martin Hemler

E-Mail: martin_hemler@dfci.harvard.edu

5d. PROJECT NUMBER

5e. TASK NUMBER

5f. WORK UNIT NUMBER

7. PERFORMING ORGANIZATION NAME(S) AND ADDRESS(ES)

Dana-Farber Cancer Institute
Boston, MA 02115

8. PERFORMING ORGANIZATION REPORT NUMBER

9. SPONSORING / MONITORING AGENCY NAME(S) AND ADDRESS(ES)
U.S. Army Medical Research and Materiel Command
Fort Detrick, Maryland 21702-5012

10. SPONSOR/MONITOR'S ACRONYM(S)

11. SPONSOR/MONITOR'S REPORT NUMBER(S)

12. DISTRIBUTION / AVAILABILITY STATEMENT
Approved for Public Release; Distribution Unlimited

13. SUPPLEMENTARY NOTES

14. ABSTRACT

The proteolytic enzyme MT1-MMP, which is frequently upregulated on the surface of breast cancer cells compared to normal breast cells, makes a major contribution towards breast cancer growth, invasion and metastasis. Another protease, called ADAM10, also contributes to breast cancer. The purpose of our studies was to investigate how tetraspanin proteins regulate the maturation and functions of proteases MT1-MMP and ADAM10. We hypothesized that manipulation/alteration of tetraspanin proteins (e.g. CD9, CD81, TSPAN12) could diminish the functions of associated cell surface proteases (e.g. MT1-MMP, ADAM10), thereby limiting breast cancer cell functions. Results obtained strongly support this hypothesis, as we found that alteration of tetraspanin complexes had a major effect on the functions of cell surface proteases. More specifically, we demonstrated three different strategies for disrupting tetraspanin functions: i) RNAi ablation, ii) Dominant negative mutation, and iii) C-terminal tail disruption. Also, we determined that EWI-2 action as a tumor suppressor may involve displacement of MT1-MMP from tetraspanin complexes. This could possibly be exploited using synthetic mimics of EWI-2 as anti-tumor agents. In conclusion, our results suggest that perturbation of tetraspanin proteins may provide an unconventional approach towards limiting the growth, invasion and metastasis of breast cancer cells.

15. SUBJECT TERMS

Membrane type-1 matrix metalloprotease (MT1-MMP); Metalloprotease ADAM10; Tetraspanin protein CD9; Tetraspanin protein CD81; Tetraspanin protein TSPAN12; Ig superfamily protein EWI-2; Tetraspanin enriched microdomains (TEMs)

16. SECURITY CLASSIFICATION OF:			17. LIMITATION OF ABSTRACT	18. NUMBER OF PAGES	19a. NAME OF RESPONSIBLE PERSON
a. REPORT	b. ABSTRACT	c. THIS PAGE			USAMRMC
U	U	U	UU	51	19b. TELEPHONE NUMBER *(include area code)*

Table of Contents

Introduction

The proteolytic enzyme MT1-MMP, which is frequently upregulated on the surface of breast cancer cells compared to normal breast cells, makes a major contribution towards breast cancer growth, invasion and metastasis. Another protease, called ADAM10, also contributes to breast cancer. Despite the importance of these critical enzymes on the surface of cancer cells, little is known about their lateral binding partners and how they may regulate MT1-MMP and ADAM10 functions. Tetraspanins are a family of cell surface proteins which function as molecular organizers of multiprotein membrane complexes, thereby influencing events such as cell proliferation, fusion, signaling and migration. Tetraspanins associate with each other and with several other proteins to form a novel type of specialized membrane microdomain called Tetraspanin Enriched Microdomains (TEMs). We have undertaken an unconventional approach towards limiting the growth, invasion and metastasis of breast cancer cells. We hypothesized that manipulation/alteration of tetraspanin proteins (e.g. CD9, CD81, TSPAN12) could diminish the functions of associated cell surface proteases (e.g. MT1-MMP, ADAM10), thereby limiting breast cancer cell functions. Results obtained strongly support this hypothesis. We have discovered novel strategies, involving the manipulation of tetraspanin proteins, which lead to diminished MT1-MMP and ADAM10 functions and markedly altered tumor cell behavior.

Body

Here we describe research accomplishments associated with each task described in the statement of work.

Aim #1: We will test the effects of CD9 and CD81 ablation on MT1-MMP-dependent breast tumor progression in vivo, in breast cancer cells which either lack or express MT1-MMP.

1. Regulatory review and approval of animal protocol for aims #1 and #3 has been achieved.
2. RNAi knockdown of tetraspanin proteins CD9, CD81, TSPAN12, and CD151 in breast cancer cell lines has been carried out {142, 143}.
3. Efficient knockdown of CD9, CD81, TSPAN12 and CD151 has been confirmed {142, 143}.
4. Study of in vivo orthotopic tumor growth was given a low priority, due to unexpected in vitro results. Since tetraspanin ablation markedly decreased MT1-MMP expression {142}, it no longer seemed as necessary to analyze function in vivo, when expression was diminished.
5. Study of in vivo tail vein injection was also given a low priority, for reasons mentioned in point #4.
6. We now clearly establish that CD9, CD81, and TSPAN12 knockdown can markedly diminish cell growth and invasion in 3D, but not 2D collagen assays {142}. Notably, these results are dependent on the presence of MT1-MMP in the breast cancer cells, consistent with the formation of a functional complex between tetraspanins and MT1-MMP {142}.

Aim #2: We will select monoclonal antibodies best able to disrupt associations between CD9/CD81 and MT1-MMP. Biochemical assays involving tetraspanin-protein interactions will be accompanied by subcellular localization studies.

1. All available monoclonal antibodies recognizing CD9, CD81 and MT1-MMP were tested for ability to disrupt associations between CD9/CD81 and MT1-MMP. Several antibodies to CD9 and to CD81 successfully co-immunoprecipitated MT1-MMP, but none of these antibodies caused a disruption of the complexes (1).
2. Because disrupting monoclonal antibodies were not available, we sought alternative means to disrupt tetraspanin –protease complexes. Expression of Ig superfamily protein EWI-2 caused a major disruption in MT1-MMP association with tetraspanin proteins [see Fig. 5E in (2)], which may help to explain decreased tumor growth (2). In a second strategy, a dominant negative mutation was made in tetraspanin protein TSPAN12, resulting in loss of association with the protease ADAM10, accompanied by decreased ADAM10 maturation and function (3). In a third strategy, a mutation in the cytoplasmic tail of CD9 was engineered, resulting in a) markedly diminished assembly of CD9 complexes with partner proteins, and b) loss of several CD9-dependent functions (4).
3. As mentioned above (point #2), expression of IgSF protein EWI-2 causes disruption of MTa-MMP association with tetraspanins (2). Notably, EWI-2 expression does not disrupt other tetraspanin associations. In fact, CD9-CD81 associations are increased (2). Hence, EWI-2 exerts a strong selective effect on MT1-MMP associations.
4. Based on our preliminary data, ablation of CD9 and CD81 lead to diminished MT1-MMP cell surface expression. To confirm this result, we carried out flow cytometry. Indeed, CD9 and CD81 ablation did cause loss of cell surface MT1-MMP expression (1). Furthermore, we assessed MT1-MMP turnover using 35S methionine pulse-chase labeling. These results showed that tetraspanin ablation did not affect initial biosynthesis of MT1-MMP, but did facilitate premature lysosomal degradation of MT1-MMP (1). Confocal microscopy experiments showed that antibodies to CD9 or CD81, but not control antibodies, triggered the co-clustering of MT1-MMP with tetraspanins (1). In a related experiment, expression of mutant TSPAN12 in a breast cancer cell line markedly altered the distribution of wild type TSPAN12, which associates with the protease ADAM10 (3). Both of these results demonstrate that alteration of subcellular distribution of a cell surface protease (e.g. MT1-MMP, ADAM10) likely underlies tetraspanin effects on protease maturation and function.

Aim #3: Antibodies that inhibit CD9/CD81 associations with MT1-MMP will be tested for effects on MT1-MMP-dependent invasive functions, both in vitro and in vivo.

1. MCF-7-MT1-MMP cells (and control MCF-7 cells) were embedded in 3D collagen gels and it was shown that ablation of tetraspanins CD9 and CD81 greatly diminished MT1-MMP-dependent in vitro invasion and growth (1).
2. MCF-7-MT1-MMP cells (and contol MCF-7 cells) were embedded in 3D fibrin gels and it was shown that ablation of CD9 and CD81 markedly impaired MT1-MMP-dependent in vitro invasion and growth (1).

3. MCF-7-MT1-MMP cells (and control MCF-7 cells) were plated on fibronectin coated slides and it was then shown that ablation of CD9 and CD81 markedly diminished fibronectin proteolysis by MT1-MMP, as analyzed by fluorescence microscopy (1).
4. In vivo experiments involving antibody disruption of primary tumor growth were not carried out because disrupting antibodies did not become available. However, alternative strategies have been developed (see points #2.2, 2.3), and these approaches should be feasible for in vivo testing in the future, using orthotopic mammary fat pad injection.
5. In vivo experiments involving antibody disruption of secondary (i.e. metastatic) tumor growth were not carried out because disrupting antibodies did not become available. However, alternative strategies have been developed (see points #2.2, 2.3) and these approaches should be feasible for future in vivo testing, using tail vein injection into nude mice to monitor metastatic potential.

Key research accomplishments

- Cell surface protease MT1-MMP expression and maturation depends on tetraspanin proteins (1).
- Cell surface protease MT1-MMP support of tumor cell growth and invasion depends on tetraspanin protein associations (1).
- Cell surface protease MT1-MMP association with tetraspanin proteins can be negatively regulated by EWI-2 (2).
- Cell surface protease ADAM10 expression, maturation and function depends on a tetraspanin protein (3).
- Tetraspanin CD9 association with partner proteins depends on CD9 having an intact C-terminal tail (4).
- Tetraspanin CD9 functions depend on CD9 having an intact C-terminal tail (4).

Reportable outcomes

Manuscripts resulting from this research include:

Lafleur MA, Xu D, Hemler, ME. Tetraspanin proteins regulate membrane type-1 matrix metalloproteinase (MT1-MMP)-dependent pericellular proteolysis. **Mol Biol Cell**. 2009; 20:2030-40.

Kolesnikova TV, Kazarov AR, Lemieux M, Lafleur MA, Kesari S, Kung AL, Hemler ME. glioblastoma inhibition by cell surface immunoglobulin protein EWI-2, in vitro and in vivo. **Neoplasia**. 2009. 11:77-86.

Xu D, Sharma C, Hemler ME. Tetraspanin12 regulates ADAM10-dependent cleavage of amyloid precursor protein. **FASEB Journal**. 2009; 23:3674-81.

Wang H-X, Kolesnikova TV, Denison C, Gygi S, Hemler ME. C-terminal tail contributions to tetraspanin CD9 function and molecular organization. **Journal of Cell Science**. 2011; 124:2702-2710.

Presentations:

Dr. Martin E. Hemler presented a poster, entitled "Contributions of MT1-MMP and tetraspanin proteins (CD9, CD81, CD151) to human breast cancer invasion and growth ", at the Department of Defense Era Of Hope Breast Cancer Meeting in Orlando, FL, August, 2011.

Employment received:

Based largely on his success in carrying out this research project, Dr. Marc A. Lafleur was employed by Amgen Co. as a research scientist.

Conclusions

a. We have discovered that cell surface protease MT1-MMP expression and maturation depends on tetraspanin proteins (1). Consequently, cell surface protease MT1-MMP support of tumor cell growth and invasion depends on tetraspanin protein associations (1). This result indicates a novel possibility for interfering with MT1-MMP contributions towards breast cancer.

b. We have learned that cell surface protease MT1-MMP association with tetraspanin proteins can be negatively regulated by EWI-2 (2), which may explain EWI-2 causing diminished tumor growth (2). These results point to EWI-2 having a potential tumor suppressor function, at least partly acting through MT1-MMP.

c. We discovered that cell surface protease ADAM10 expression, maturation and function depends on the tetraspanin protein TSPAN12 (3). As seen for MT1-MMP, ADAM10 has emerged as a novel tumor target in breast cancer and other cancers. Consequently, disruption of TSPAN12 may have therapeutic benefit.

d. Of particular interest, a TSPAN12 mutant was generated which had dominant-negative-like properties (3). This type of dominant negative mutation (replacement of membrane-proximal cysteines) could be applicable for the disruption of the functions of many of the other tetraspanin proteins.

e. We learned that tetraspanin CD9 association with partner proteins depends on CD9 having an intact C-terminal tail (4), and that CD9 functions depend on CD9 having an intact C-terminal tail (4). This result leads to the suggestion that the C-termini of many other tetraspanins may be critical for their functions.

f. To summarize results in terms of specific “knowledge products”, we have produced the following:

- A novel demonstration that major cell surface proteases contributing to tumor growth and invasion can be inhibited by disrupting lateral interactions – this had not been done before.
- Demonstration of three different strategies for disrupting tetraspanin functions: i) RNAi ablation, ii) Dominant negative mutation, and iii) C-terminal tail disruption.
- A determination that EWI-2 action as a tumor suppressor may involve displacement of MT1-MMP from tetraspanin complexes. This could possibly be exploited using synthetic mimics of EWI-2 as anti-tumor agents.

References

1. Lafleur MA, Xu D, Hemler, ME. Tetraspanin proteins regulate membrane type-1 matrix metalloproteinase (MT1-MMP)-dependent pericellular proteolysis. **Mol Biol Cell**. 2009; 20:2030-40.

2. Kolesnikova TV, Kazarov AR, Lemieux M, Lafleur MA, Kesari S, Kung AL, Hemler ME. glioblastoma inhibition by cell surface immunoglobulin protein EWI-2, in vitro and in vivo. **Neoplasia**. 2009. 11:77-86.

3. Xu D, Sharma C, Hemler ME. Tetraspanin12 regulates ADAM10-dependent cleavage of amyloid precursor protein. **FASEB Journal**. 2009; 23:3674-81.

4. Wang H-X, Kolesnikova TV, Denison C, Gygi S, Hemler ME. C-terminal tail contributions to tetraspanin CD9 function and molecular organization. **Journal of Cell Science**. 2011; 124:2702-2710.

Appendices

Copies of the following manuscripts are included in the appendix:

Lafleur MA, Xu D, Hemler, ME. Tetraspanin proteins regulate membrane type-1 matrix metalloproteinase (MT1-MMP)-dependent pericellular proteolysis. **Mol Biol Cell**. 2009; 20:2030-40.

Kolesnikova TV, Kazarov AR, Lemieux M, Lafleur MA, Kesari S, Kung AL, Hemler ME. glioblastoma inhibition by cell surface immunoglobulin protein EWI-2, in vitro and in vivo. **Neoplasia**. 2009. 11:77-86.

Xu D, Sharma C, Hemler ME. Tetraspanin12 regulates ADAM10-dependent cleavage of amyloid precursor protein. **FASEB Journal**. 2009; 23:3674-81.

Wang H-X, Kolesnikova TV, Denison C, Gygi S, Hemler ME. C-terminal tail contributions to tetraspanin CD9 function and molecular organization. **Journal of Cell Science**. 2011; 124:2702-2710.

Molecular Biology of the Cell
Vol. 20, 2030–2040, April 1, 2009

Tetraspanin Proteins Regulate Membrane Type-1 Matrix Metalloproteinase-dependent Pericellular Proteolysis

Marc A. Lafleur, Daosong Xu, and Martin E. Hemler

Department of Cancer Immunology and AIDS, Dana-Farber Cancer Institute, Boston, MA 02115

Submitted November 26, 2008; Revised January 27, 2009; Accepted January 29, 2009
Monitoring Editor: Jean E. Schwarzbauer

Membrane type-1 matrix metalloproteinase (MT1-MMP) supports tumor cell invasion through extracellular matrix barriers containing fibrin, collagen, fibronectin, and other proteins. Here, we show that simultaneous knockdown of two or three members of the tetraspanin family (CD9, CD81, and TSPAN12) markedly decreases MT1-MMP proteolytic functions in cancer cells. Affected functions include fibronectin proteolysis, invasion and growth in three-dimensional fibrin and collagen gels, and MMP-2 activation. Tetraspanin proteins (CD9, CD81, and TSPAN2) selectively coimmunoprecipitate and colocalize with MT1-MMP. Although tetraspanins do not affect the initial biosynthesis of MT1-MMP, they do protect the newly synthesized protein from lysosomal degradation and support its delivery to the cell surface. Interfering with MT1-MMP-tetraspanin collaboration may be a useful therapeutic approach to limit cancer cell invasion and metastasis.

INTRODUCTION

Matrix metalloproteinases (MMPs) are a family of soluble and membrane-anchored proteolytic enzymes that can remodel the extracellular matrix (ECM) and cleave several other substrates, including cell–cell and cell–matrix adhesion molecules, chemokines, cytokines, latent growth factors, and cell surface receptors (Egeblad and Werb, 2002). Membrane type-1 MMP (MT1-MMP; MMP-14) is of particular interest because MT1-MMP knockout mice show severe defects, including skeletal abnormalities and fibrosis (Holmbeck *et al*., 1999). MT1-MMP also plays critical roles during tumor malignancy and is one of the best-validated proteolytic enzyme targets on cancer cells. First, MT1-MMP is up-regulated in several tumor types, including breast, cervical, and ovarian cancer (Drew *et al*., 2004; Zhai *et al*., 2005; Jiang *et al*., 2006) and is significantly associated with adverse outcome (Jiang *et al*., 2006). Second, overexpression of MT1-MMP in the mammary gland of mice results in hyperplasia and spontaneous adenocarcinomas (Ha *et al*., 2001). Third, ectopic expression of MT1-MMP and MT2-MMP, but not soluble MMPs, enables tumor cell penetration of three-dimensional (3D) collagen gels (Hotary *et al*., 2000). Similarly, introduction of MT1-MMP into poorly invasive MCF-7 breast cancer cells renders those cells more invasive in vitro and more tumorigenic in vivo (Borrirukwanit *et al*., 2007). Finally, silencing of endogenous MT1-MMP markedly decreases invasive and migratory properties of breast cancer cells (Jiang *et al*., 2006).

This article was published online ahead of print in *MBC in Press* (http://www.molbiolcell.org/cgi/doi/10.1091/mbc.E08–11–1149) on February 11, 2009.

Address correspondence to: Martin E. Hemler (martin_hemler@dfci.harvard.edu).

Abbreviations used: GFP, green fluorescent protein; MMP, matrix metalloproteinase; MT1-MMP, membrane type-1 matrix metalloproteinase; TEM, tetraspanin-enriched microdomain.

MT1-MMP is regulated at the level of gene transcription, proenzyme activation, subcellular localization, internalization/recycling, dimerization, shedding, inhibition by natural inhibitors (tissue inhibitor of metalloproteinases, RECK), and posttranslational modifications (Itoh and Seiki, 2006). In addition MT1-MMP associates with cell surface molecules such as β1 integrins (Galvez *et al*., 2002), CD44 (Mori *et al*., 2002), and tetraspanin proteins such as CD63 (Takino *et al*., 2003), CD151 (Yanez-Mo *et al*., 2008), CD81, and others (Kolesnikova *et al*., 2009). Tetraspanins are a family of cell surface proteins (33 human members), each with four conserved transmembrane domains, characteristic extracellular loops, and short cytoplasmic domains (Hemler, 2003). These relatively small proteins (typically 22–30 kDa) generally do not function as classical cell surface receptors. Rather, they serve as molecular organizers of multiprotein membrane complexes, thereby influencing cell proliferation, fusion, signaling, and migration (Stipp *et al*., 2003b). Tetraspanins can associate with each other and with other proteins such as integrins, immunoglobulin (Ig) superfamily members, proteoglycans, ligands, and growth factor receptors to form specialized membrane structures called tetraspanin-enriched microdomains (TEMs) (Hemler, 2005). The tendency of different tetraspanins to associate closely within TEMs probably underlies the ability of distinct tetraspanins to provide functional compensation for each other (Fradkin *et al*., 2002; Kaji *et al*., 2002). On cancer cells, some tetraspanins (CD151 and CO-029) promote invasion (Claas *et al*., 1998; Yang *et al*., 2008), whereas others (NET-6, CD82, and CD9) behave more as tumor suppressors (Liu and Zhang, 2006; Huang *et al*., 2007; Takeda *et al*., 2007).

Given their tendency to localize into cellular lamellipodia and filopodia (Penas *et al*., 2000), tetraspanins are well positioned on the cell surface to orchestrate events such as pericellular proteolysis by membrane-anchored proteases. In this regard, tetraspanin CD151 association with endothelial cell MT1-MMP may inhibit MT1-MMP–dependent MMP-2 activation, while paradoxically supporting MT1-MMP–dependent collagen degradation (Yanez-Mo *et al*., 2008). In another study, association with tetraspanin CD63

was suggested to accelerate lysosomal degradation of MT1-MMP in HeLa cells (Takino *et al*., 2003). Given the importance of MT1-MMP as a proinvasive protease in cancer cells, we set out to identify the functional importance of tetraspanin-MT1-MMP associations in cancer cells. Among seven different tetraspanins analyzed, CD9, CD81, and TSPAN12 showed the most readily detectable associations with MT1-MMP. Hence, functional studies focused mostly on those tetraspanins. To ensure sufficient disruption of TEMs and to minimize functional compensation, we knocked down these tetraspanins two to three at a time. Furthermore, because tetraspanins had been shown to have conflicting effects on MT1-MMP functions, we undertook a comprehensive functional analysis, by using four different assays for MT1-MMP function. In addition, we provide mechanistic insight into how tetraspanins regulate MT1-MMP function.

MATERIALS AND METHODS

Cell Culture

Cell lines were from American Type Culture Collection (Manassas, VA). MCF-7 cells were stably transfected with MT1-MMP-FLAG (MCF-7-MT1), MT1-MMP-green fluorescent protein (GFP) (MCF-7-MT1-GFP, GFP at C terminus), or vector only using FuGENE6 (Roche Diagnostics, Indianapolis IN). FLAG-MT1-MMP from M. Seiki (University of Tokyo, Tokyo, Japan), was cloned into pcDNA3.1 (Invitrogen, Carlsbad CA). MT1-MMP-GFP is from wild type (wt) MT1-MMP cloned into phosphorylated enhanced green fluorescent protein (BD BioSciences, Palo Alto CA) and subcloned into pcDNA3.1. Stable cell lines were sorted as a pool population by flow cytometry. HT1080-FLAG–tagged MT1-MMP cells were generated as described above. TSPAN12-FLAG was cloned into pLXIZ and transfected into the pT67 packaging cell line. HT1080 cells were infected with viral supernatants to generate stable cell lines. All cells were maintained in DMEM (Invitrogen) with 10% fetal bovine serum (FBS).

Reagents and Antibodies

Bafilomycin A1 (vacuolar type H^+ ATPase inhibitor), cytochalasin D, thrombin, pepstatin A (aspartyl peptidase inhibitor), E64, 4-(2-aminoethyl)benzenesulfonyl fluoride (AEBSF), anti-FLAG (M2) antibody, anti-β actin antibody, and secondary horseradish peroxidase (HRP)-conjugated goat anti-mouse antibody were from Sigma-Aldrich (St. Louis, MO). ALLM and MG132 were obtained from BIOMOL Research Laboratories (Plymouth Meeting, PA). Plasminogen-depleted fibrinogen was from Calbiochem (San Diego, CA). Protein G-agarose beads, aprotinin, and leupeptin (serine and thiol protease inhibitor) were from Roche Diagnostics. MT1-MMP antibodies (AB815 and LEM2/15.8) and GM6001 were from Millipore Bioscience Research Reagents (Billerica, MA). MT1-MMP antibody (28209) was from Abcam (Cambridge, MA). Anti-GFP antibody was from Clontech (Mountain View, CA). Anti-CD71 and anti-E-cadherin (G-10) antibodies were from Santa Cruz Biotechnology (Santa Cruz, CA). Fibronectin and anti-fibronectin antibody were from BD Biosciences. Secondary HPR-conjugated goat anti-rabbit light chain was from Zymed Laboratories (South San Francisco, CA). Alexa 546-fibrinogen, Alexa 546-phalloidin, ProLong Gold antifade mounting media with 4,6-diamidino-2-phenylindole (DAPI), Alexa 488-donkey anti-rabbit, Alexa 488-donkey anti-mouse, and Alexa 546 goat anti-mouse were from Invitrogen. Type I collagen was from Inamed (Fremont, CA). Antibodies to CD9 included MM2/57 (BioSource International, Camarillo, CA), MEM-61 (GeneTex, San Antonio, TX) and ALB6 (Immunotech, Marseille, France). Other antibodies are TSPAN4 (Tachibana *et al*., 1997), MHC I (W6/32) (Barnstable *et al*., 1978), CD98 (4F2) (Hemler and Strominger, 1982), CD147 (8G6), α3 integrin (A3X8), CD63 (6H1), CD81 (M38), CD82 (M104), and CD151 (5C11) (Yang *et al*., 2002).

Immunoprecipitation, Western Blotting, and Zymography

Cells were lysed in 25 mM HEPES, 150 mM NaCl, 5 mM $MgCl_2$, and 5 mM $CaCl_2$ with protease inhibitor cocktail (Roche Diagnostics) and 1% detergent (Triton X-100, Brij 96, Brij 99, or 3-[(3-cholamidopropyl)dimethylammonio]propanesulfonate [CHAPS]) at 4°C. Radioimmunoprecipitation assay contained the above-mentioned components with 1% deoxycholate, 1% Triton X-100, and 0.1% SDS. In some cases, lysates were ultracentrifuged (Beckman L8-80M) at 100,000 $\times$ *g*. Equal lysate volumes were precleared with protein G-agarose beads and then immunoprecipitated with indicated antibodies and protein G overnight at 4°C. Beads were washed and eluted with SDS-sample buffer (50 mM Tris-HCl, pH 6.8, 1% SDS, 0.025% bromophenol blue, and 10% glycerol). Western blot analysis for MT1-MMP and antibody validation was performed as described previously (Lafleur *et al*., 2006). Western blot analysis for CD9, CD81, and actin and antibody validation was performed as described previously (Stipp *et al*., 2003a; Kovalenko *et al*., 2007). For zymography, samples were separated on a 10% polyacrylamide gel copolymerized with 1 mg/ml gelatin (Sigma-Aldrich) and developed as described previously (Lafleur *et al*., 2006).

Small Interfering RNA (siRNA) Transfection

Cells were transfected with 10 nM (MCF-7 cells) or 25 nM (HT1080 cells) of indicated siRNAs (Dharmacon RNA Technologies, Lafayette, CO) with Lipofectamine RNAiMAX (Invitrogen). The sense sequences for the siRNAs are as follows: CD9#1, CCAAGAAGGACGUACUCGAUU; CD9#2, UUAAGGAAGUCCAGGAGUU; CD81#1, CCACCAACCUCCUGUAUCUUU; CD81#2, CCAACAACGCCAAGGCUGU; CD151#1, CCUCAAGAGUGACUACAUCUU; TSPAN12#1, GCAAACAGCUUUAAUACACUU; TSPAN12#2, GUACAAUGGUCAGAUAUGGUU; and control#1, UAGCGACUAAACACAUCAA.

3D Collagen and Fibrin Gels

Two days after siRNA transfection, cells were embedded into fibrin or collagen gels. For collagen gels, 5×10^4 cells were resuspended in 400 μl of neutralized and buffered collagen gels (2 mg/ml) and polymerized for 1 h at 37°C. Finally, cells were covered in growth media. For fibrin gels, 5×10^4 cells were resuspended in 400 μl of 2.5 mg/ml fibrinogen in serum-free media and polymerized with thrombin (1 U/ml) for 30 min at 37°C. Then, they were covered with growth media containing 50 μg/ml aprotinin.

Fibronectin Immunofluorescence

siRNA-treated cells were cultured on fibronectin coated (10 μg/ml) Lab-Tek chamber slides (Nalge Nunc International, Rochester, NY) for 24 h in serum-free media with protease inhibitors: 100 μg/ml aprotinin, 5 μM leupeptin, 20 μM E64, 20 μM pepstatin A, and 100 μM AEBSF. Cells were fixed with 4% paraformaldehyde, blocked/permeabilized with 5% bovine serum albumin (BSA)/phosphate-buffered saline (PBS)/0.25% Triton X-100, and immunostained with an anti-fibronectin antibody for 1 h at 20°C. Cells were then incubated with an Alexa 488 secondary antibody and Alexa 546-phalloidin for 1 h at 20°C. Cells were mounted with ProLong Gold antifade mounting media containing DAPI. Specificity of the anti-fibronectin antibody was obtained by negative staining of collagen coated slides (data not shown).

MTT Proliferation and Flow Cytometry

MCF-7-MT1 cells transfected with indicated siRNAs were plated in 96-well plates (2000 cells/well) in triplicate for 1–7 d. An MTT proliferation assay (Roche Diagnostics) was performed each day using an Opsys MR Thermo Lab Systems plate reader. For flow cytometry, cells were blocked with 5% goat serum/1% BSA/0.02% NaN_3 in PBS at 4°C and then stained with primary antibodies for 1 h at 4°C. Cells were washed and incubated with Alexa 488-conjugated donkey anti-rabbit or anti-mouse secondary antibodies for 1 h at 4°C and washed before analysis.

Internalization

MCF-7-MT1-GFP cells were incubated with 0.5 mg/ml EZ-link Sulfo-NHS-SS-biotin (Pierce Chemical, Rockford, IL) at 4°C for 1 h. Cells were washed in PBS and incubated in serum-free media for 0, 10, or 30 min at 37°C. Cells were washed and incubated with reducing solution (42 mM glutathione, 75 mM NaCl, 1 mM EDTA, 1% BSA, and 75 mM NaOH) for 40 min at 4°C. Cells were washed with PBS, lysed as described above for immunoprecipitation with 1% Triton X-100 lysis buffer, and MT1-MMP was immunoprecipitated with an anti-GFP antibody. Eluates were analyzed by Western blotting using ExtrAvidin-HRP.

Pulse-Chase

MCF-7-MT1-FLAG cells were incubated with DMEM lacking L-cysteine and L-methionine (Invitrogen), 10% dialyzed FBS, 25 mM HEPES, L-glutamine, and penicillin/streptomycin for 30 min at 37°C. Cells were pulsed (30 min) with the above-mentioned media with 0.2 mCi/ml EasyTag Expression Protein Labeling Mix [^{35}S]L-methionine and [^{35}S]L-cysteine (PerkinElmer Life and Analytical Sciences, Waltham, MA). Cells were chased with DMEM lacking L-cysteine and L-methionine, 10% dialyzed FBS, 25 mM HEPES, L-glutamine, penicillin/streptomycin, 0.2 mM L-cysteine, and 0.2 mM L-methionine. Cells were lysed as described above for immunoprecipitation with 1% Triton X-100 lysis buffer with 10 mg/ml BSA. Lysates were precleared and immunoprecipitated using 28209 anti-MT1-MMP antibody. Eluates were separated on a 4–20% gradient gel (Invitrogen), transferred to polyvinylidene difluoride membrane, and exposed to a PhosphorImager screen (GE Healthcare, Chalfont St. Giles, Buckinghamshire, United Kingdom) overnight. Cell surface pulse-chase experiments were as described above, except that before immunoprecipitation, intact cells were cooled to 4°C and then incubated with the M2 anti-FLAG antibody for 2 h at 4°C, and then lysed.

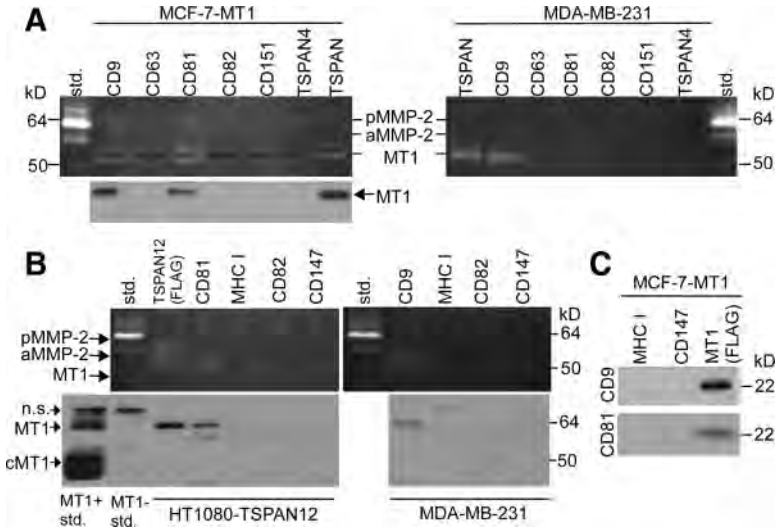

Figure 1. Specific tetraspanins associating with MT1-MMP. (A) MCF-7-MT1 and MDA-MB-231 cells were lysed in 1% Brij 99 lysis buffer, and the indicated tetraspanins were immunoprecipitated (TSPAN, cocktail of tetraspanin antibodies against CD9, CD63, CD81, CD82, CD151, and TSPAN4). Eluates were analyzed by gelatin zymography and by Western blotting for MT1-MMP, using the anti-catalytic domain LEM2/15.8 antibody. Std, MMP-2 standard; pMMP-2, pro-MMP-2; aMMP-2, active MMP-2; n.s., nonspecific. All antibodies used in these and other immunoprecipitation experiments have been previously shown to immunoprecipitate their target antigens (Barnstable *et al.*, 1978; Tachibana *et al.*, 1997; Yang *et al.*, 2002). (B) HT1080 cells stably expressing TSPAN12 and MDA-MB-231 cells were lysed in 1% Brij 99, cell surface proteins were immunoprecipitated, and eluates were analyzed by gelatin zymography and by MT1-MMP Western blotting using the anti-hinge AB815 antibody. cMT1, cleaved MT1. MT1 Standards are from MCF-7 cells (negative for MT1) or MCF-7 cells stably expressing MT1-MMP. (C) FLAG-MT1-MMP, MHC1, and CD147 were immunoprecipitated from MCF-7-MT1 cells (lysed in 1% Brij 99) and eluates were Western blotted for CD9 and CD81.

RNA Isolation and Reverse Transcription-Polymerase Chain Reaction (RT-PCR)

RNA was harvested using RNeasy mini columns (QIAGEN, Valencia CA). Reverse transcription was performed with the SuperScript first-strand synthesis system (Invitrogen). PCR was performed with PCR buffer (1.5 mM $MgCl_2$), 200 μM dNTPs (Roche Diagnostics), 200 nM forward and reverse primers, 5 U of *Taq* DNA polymerase (Roche Diagnostics), and template. PCR conditions were as follows: 94°C for 2 min and then 35 cycles (TSPAN12) or 25 cycles (glyceraldehyde-3-phosphate dehydrogenase [GAPDH]) of 94°C 15 s, 60°C 30 s, and 72°C 1 min by using a DNA Engine Peltier thermal cycler (Bio-Rad, Hercules, CA).

Primers used were as follows: TSPAN12 5′, CTCTTGATAAAGGTCACTGAGATC; TSPAN12 3′, TGTTGCTTCTTGCATGGTACTTTG; GAPDH 5′, CGGAGTCAACGGATTTGGTCGTAT; and GAPDH 3′, AGCCTTCTCCATGGTGGTGAAGAC.

Statistical Analysis

Where indicated, a *t* test (2-tailed, unequal variance) was performed when comparing two groups; control versus tetraspanin knockdown. The p values were obtained for each tetraspanin knockdown condition (single, double, or triple) compared with the control.

Image and Data Acquisition, Including Microscopy

For zymograms and Western blots, original gels or films, respectively, were scanned using an Epson perfection 1650 scanner. Images were cropped using Adobe Photoshop 6.0 (Adobe Systems, Mountain View, CA) and imported into Canvas 9.0 for labeling. For ^{35}S pulse-chase experiments, images were obtained by PhosphorImager (Scanner Control, version 4.1; GE Healthcare). For all RT-PCR, DNA images were acquired with a Gene Genius Bio Imaging System and GeneSnap software version 4.0. Where indicated, densitometry was performed with ImageQuant version 5.2 (GE Healthcare). Phase-contrast images were acquired using an Axiovert 135 microscope (Carl Zeiss, Jena, Germany) and RT monochrome Spot camera and software, version 3.3 (Diagnostic Instruments, Sterling Heights, MI) with a 40× objective (Figure 2D) or a 10× objective (Figure 3A). Growth area in Figure 3 was quantitated using Scion Image, version 1.62, while focused on the same plane for each sample. Immunofluorescent images were acquired with a Nikon Eclipse TE300 fluorescent microscope and RT SE. Spot camera and software, version 4.6 (Diagnostic Instruments) with a 40× objective. Fibronectin degradation was quantitated by measuring pixel density (using ImageQuant 5.2) within comparably sized areas of fibronectin proteolysis. Confocal images were acquired with a Zeiss LSM 510 META confocal microscope (Harvard NeuroDiscovery Center, Boston, MA). Z-stack reconstructions (143.4 × 143.4 × 22.1 μm) were performed from images taken every 1.1 μm with a 63× objective, and images were viewed with a Zeiss LSM Image Browser, version 3.5.0.223. Flow cytometry data acquisition was performed using a FACSCalibur flow cytometer with CellQuest software, version 3.3, with data analyzed using FlowJo software, version 6.4.4 (BD Biosciences).

RESULTS

MT1-MMP Association with Tetraspanin Proteins

MT1-MMP may associate with at least four different tetraspanin proteins (Takino *et al.*, 2003; Yanez-Mo *et al.*, 2008; Kolesnikova *et al.*, 2009). To clarify which might associate best with MT1-MMP on tumor cell lines, we immunoprecipitated CD9, CD63, CD81, CD82, CD151, and TSPAN4 from MCF-7-MT1 and MDA-MB-231 cells (Figure 1A). CD9 and CD81 yielded the most MT1-MMP, as seen by gelatin zymography and Western blot. TSPAN12 also associated with MT1-MMP, as seen upon immunoprecipitating TSPAN12-FLAG from HT1080 cells (Figure 1B). Antibodies to other tetraspanins (CD63, CD82, and CD151) or other abundant cell surface proteins (major histocompatibility complex I [MHC I], CD147) yielded little or no MT1-MMP (Figures 1, A and B). All tetraspanins and negative control proteins analyzed were well expressed by MCF-7-MT1, HT1080, and MDA-MB-231 cells with the exception of CD9 in HT1080 cells (Supplemental Table 1). In a reciprocal experiment, immunoprecipitation of MT1-MMP-FLAG but not control proteins (MHC I and CD147) yielded CD9 and CD81 (Figure 1C).

CD81 immunoprecipitation from HT1080 cells yielded MT1-MMP regardless of whether lysates were centrifuged at 100,000 × *g* (Supplemental Figure 1A). Hence, MT1-MMP-tetraspanin associations are not a protein insolubility artifact. MT1-MMP-tetraspanin association was also observed in MDA-MB-231, BT549, 293, U87, and NT2 cancer cells. Cells with minimal MT1-MMP expression (HeLa, LN827, MCF-7, A549, and K562) did not yield MT1-MMP zymogram activity (Supplemental Figure 1B).

Choice of lysis buffer is critical in these experiments. Immunoprecipitation of TSPAN12 yielded MT1-MMP in relatively stringent conditions (1% Brij 96 or TX-100), whereas CD9 and CD81 associations were seen in less stringent conditions (1% Brij 99 and CHAPS) (Supplemental Figure 2A and Supplemental Table 2). To confirm that tetraspanin-MT1-MMP associations are not postlysis artifacts, HT1080 1% Brij 99 lysates, containing TSPAN12-FLAG or MT1-MMP-GFP, were either mixed 1:1 or kept separate. Immunoprecipitation of FLAG yielded TSPAN12-FLAG and immunoprecipitation of GFP yielded MT1-MMP-GFP. There was no evidence of postlysis association between FLAG- and GFP-tagged proteins (Supplemental Figure 2B). As a positive control, immunoprecipitation of TSPAN12-FLAG yielded endogenous MT1-MMP (Supplemental Figure 2B, bottom left). Immunoprecipitation of CD81 yielded comparable amounts of both endogenous MT1-MMP and MT1-MMP-GFP (Supplemental Figure 2B, right). Hence, the GFP

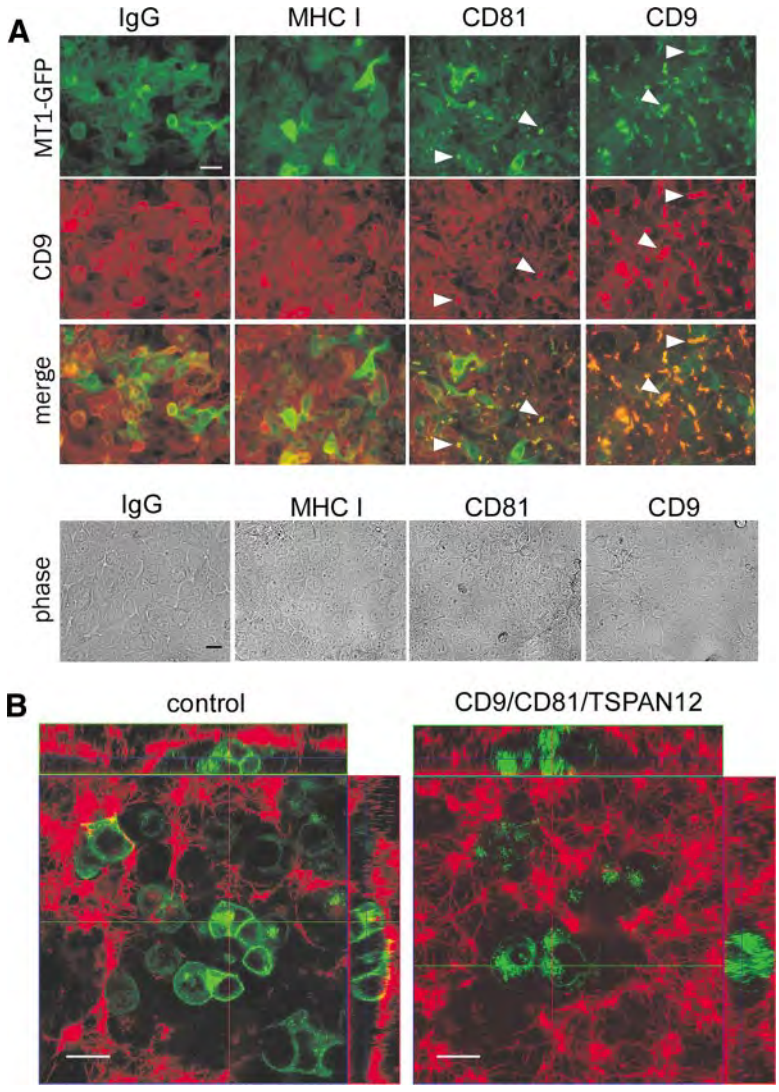

Figure 2. Tetraspanin effects on MT1-MMP subcellular localization. (A) MCF-7-MT1-GFP cells were treated with the indicated control (IgG and MHC I) and tetraspanin (CD9 and CD81) antibodies (50 μg/ml for 2 d), fixed (in 4% paraformaldehyde), blocked in 5% BSA/PBS, incubated at 20°C with Alexa Fluor 546-conjugated anti-CD9 antibody (ALB6), and analyzed by fluorescence or phase-contrast microscopy. Bar, 20 μm. White arrowheads indicate coclustering of MT1-MMP-GFP with CD9 or CD81. (B) MCF-7-MT1-GFP cells were transfected with control or CD9/CD81/TSPAN12 siRNAs and plated within fibrin gels 2 d after siRNA transfection. Fibrin gels were spiked with 1% Alexa 546-labeled fibrinogen before addition of thrombin to form the gel. After 2 d, cells were visualized by confocal microscopy. Green, MT1-MMP-GFP; red, fibrin matrix. Laser power was adjusted to show similar green intensities between control and tetraspanin knockdown cells. Bar, 20 μm. Horizontal (green) and vertical (red) lines within the central XY image correspond to the planes chosen for XZ (up) and YZ (right) images, respectively.

moiety does not interfere with MT1-MMP-GFP-tetraspanin association.

We also treated MCF-7-MT1-GFP cells with anti-CD9, anti-CD81, or control antibodies. Cells were then fixed and assessed for MT1-MMP-GFP and CD9 expression. Antibodies to CD9 or CD81, but not control antibodies (IgG or anti-MHC I), triggered coclustering of MT1-MMP-GFP (green) and CD9 (red) into overlapping punctate complexes (Figure 2A, white arrowheads). Cell morphology was not noticeably altered by antibody treatment (Figure 2A, bottom). These results support the conclusion that MT1-MMP associates with tetraspanins CD9 and CD81.

Tetraspanins Promote MT1-MMP–dependent Functions

In previous studies, tetraspanins CD63 and CD151 were suggested to inhibit MT1-MMP–dependent MMP-2 activation (Takino *et al*., 2003; Yanez-Mo *et al*., 2008), while paradoxically promoting collagen degradation (Yanez-Mo *et al*., 2008). Here, we undertook a comprehensive assessment of the effects of tetraspanins (CD9, CD81, and TSPAN12) on tumor cell MT1-MMP, by using four different functional assays. To focus attention on MT1-MMP, we mostly compared the functions of MCF-7-MT1 and MCF-7-VC cells. The former cells are stably transfected to express moderate levels of MT1-MMP, whereas the latter are vector control cells, with minimal background MMP activity. To efficiently disrupt the tetraspanin network in MCF-7-VC and MCF-7-MT1 cells, we silenced tetraspanins (CD9, CD81, and TSPAN12) in combinations of two or three at a time. Evidence for efficient knockdown of CD9, CD81, and TSPAN12 is shown in Supplemental Figure 3, A–C.

Tetraspanin effects on MT1-MMP function were first analyzed using Alexa 546-labeled 3D fibrin gels. During a 2-d growth interval, control siRNA-treated MCF7-MT1-GFP cells created large fibrin-depleted boroughs, as seen in both XY planes and in Z stacks (Figure 2B, left). By contrast, CD9/CD81/TSPAN12 siRNA-treated cells showed smaller regions of fibrin proteolysis (Figure 2A, right). Also evident were striking differences in MT1-MMP-GFP localization. In control siRNA-treated cells, MT1-MMP-GFP was localized mainly at the periphery, with some intracellular signal (Figure 2B, left). On tetraspanin knockdown, MT1-MMP-GFP became predominantly intracellular (Figure 2B, right).

In another 3D fibrin gel experiment, embedded MCF-7-VC and MCF-7-MT1 cells were monitored for changes in invasion and growth, due to tetraspanin knockdown (Figure 3). Using MT1-MMP to escape from fibrin growth constraints (Hotary *et al*., 2003), control siRNA-treated MCF-7-

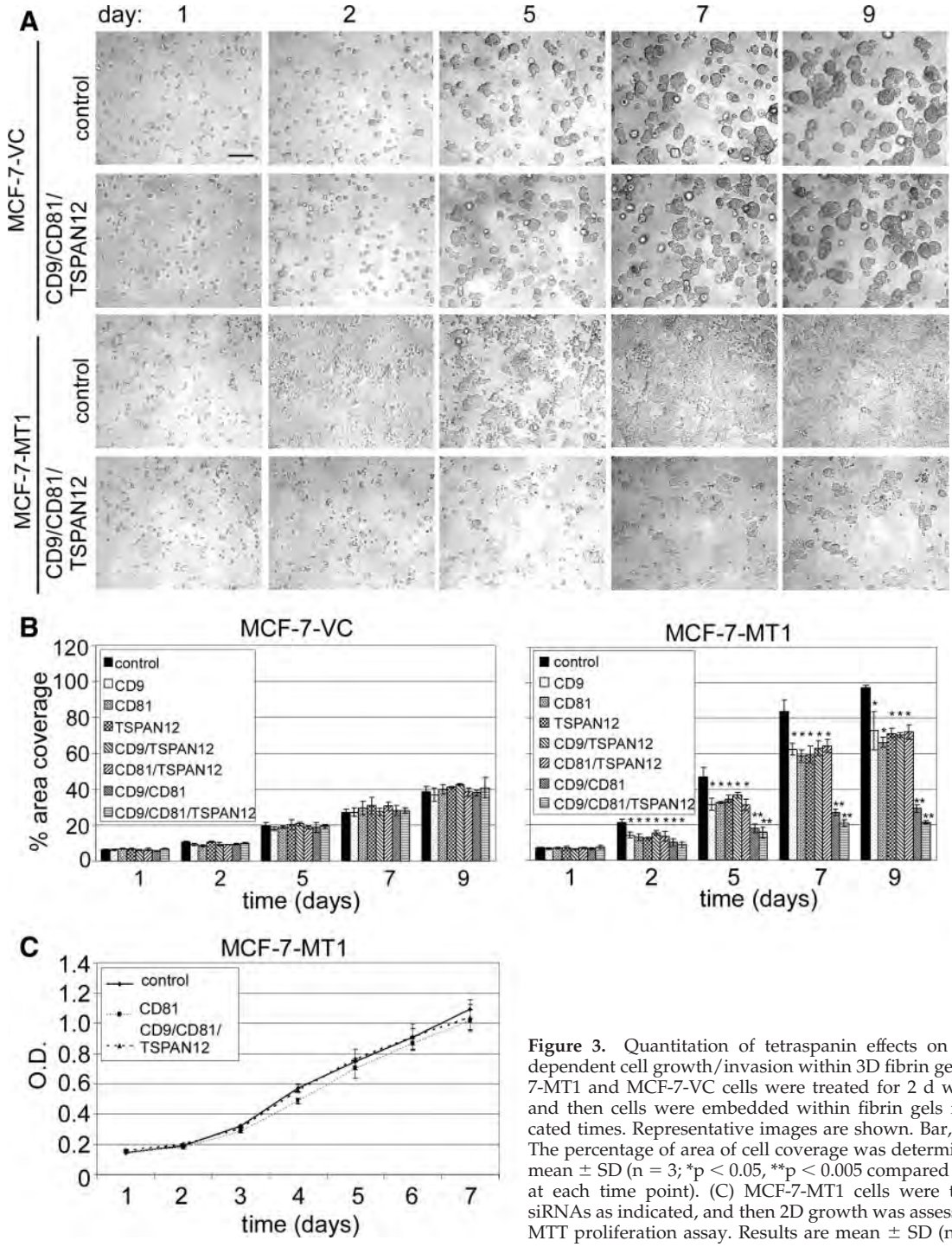

Figure 3. Quantitation of tetraspanin effects on MT1-MMP-dependent cell growth/invasion within 3D fibrin gels. (A) MCF-7-MT1 and MCF-7-VC cells were treated for 2 d with siRNAs, and then cells were embedded within fibrin gels for the indicated times. Representative images are shown. Bar, 200 μm. (B) The percentage of area of cell coverage was determined to yield mean ± SD (n = 3; *$p < 0.05$, **$p < 0.005$ compared with control at each time point). (C) MCF-7-MT1 cells were treated with siRNAs as indicated, and then 2D growth was assessed using an MTT proliferation assay. Results are mean ± SD (n = 3).

MT1 cells efficiently spread, invaded, and proliferated within fibrin gels (Figure 3A, row 3). By contrast, CD9/CD81/TSPAN12 knockdown cells showed minimal invasion and growth (Figure 3A, row 4). Double knockdown (CD9/CD81) MCF-7-MT1 cells also were markedly impaired, whereas single knockdown cells were affected to a lesser extent (Figure 3B). Because MCF-7-VC cells are minimally fibrinolytic, they were unable to escape matrix growth constraints. Consequently, they grew as immobile cysts, regardless of tetraspanin knockdown (Figure 3A, rows 1 and 2; and B). Proliferation of MCF-7-MT1 cells was not significantly affected by tetraspanin knockdown in a 2D proliferation/viability assay (Figure 3C).

Similar experiments were then carried out using 3D collagen gels. Once again, control siRNA-treated MCF7-MT1 cells, but not tetraspanin knockdown cells, escaped from a 3D growth restraint (Supplemental Figure 4B). Again, triple knockdown and CD9/CD81 double knockdown were most effective, whereas other double and single knockdowns were less effective (Supplemental Figure 4B). By contrast, tetraspanin knockdown had little effect on control MCF-7 cells (Supplemental Figure 4A).

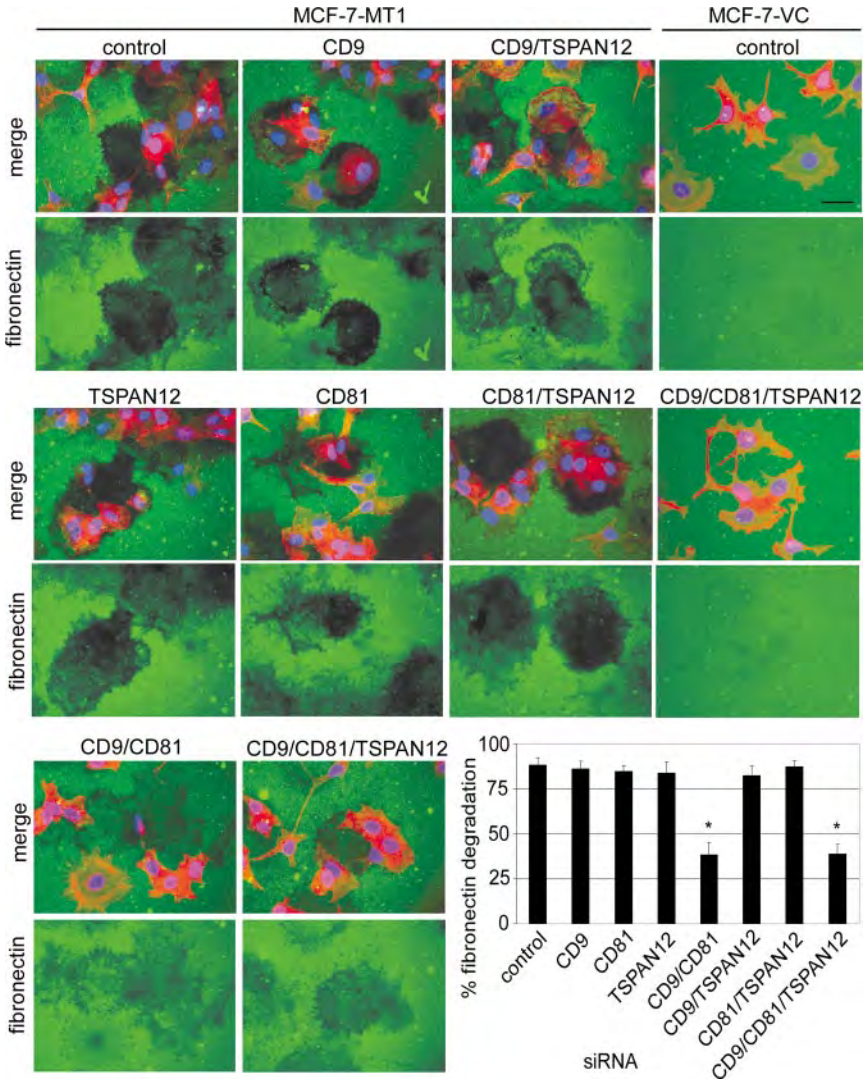

Figure 4. Tetraspanin effects on MT1-MMP-dependent fibronectin degradation. MCF-7-VC and MCF-7-MT1 cells were treated with siRNAs, plated 4 d later on fibronectin (FN)-coated slides, and then incubated overnight in serum-free media with protease inhibitors (50 μg/ml aprotinin, 2 μM leupeptin, 20 μM E64, and 20 μM pepstatin A) to prevent non-MMP proteolysis of the FN. The following day, cells were washed, fixed, and FN was detected using an anti-FN antibody followed by Alexa 488-conjugated anti-mouse secondary antibody (green). The position of the cells was determined by staining the cytoskeleton with Alexa Fluor 546-phalloidin (red) and the nuclei with DAPI (blue). Representative fluorescent images (merge green/red/blue or green only) are shown. Bar, 20 μm. For the bar graph, 100% fibronectin degradation is defined as 0 pixel density within defined proteolyzed areas, whereas 0% degradation is pixel density in the unperturbed fibronectin layer. Results are mean of percentage of fibronectin degradation ± SD (n = 3; *$p < 0.01$ compared with control). Efficient tetraspanin knockdown was obtained similarly to that shown in Supplemental Figure 3.

A third type of ECM degradation assay was then carried out, involving MT1-MMP-dependent pericellular fibronectin degradation. On plating on fibronectin overnight, MCF-7-MT1 cells efficiently cleared fibronectin, leaving dark patches in the fluorescent green lawn (Figure 4, top left). However, fibronectin degradation was significantly reduced after knockdown of CD9/CD81 or CD9/CD81/TSPAN12 (Figure 4, bottom). Other single or double knockdowns had minimal effect on MCF-7-MT1 cells (Figure 4). As expected, control MCF-7-VC cells did not degrade fibronectin, with or without tetraspanin knockdown (Figure 4, far right).

We next analyzed pro-MMP-2 activation, which is principally mediated by MT1-MMP (Sato *et al*., 1994). Compared with control knockdown, CD9/CD81/TSPAN12 knockdown in MCF-7-MT1 cells caused activation of pro-MMP-2 to be ~78% inhibited (Figure 5A). We also analyzed tetraspanin knockdown effects on endogenous MT1-MMP in HT1080 cells. Because HT1080 cells do not express CD9, we knocked down CD81, TSPAN12, and CD151 (which weakly associates with MT1-MMP). Again, tetraspanin knockdown decreased pro-MMP-2 activation, this time by ~40% (Figure 5B). The effect was particularly obvious when cytochalasin D (cyto D) was added to increase MT1-MMP protein levels in HT1080 cells. Cyto D has been shown previously to increase the transcription of MT1-MMP (Yan *et al*., 2000). Little MMP-2 activation was seen in MCF-7-VC cells (Figure 5C), thus confirming that MMP-2 activation is almost entirely MT1-MMP dependent in our MCF-7 cell system.

Mechanistic Insights: How Do Tetraspanins Affect MT1-MMP Functions?

Tetraspanin knockdown (CD9/CD81/TSPAN12) in MCF-7-MT1 cells decreased levels of both full-length and cleaved MT1-MMP (cMT1) by 75 and 80%, respectively, as seen by densitometric quantitation (Figure 6A). Cell surface expression of MT1-MMP was also diminished, by 40–60%, as seen by flow cytometry using two different anti-MT1-MMP antibodies (Figure 6B). Surface expressions of other abundant cell surface proteins (MHC I, E-cadherin, and α3 integrin) were mostly unaffected, whereas CD9 and CD81 were appropriately diminished (Figure 6B). To confirm CD9/CD81/TSPAN12 knockdown results above, a second set of CD9, CD81, and TSPAN12 siRNAs were tested. Again, substantial knockdown of CD9, CD81, and TSPAN12 was accompanied by ~50% reduction in expression of MT1-MMP (Supplemental Table 3).

Tetraspanin knockdown (CD81/TSPAN12/CD151) also decreased expression of total endogenous MT1-MMP (full

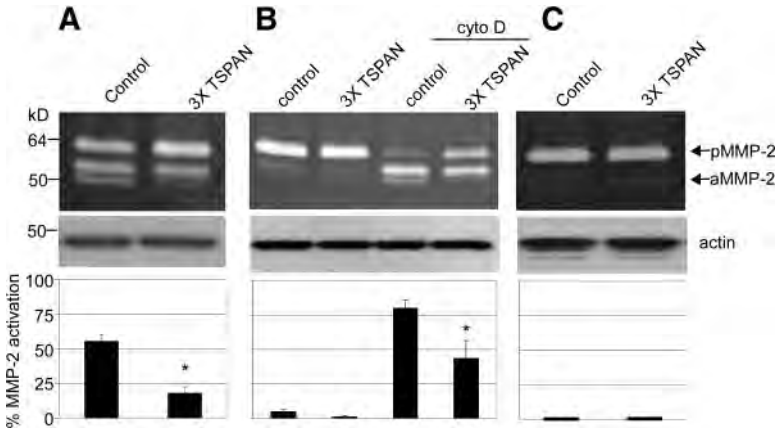

Figure 5. Tetraspanin effects on MT1-MMP–dependent pro-MMP-2 activation. (A) MCF-7-MT1 cells were treated with control or CD9/CD81/TSPAN12 (3xTSPAN) siRNAs and after 4 d, cells were plated and incubated overnight in serum-free media supplemented with conditioned media from MCF-7 cells stably expressing MMP-2. Eighteen hours later, conditioned media and lysates were collected and analyzed for pro-MMP-2 activation by gelatin zymography or actin expression by Western blotting (as loading control), respectively. Densitometry was performed on zymograms and results displayed as percentage of active MMP-2 ± SD (n = 3; *$p < 0.01$ compared with control). (B) HT1080 cells were transfected with control or CD81/CD151/TSPAN12 (3xTSPAN) siRNAs. After 4 d, cells were plated and then incubated overnight in serum-free media with or without 4 μM cyto D. Conditioned media were then collected and analyzed by gelatin zymography for pro-MMP-2 activation. Zymogram densitometry was performed (n = 4; *$p < 0.05$ compared with control). (C) MCF-7-VC cells were treated and analyzed as described in A (n = 2).

length and cMT1) in HT1080 cells. Expression decreased by 45–55%, depending on whether cytochalasin D was absent or present (Figure 6C). Cell surface expression of endogenous HT1080 MT1-MMP also showed a significant decrease (~30%), as detected by flow cytometry using two different anti-MT1-MMP antibodies. Control experiments confirmed knockdown of CD81, CD151, and TSPAN12 (Figure 6D and Supplemental Figure 4D), whereas other abundant cell surface proteins (MHC I and CD98) were unaffected (Figure 6D).

To address the mechanism whereby tetraspanins affect MT1-MMP protein levels, we first analyzed cell surface internalization. Knockdown of CD9/CD81/TSPAN12 did not affect MT1-MMP internalization in MCF-7-MT1-GFP cells, as determined using a reducible biotin accessibility assay (Supplemental Figure 5). Next, we used pulse-chase [^{35}S]Met/Cys labeling to assess MT1-MMP delivery to the cell surface. After siRNA treatment, MCF-7-MT1 cells were pulsed (30 min) and then chased for 0, 20, 45, 90, or 210 min. Before lysis, cells were incubated with anti-FLAG antibody, which bound to extracellular pro- and active MT1-MMP-FLAG. After lysis, cell surface MT1-MMP-FLAG proteins were immunoprecipitated and analyzed (Figure 7A). Already at 30-min pulse, 0-min chase, there was less newly synthesized MT1-MMP delivered to the surface of CD9/CD81/TSPAN12 knockdown cells (Figure 7A), despite there being similar amounts of total MT1-MMP synthesized in control and tetraspanin knockdown cells (Figure 7B, time zero). Later time points (20-, 45-, and 90-min chase) confirmed the deficit in cell surface delivery caused by tetraspanin knockdown (Figure 7A). Figure 7D confirmed CD9 and CD81 knockdown and decreased levels of total MT1-MMP. Pulse-chase analysis of total MT1-MMP (Figure 7B) showed that tetraspanin knockdown did not diminish total MT1-MMP synthesis rates nor affect much the rapid conversion of pro- to active form. However, total MT1-MMP was degraded at a faster rate, and very little of the autocatalytically generated cMT1 was produced upon CD9/CD81/TSPAN12 knockdown. These results indicate that silencing of CD9/CD81/TSPAN12 causes less MT1-MMP to reach the cell surface. Instead, it seems to be rerouted to an intracellular compartment and degraded at a faster rate.

To gain further insight into MT1-MMP degradation, we treated control or CD9/CD81/TSPAN12-silenced MCF-7-MT1-GFP cells with lysosome and proteasome inhibitors. Lysosome inhibitors (chloroquine, bafilomycin A1, and pepstatin A/leupeptin combination) largely protected total MT1-MMP from CD9/CD81/TSPAN12 knockdown-induced degradation (Figure 7C). By contrast, proteasome inhibitors (MG132 and lactacystin) did not protect MT1-MMP from degradation.

DISCUSSION

The role of MT1-MMP as a proinvasive protease during tumor cell invasion has been well established (Osenkowski *et al.*, 2004; Itoh and Seiki, 2006). MT1-MMP associates with various tetraspanin proteins (Takino *et al.*, 2003; Yanez-Mo *et al.*, 2008; Kolesnikova *et al.*, 2009), resulting in possible negative regulation of expression (Takino *et al.*, 2003), and both negative and positive functional regulation (Yanez-Mo *et al.*, 2008). Here, we describe how multiple tetraspanins associate with newly synthesized MT1-MMP in cancer cells, thereby preventing its lysosomal degradation, supporting cell surface expression and uniformly enhancing MT1-MMP functions in multiple proteolysis assays.

Functional Consequences of Tetraspanin Association

Among seven tetraspanins tested, CD9, CD81, and TSPAN12 showed the most robust MT1-MMP association, as seen by reciprocal coimmunoprecipitation and antibody-induced colocalization. Removal of tetraspanins CD9, CD81, and/or TSPAN12 markedly diminished all MT1-MMP–dependent functions tested. MT1-MMP promotes fibronectin proteolysis, leading to enhanced cell migration and invasion (Takino *et al.*, 2007). Tetraspanin knockdown impaired MT1-MMP–dependent proteolysis of two-dimensional fibronectin, which should lead to impaired cell migration and invasion. MT1-MMP also supports tumor proliferation by relieving growth constraints imposed by 3D ECM (Hotary *et al.*, 2003). Tetraspanin knockdown markedly diminished cancer cell invasion and proliferation within 3D fibrin and collagen gels, consistent with relief of growth constraints. These results may help to explain why loss of tetraspanin-MT1-MMP association correlated with diminished glioblastoma growth within a 3D in vivo setting (Kolesnikova *et al.*, 2009). Another important function of MT1-MMP is to activate MMP-2 (Sato *et al.*, 1994). Tetraspanin knockdown markedly diminished activation of MMP-2 by MT1-MMP (either endogenous or overexpressed) in two different tumor cell lines. Given that MMP-2 also can be a key player during tumor cell invasion/tumor progression (Itoh *et al.*, 1998),

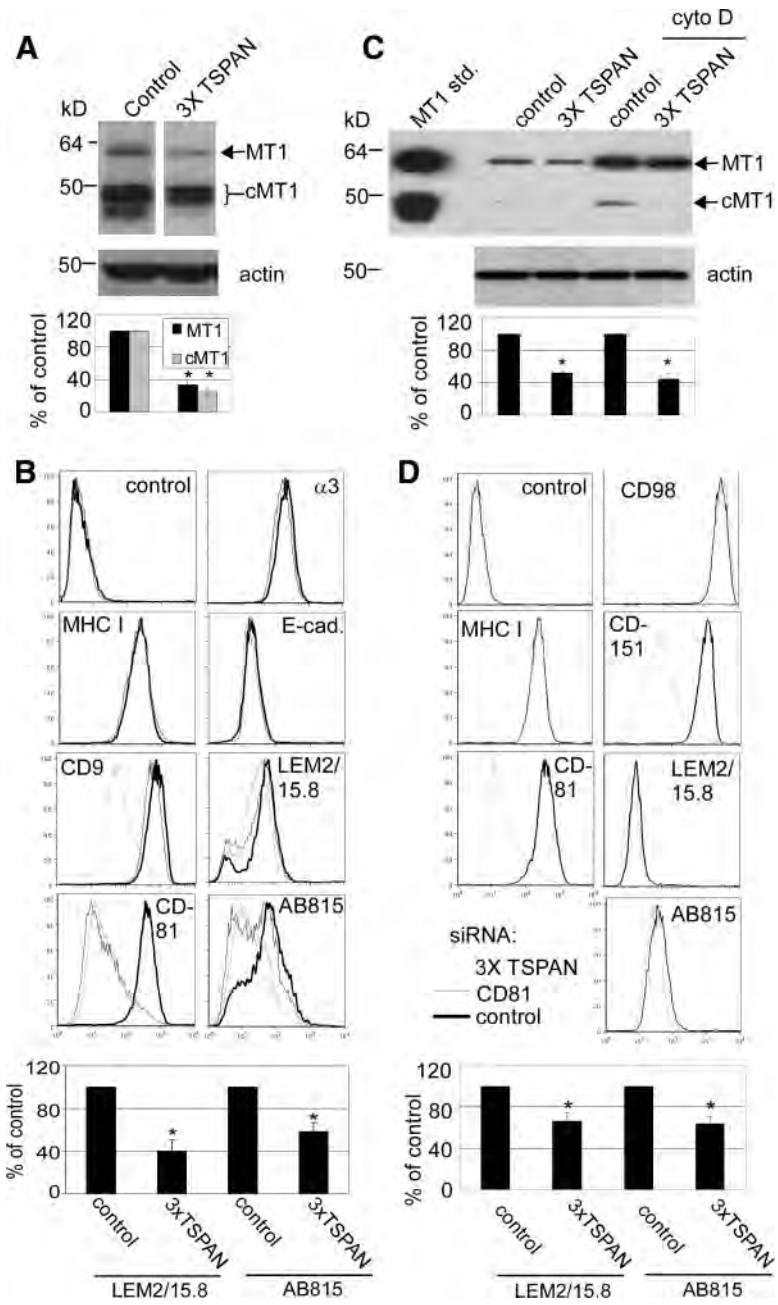

Figure 6. Tetraspanin effects on MT1-MMP expression. (A) TX114 cell lysates from MCF-7-MT1 samples in Figure 5A were blotted for MT1-MMP (AB815 antibody) and actin. Densitometry was performed on Western blots to yield indicated percent values relative to control lanes ± SD (n = 3; *p < 0.05 compared with control); cMT1 is cleaved MT1 lacking the catalytic domain (generated via an autocatalytic cleavage event). (B) MCF-7-MT1 cells were treated with control, CD81, or CD9/CD81/TSPAN12 (3xTSPAN) siRNAs. After 4 d, cell surface expression of MHC I, E-cadherin, α3 integrin, CD9, CD81, and MT1-MMP was determined by flow cytometry. For MT1-MMP, AB815 is anti-hinge antibody (detects both full-length and cleaved MT1-MMP) and LEM2/15.8 is anti-catalytic domain antibody (detects full-length MT1-MMP only). Quantitation of flow cytometry mean fluorescent intensity (MFI) values of MT1-MMP by using either AB815 or LEM2/15.8 antibodies is shown and expressed as percentage of control ± SD (n = 4; *p < 0.05 compared with control for each antibody). (C) Cell lysates from HT1080 samples in Figure 5B were blotted for MT1-MMP (AB815 antibody) or actin. Densitometry of total MT1-MMP was expressed as percentage relative to controls ± SD (n = 3; *p < 0.01 compared with control). cMT1 is cleaved MT1-MMP. MT1-MMP standard was prepared as described in Figure 1B. (D) HT1080 cells were transfected with control or CD81/CD151/TSPAN12 (3xTSPAN) siRNAs, and flow cytometry was performed 4 d after transfection for MHC I, CD98, CD81, CD151, and MT1-MMP (AB815 and LEM2/15.8) with cyto D stimulation 1 d before flow cytometry. Quantitation of flow cytometry MFI values of MT1-MMP is shown and expressed as percentage of control ± SD (n = 5; *p < 0.05 compared with control for each antibody).

loss of MMP-2 activation likely contributes to impaired tumor cell functions caused by tetraspanin knockdown.

Deletion of individual tetraspanins in mice and flies has yielded relatively minor developmental effects (Hemler, 2005), likely due to functional compensation among different tetraspanins (Fradkin *et al*., 2002; Kaji *et al*., 2002). Here, compared with single tetraspanin knockdowns, depletion of two or three tetraspanins more notably diminished MT1-MMP expression and functions. Among combinations tested, CD9/CD81 knockdown was most effective, consistent with these molecules providing overlapping (i.e., partly compensating) contributions toward MT1-MMP expression and function. In this regard, the structurally similar CD9 and CD81 molecules partially compensate for each other during oocyte fertilization (Rubinstein *et al*., 2006). CD9 and CD81 are not known to support tumor invasion and growth, perhaps because they are usually studied one at a time. Notably, CD9/CD81 null and MT1-MMP null mice show striking similarities. Both strains show diminished size, abnormal bone-associated phenotypes (e.g., osteopenia), and alveolar airspace enlargement (Holmbeck *et al*., 1999; Hemler, 2003; Takeda *et al*., 2003; Atkinson *et al*., 2005). Hence, the CD9/CD81 null mouse phenotype could arise, at least partly, from altered MT1-MMP regulation.

Compared with CD9/CD81 double knockdown results, TSPAN12/CD9/CD81 triple knockdown effects were only slightly more obvious, possibly because endogenous TSPAN12 protein is less abundant than CD9 and CD81. Nonetheless, knockdown of endogenous TSPAN12 individually did have a small but significant effect on MT1-MMP functions within 3D fibrin and collagen matrices, suggesting that TSPAN12 can be a contributor. Its wide expression

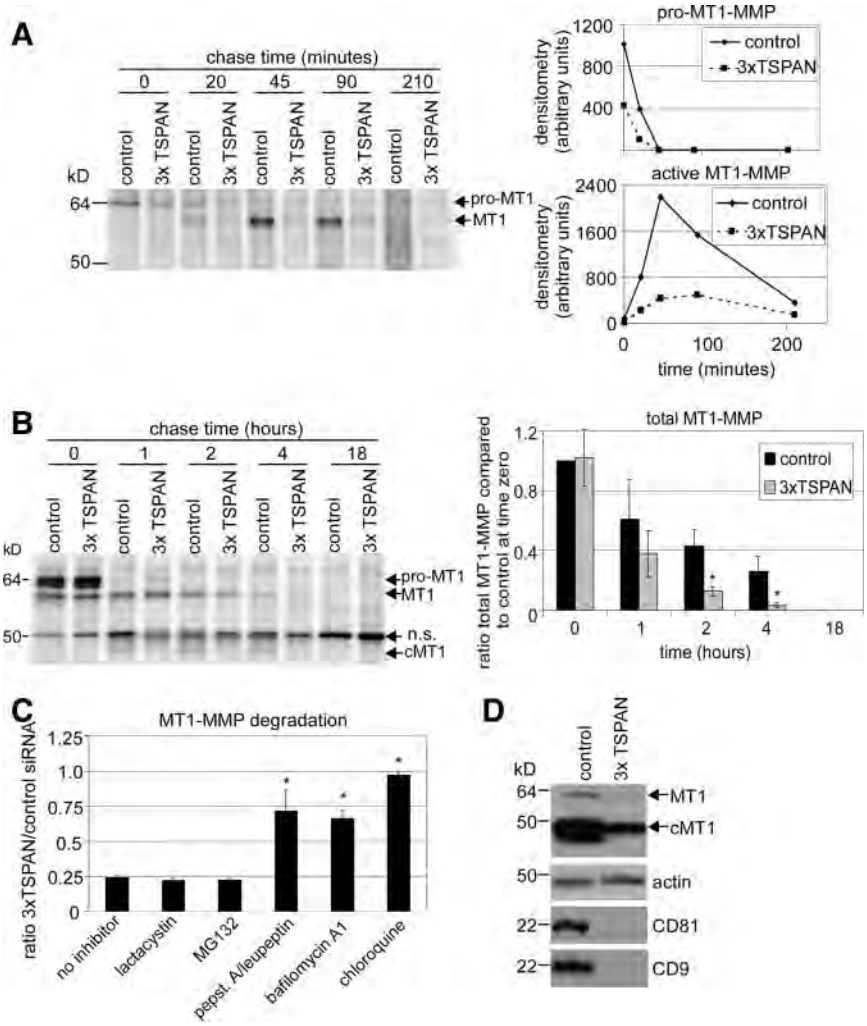

Figure 7. Tetraspanins affect MT1-MMP trafficking and stability. (A) MCF-7-MT1 cells were transfected with control or CD9/CD81/TSPAN12 (3xTSPAN) siRNAs. After 4 d, the cell surface subset of MT1-MMP was analyzed by [^{35}S]Met/Cys pulse-chase (see *Materials and Methods*). Appearance and processing of cell surface MT1-MMP was quantitated by densitometry and plotted as raw densitometric values for both pro- and active MT1-MMP as line graphs. (B) Four days after siRNA treatment, total MT1-MMP was analyzed by [^{35}S]Met/Cys pulse-chase, and densitometry was performed on total labeled MT1-MMP protein and expressed as ratio compared with control at time zero ± SD ($n = 3$; *$p < 0.05$ compared with control at each time point). cMT1 is cleaved MT1. (C) MCF-7-MT1-GFP cells were transfected with control or CD9/CD81/TSPAN12 (3xTSPAN) siRNAs. Two days after siRNA treatment, cells were treated with either lactacystin (10 μM), MG132 (2.5 μM), pepstatin A (50 μM)/leupeptin (10 μM), bafilomycin A1 (25 nM), or chloroquine (50 μM) for 2 d. Cell lysates were then collected, and MT1-MMP was analyzed by Western blotting. Densitometry was performed on total MT1-MMP and represented as ratio of total MT1-MMP for 3xTSPAN/control for each inhibitor ± SD ($n = 3$; *$p < 0.05$ compared with no inhibitor). Note that all the lysosomal inhibitors stimulated MT1-MMP expression in control siRNA-treated cells compared with no inhibitor, consistent with normal degradation of MT1-MMP in lysosomes (data not shown). (D) Tetraspanin knockdown was confirmed by Western blotting of CD9 and CD81 from cell lysates. Decreased MT1-MMP expression with tetraspanin knockdown is shown by Western blotting. TSPAN12 mRNA was also appropriately decreased (data not shown).

(Serru *et al.*, 2000) should enable collaboration with MT1-MMP on many cancer cell types. Further study of endogenous TSPAN12 protein awaits the development of appropriate antibody reagents.

Our CD81/CD151/TSPAN12 knockdown diminished MT1-MMP-dependent MMP-2 activation in HT1080 cells. Elsewhere, CD151 knockdown stimulated MT1-MMP–dependent MMP-2 activation on endothelial cells (Yanez-Mo *et al.*, 2008). These results are not necessarily contradictory because 1) knockdown of CD151 alone may be insufficient to disrupt MT1-MMP function within TEMs, and 2) regulation of MT1-MMP may differ in primary endothelial cells compared with tumor cell lines. In addition, in tumor cell lines MT1-MMP associations are much more robust with CD9 and CD81 (compared with CD151).

Tetraspanin Effects on MT1-MMP: Mechanistic Insights

Tetraspanin knockdown decreased MT1-MMP expression (both cell surface and total) in both overexpressed and endogenous systems. Hence, combinations of tetraspanins (especially CD9, CD81, TSPAN12, and CD151) support MT1-MMP expression. Elsewhere, knockdown of CD151 alone did not affect MT1-MMP expression (Yanez-Mo *et al.*, 2008), and CD63 knockdown increased rather than decreased MT1-MMP expression (Takino *et al.*, 2003). Because we did not observe CD63 association with MT1-MMP, we did not pursue CD63 further. MT1-MMP association with other cell surface proteins, including CD44, syndecan, and αV integrins (Barbolina and Stack, 2008), leads to shedding and/or proteolytic processing. However, MT1-MMP does not seem to cause tetraspanin proteolysis.

For total MT1-MMP, initial synthesis and stability were unaltered upon tetraspanin removal—decreased expression was not seen until later time points (e.g., 2- to 4-h chase). However, cell surface MT1-MMP expression was greatly diminished even at early time points. Rather than going to the cell surface, newly synthesized MT1-MMP is apparently diverted to an intracellular compartment and subsequently degraded at an accelerated rate. Consistent with this, confocal microscopy showed that MT1-MMP was not only diminished in tetraspanin knockdown cells but also shifted away from the surface and into intracellular compartments. We considered that tetraspanin knockdown might cause MT1-MMP to be rapidly removed soon after it arrives at the cell surface. However, we did not observe increases in MT1-MMP internalization or shedding into exosome/microvesicle particles (unpublished data), again consistent with MT1-MMP not reaching the cell surface. After tetraspanin silencing, MT1-MMP disappearance was inhibited by lysosomal protease inhibitors chloroquine, bafilomycin A1, and pepstatin A/leupeptin combination. These results suggest that

MT1-MMP is diverted into lysosomal compartments and degraded.

There is precedent for tetraspanins supporting partner protein surface expression. CD81 facilitates EWI-2 (Stipp *et al*., 2003a) and CD19 (Shoham *et al*., 2006) surface expression, and tetraspanins UP1a and UP1b enable UPII and UPIII surface expression (Hu *et al*., 2005). However, in these cases, tetraspanin absence impairs intracellular maturation. By contrast, diminished cell surface MT1-MMP is not accompanied by delayed maturation (Figure 7B). Hence, tetraspanins may affect MT1-MMP at a post-endoplasmic reticulum/Golgi stage, by a novel mechanism.

Because tetraspanins such as CD9, CD81, CD151 (Berditchevski, 2001), and TSPAN12 (our unpublished data) associate with integrins, MT1-MMP should be brought into proximity with integrins, as demonstrated in endothelial cells for CD151 and MT1-MMP (Yanez-Mo *et al*., 2008). Hence, tetraspanins may coordinate processes of cell adhesion and ECM proteolysis during cell invasion and migration. Within invading cells, MT1-MMP in lamellipodia and invadopodia is well positioned for localized ECM degradation (Itoh, 2006). Indeed, silencing of proteins such as TI-VAMP/VAMP-7, Sec3/Sec8/IQGAP1, or RAb8 leads to disruption of invadopodia formation and/or loss of MT1-MMP-dependent tumor cell invasion (Bravo-Cordero *et al*., 2007; Sakurai-Yageta *et al*., 2008; Steffen *et al*., 2008). Tetraspanin protein complexes contribute to the organization of lamellipodia, filopodia, and uropodia (Shigeta *et al*., 2003; Stipp *et al*., 2003a) and therefore should also contribute to invadopodia. However, it remains to be seen whether ablation of tetraspanins, and loss of cell surface MT1-MMP expression, is accompanied by disruption of invadopodia.

Implications

Broad-spectrum synthetic inhibitors, targeting MMP active sites, have undergone extensive clinical testing. Unfortunately, these agents failed to provide useful cancer therapy in humans (Overall and Kleifeld, 2006). Hence, the challenge remains to target MMPs successfully with minimal harmful side effects. For a membrane-bound protease, interfering with subcellular localization may be a beneficial alternative to typical active site inhibition approaches. Anti-tetraspanin antibody effects on MT1-MMP localization may represent a promising step in this direction. Furthermore, because adult mice survive well without CD9 and CD81 expression (Takeda *et al*., 2003), therapies targeting these molecules should not be excessively toxic. This approach could potentially provide alternative treatment options for tumor invasion and metastasis and other pathological conditions dependent on pericellular proteolysis.

ACKNOWLEDGMENTS

This work was supported by National Institutes of Health grant GM-38903 and a Canadian Institutes of Health Research (CIHR) fellowship (to M.A.L.).

REFERENCES

Atkinson, J. J., Holmbeck, K., Yamada, S., Birkedal-Hansen, H., Parks, W. C., and Senior, R. M. (2005). Membrane-type 1 matrix metalloproteinase is required for normal alveolar development. Dev. Dyn. *232*, 1079–1090.

Barbolina, M. V., and Stack, M. S. (2008). Membrane type 1-matrix metalloproteinase: substrate diversity in pericellular proteolysis. Semin. Cell Dev. Biol. *19*, 24–33.

Barnstable, C. J., Bodmer, W. F., Brown, G., Galfre, G., Milstein, C., Williams, A. F., and Ziegler, A. (1978). Production of monoclonal antibodies to group A erythrocytes, HLA and other human cell surface antigens-new tools for genetic analysis. Cell *14*, 9–20.

Berditchevski, F. (2001). Complexes of tetraspanins with integrins: more than meets the eye. J. Cell Sci. *114*, 4143–4151.

Borrirukwanit, K., Lafleur, M. A., Mercuri, F. A., Blick, T., Price, J. T., Fridman, R., Pereira, J. J., Leardkamonkarn, V., and Thompson, E. W. (2007). The type I collagen induction of MT1-MMP-mediated MMP-2 activation is repressed by alphaVbeta3 integrin in human breast cancer cells. Matrix Biol. *26*, 291–305.

Bravo-Cordero, J. J., Marrero-Diaz, R., Megias, D., Genis, L., Garcia-Grande, A., Garcia, M. A., Arroyo, A. G., and Montoya, M. C. (2007). MT1-MMP proinvasive activity is regulated by a novel Rab8-dependent exocytic pathway. EMBO J. *26*, 1499–1510.

Claas, C., Seiter, S., Claas, A., Savelyeva, L., Schwab, M., and Zoller, M. (1998). Association between the rat homologue of CO-029, a metastasis-associated tetraspanin molecule and consumption coagulopathy. J. Cell Biol. *141*, 267–280.

Drew, A. F., Blick, T. J., Lafleur, M. A., Tim, E. L., Robbie, M. J., Rice, G. E., Quinn, M. A., and Thompson, E. W. (2004). Correlation of tumor- and stromal-derived MT1-MMP expression with progression of human ovarian tumors in SCID mice. Gynecol. Oncol. *95*, 437–448.

Egeblad, M., and Werb, Z. (2002). New functions for the matrix metalloproteinases in cancer progression. Nat. Rev. Cancer *2*, 161–174.

Fradkin, L. G., Kamphorst, J. T., DiAntonio, A., Goodman, C. S., and Noordermeer, J. N. (2002). Genomewide analysis of the *Drosophila* tetraspanins reveals a subset with similar function in the formation of the embryonic synapse. Proc. Natl. Acad. Sci. USA *99*, 13663–13668.

Galvez, B. G., Matias-Roman, S., Yanez-Mo, M., Sanchez-Madrid, F., and Arroyo, A. G. (2002). ECM regulates MT1-MMP localization with beta1 or alphavbeta3 integrins at distinct cell compartments modulating its internalization and activity on human endothelial cells. J. Cell Biol. *159*, 509–521.

Ha, H. Y., *et al*. (2001). Overexpression of membrane-type matrix metalloproteinase-1 gene induces mammary gland abnormalities and adenocarcinoma in transgenic mice. Cancer Res. *61*, 984–990.

Hemler, M. E. (2003). Tetraspanin proteins mediate cellular penetration, invasion, and fusion events and define a novel type of membrane microdomain. Annu. Rev. Cell Dev. Biol. *19*, 397–422.

Hemler, M. E. (2005). Tetraspanin functions and associated microdomains. Nat. Rev. Mol. Cell. Biol. *6*, 801–811.

Hemler, M. E., and Strominger, J. L. (1982). Characterization of antigen recognized by the monoclonal antibody (4F2): different molecular forms on human T and B lymphoblastoid cell lines. J. Immunol. *129*, 623–628.

Holmbeck, K., *et al*. (1999). MT1-MMP-deficient mice develop dwarfism, osteopenia, arthritis, and connective tissue disease due to inadequate collagen turnover. Cell *99*, 81–92.

Hotary, K., Allen, E., Punturieri, A., Yana, I., and Weiss, S. J. (2000). Regulation of cell invasion and morphogenesis in a three-dimensional type I collagen matrix by membrane-type matrix metalloproteinases 1, 2, and 3. J. Cell Biol. *149*, 1309–1323.

Hotary, K. B., Allen, E. D., Brooks, P. C., Datta, N. S., Long, M. W., and Weiss, S. J. (2003). Membrane type I matrix metalloproteinase usurps tumor growth control imposed by the three-dimensional extracellular matrix. Cell *114*, 33–45.

Hu, C. C., Liang, F. X., Zhou, G., Tu, L., Tang, C. H., Zhou, J., Kreibich, G., and Sun, T. T. (2005). Assembly of urothelial plaques: tetraspanin function in membrane protein trafficking. Mol. Biol. Cell *16*, 3937–3950.

Huang, H., Sossey-Alaoui, K., Beachy, S. H., and Geradts, J. (2007). The tetraspanin superfamily member NET-6 is a new tumor suppressor gene. J. Cancer Res. Clin. Oncol. *133*, 761–769.

Itoh, T., Tanioka, M., Yoshida, H., Yoshioka, T., Nishimoto, H., and Itohara, S. (1998). Reduced angiogenesis and tumor progression in gelatinase A-deficient mice. Cancer Res. *58*, 1048–1051.

Itoh, Y. (2006). MT1-MMP: a key regulator of cell migration in tissue. IUBMB Life *58*, 589–596.

Itoh, Y., and Seiki, M. (2006). MT1-MMP: a potent modifier of pericellular microenvironment. J. Cell. Physiol. *206*, 1–8.

Jiang, W. G., Davies, G., Martin, T. A., Parr, C., Watkins, G., Mason, M. D., and Mansel, R. E. (2006). Expression of membrane type-1 matrix metalloproteinase, MT1-MMP in human breast cancer and its impact on invasiveness of breast cancer cells. Int. J. Mol. Med. *17*, 583–590.

Kaji, K., Oda, S., Miyazaki, S., and Kudo, A. (2002). Infertility of CD9-deficient mouse eggs is reversed by mouse CD9, human CD9, or mouse CD81; polyadenylated mRNA injection developed for molecular analysis of sperm-egg fusion. Dev. Biol. *247*, 327–334.

Kolesnikova, T., Kazarov, A., Lemieux, M. E., Lafleur, M. A., Kesari, S., Kung, A. L., and Hemler, M. E. (2009). Glioblastoma Inhibition by Cell Surface Immunoglobulin Protein EWI-2, In Vitro and In Vivo. Neoplasia *11*, 77–86.

Kovalenko, O. V., Yang, X. H., and Hemler, M. E. (2007). A novel cysteine cross-linking method reveals a direct association between claudin-1 and tetraspanin CD9. Mol. Cell Proteomics *6*, 1855–1867.

Lafleur, M. A., Mercuri, F. A., Ruangpanit, N., Seiki, M., Sato, H., and Thompson, E. W. (2006). Type I collagen abrogates the clathrin-mediated internalization of membrane type 1 matrix metalloproteinase (MT1-MMP) via the MT1-MMP hemopexin domain. J. Biol. Chem. *281*, 6826–6840.

Liu, W. M., and Zhang, X. A. (2006). KAI1/CD82, a tumor metastasis suppressor. Cancer Lett. *240*, 183–194.

Mori, H., Tomari, T., Koshikawa, N., Kajita, M., Itoh, Y., Sato, H., Tojo, H., Yana, I., and Seiki, M. (2002). CD44 directs membrane-type 1 matrix metalloproteinase to lamellipodia by associating with its hemopexin-like domain. EMBO J. *21*, 3949–3959.

Osenkowski, P., Toth, M., and Fridman, R. (2004). Processing, shedding, and endocytosis of membrane type 1-matrix metalloproteinase (MT1-MMP). J. Cell. Physiol. *200*, 2–10.

Overall, C. M., and Kleifeld, O. (2006). Tumour microenvironment–opinion: validating matrix metalloproteinases as drug targets and anti-targets for cancer therapy. Nat. Rev. Cancer *6*, 227–239.

Penas, P. F., Garcia-Diez, A., Sanchez-Madrid, F., and Yanez-Mo, M. (2000). Tetraspanins are localized at motility-related structures and involved in normal human keratinocyte wound healing migration. J. Invest. Dermatol. *114*, 1126–1135.

Rubinstein, E., Ziyyat, A., Prenant, M., Wrobel, E., Wolf, J. P., Levy, S., Le Naour, F., and Boucheix, C. (2006). Reduced fertility of female mice lacking CD81. Dev. Biol. *290*, 351–358.

Sakurai-Yageta, M., Recchi, C., Le Dez, G., Sibarita, J. B., Daviet, L., Camonis, J., D'Souza-Schorey, C., and Chavrier, P. (2008). The interaction of IQGAP1 with the exocyst complex is required for tumor cell invasion downstream of Cdc42 and RhoA. J. Cell Biol. *181*, 985–998.

Sato, H., Takino, T., Okada, Y., Cao, J., Shinagawa, A., Yamamoto, E., and Seiki, M. (1994). A matrix metalloproteinase expressed on the surface of invasive tumour cells. Nature *370*, 61–65.

Serru, V., Dessen, P., Boucheix, C., and Rubinstein, E. (2000). Sequence and expression of seven new tetraspans. Biochim. Biophys. Acta *1478*, 159–163.

Shigeta, M., Sanzen, N., Ozawa, M., Gu, J., Hasegawa, H., and Sekiguchi, K. (2003). CD151 regulates epithelial cell-cell adhesion through PKC- and Cdc42-dependent actin cytoskeletal reorganization. J. Cell Biol. *163*, 165–176.

Shoham, T., Rajapaksa, R., Kuo, C. C., Haimovich, J., and Levy, S. (2006). Building of the tetraspanin web: distinct structural domains of CD81 function in different cellular compartments. Mol. Cell. Biol. *26*, 1373–1385.

Steffen, A., Le Dez, G., Poincloux, R., Recchi, C., Nassoy, P., Rottner, K., Galli, T., and Chavrier, P. (2008). MT1-MMP-dependent invasion is regulated by TI-VAMP/VAMP7. Curr. Biol. *18*, 926–931.

Stipp, C. S., Kolesnikova, T. V., and Hemler, M. E. (2003a). EWI-2 regulates alpha3beta1 integrin-dependent cell functions on laminin-5. J. Cell Biol. *163*, 1167–1177.

Stipp, C. S., Kolesnikova, T. V., and Hemler, M. E. (2003b). Functional domains in tetraspanin proteins. Trends Biochem. Sci. *28*, 106–112.

Tachibana, I., Bodorova, J., Berditchevski, F., Zutter, M. M., and Hemler, M. E. (1997). NAG-2, a novel transmembrane-4 superfamily (TM4SF) protein that complexes with integrins and other TM4SF proteins. J. Biol. Chem. *272*, 29181–29189.

Takeda, T., Hattori, N., Tokuhara, T., Nishimura, Y., Yokoyama, M., and Miyake, M. (2007). Adenoviral transduction of MRP-1/CD9 and KAI1/CD82 inhibits lymph node metastasis in orthotopic lung cancer model. Cancer Res. *67*, 1744–1749.

Takeda, Y., *et al*. (2003). Tetraspanins CD9 and CD81 function to prevent the fusion of mononuclear phagocytes. J. Cell Biol. *161*, 945–956.

Takino, T., Miyamori, H., Kawaguchi, N., Uekita, T., Seiki, M., and Sato, H. (2003). Tetraspanin CD63 promotes targeting and lysosomal proteolysis of membrane-type 1 matrix metalloproteinase. Biochem. Biophys. Res. Commun. *304*, 160–166.

Takino, T., Saeki, H., Miyamori, H., Kudo, T., and Sato, H. (2007). Inhibition of membrane-type 1 matrix metalloproteinase at cell-matrix adhesions. Cancer Res. *67*, 11621–11629.

Yan, L., Moses, M. A., Huang, S., and Ingber, D. E. (2000). Adhesion-dependent control of matrix metalloproteinase-2 activation in human capillary endothelial cells. J. Cell Sci. *113*, 3979–3987.

Yanez-Mo, M., *et al*. (2008). MT1-MMP collagenolytic activity is regulated through association with tetraspanin CD151 in primary endothelial cells. Blood *112*, 3217–3226.

Yang, X., Claas, C., Kraeft, S. K., Chen, L. B., Wang, Z., Kreidberg, J. A., and Hemler, M. E. (2002). Palmitoylation of tetraspanin proteins: modulation of CD151 lateral interactions, subcellular distribution, and integrin-dependent cell morphology. Mol. Biol. Cell *13*, 767–781.

Yang, X. H., Richardson, A. L., Torres-Arzayus, M. I., Zhou, P., Sharma, C., Kazarov, A. R., Andzelm, M. M., Strominger, J. L., Brown, M., and Hemler, M. E. (2008). CD151 accelerates breast cancer by regulating alpha 6 integrin function, signaling, and molecular organization. Cancer Res. *68*, 3204–3213.

Zhai, Y., Hotary, K. B., Nan, B., Bosch, F. X., Munoz, N., Weiss, S. J., and Cho, K. R. (2005). Expression of membrane type 1 matrix metalloproteinase is associated with cervical carcinoma progression and invasion. Cancer Res. *65*, 6543–6550.

NEOPLASIA
www.neoplasia.com

Volume 11 Number 1 January 2009 pp. 77–86 77

Glioblastoma Inhibition by Cell Surface Immunoglobulin Protein EWI-2, *In Vitro* and *In Vivo*[1,2]

Tatiana V. Kolesnikova[*,†], Alexander R. Kazarov[*,†], Madeleine E. Lemieux[†,‡], Marc A. Lafleur[*,†], Santosh Kesari[§,¶], Andrew L. Kung[†,‡] and Martin E. Hemler[*,†]

*Department of Cancer Immunology and AIDS, Dana-Farber Cancer Institute, Boston, MA, USA; [†]Department of Pathology, Harvard Medical School, Boston, MA, USA; [‡]Department of Pediatric Oncology, Dana-Farber Cancer Institute, Boston, MA, USA; [§]Departments of Cancer Biology and Medical Oncology, Dana-Farber Cancer Institute, Boston, MA, USA; [¶]Department of Neurology, Brigham and Women's Hospital, Boston, MA, USA

Abstract

EWI-2, a cell surface IgSF protein, is highly expressed in normal human brain but is considerably diminished in glioblastoma tumors and cell lines. Moreover, loss of EWI-2 expression correlated with a shorter survival time in human glioma patients, suggesting that EWI-2 might be a natural inhibitor of glioblastoma. In support of this idea, EWI-2 expression significantly impaired both ectopic and orthotopic tumor growth in nude mice *in vivo*. *In vitro* assays provided clues regarding EWI-2 functions. Expression of EWI-2 in T98G and/or U87-MG malignant glioblastoma cell lines failed to alter two-dimensional cell proliferation but inhibited glioblastoma colony formation in soft agar and caused diminished cell motility and invasion. At the biochemical level, EWI-2 markedly affects the organization of four molecules (tetraspanin proteins CD9 and CD81 and matrix metalloproteinases MMP-2 and MT1-MMP), which play key roles in the biology of astrocytes and gliomas. EWI-2 causes CD9 and CD81 to become more associated with each other, whereas CD81 and other tetraspanins become less associated with MMP-2 and MT1-MMP. We propose that EWI-2 inhibition of glioblastoma growth *in vivo* is at least partly explained by the capability of EWI-2 to inhibit growth and/or invasion *in vitro*. Underlying these functional effects, EWI-2 causes a substantial molecular reorganization of multiple molecules (CD81, CD9, MMP-2, and MT1-MMP) known to affect proliferation and/or invasion of astrocytes and/or glioblastomas.

Neoplasia (2009) 11, 77–86

Introduction

Malignant gliomas constitute most primary brain tumors. Along with high proliferative capacity, invasiveness, and resistance to conventional therapies, they are characterized by a progressive rise in the number and nature of cytogenetic aberrations [1]. For multiple reasons, we considered that EWI-2, a cell surface transmembrane protein in the immunoglobulin superfamily [2], might affect glioma tumor biology. First, mRNA for EWI-2 is more elevated in brain than in any other adult human tissue [2]. Second, EWI-2 affects the motility and morphology of multiple distinct tumor cell types [3–5]. Third, EWI-2 associates closely with two proteins (tetraspanins CD9 and CD81) that have previously been linked to astrocyte-astrocytoma tumor progression and/or proliferation. Whereas CD9 expression correlates with

Abbreviations: EWI-2 and EWI-F, cell surface immunoglobulin superfamily proteins containing conserved "Glu-Trp-Ile" motifs; MT1-MMP, membrane type 1 matrix metalloproteinase; MMP-2, matrix metalloproteinase 2; TEM, tetraspanin-enriched microdomain

Address all correspondence to: Martin E. Hemler, Dana-Farber Cancer Institute, Rm D1430, 44 Binney Street, Boston, MA 02115. E-mail: martin_hemler@dfci.harvard.edu

[1]This work was supported by grants from the National Institutes of Health (GM38903, CA42368) to M.E.H., Ruth L. Kirschstein National Research Service Award (T32) to T.V.K., Sidney Kimmel Foundation grant to A.L.K., Canadian Institutes of Health Research Fellowship to M.A.L, and National Institutes of Health K08 (K08CA124804) and Sontag Foundation Distinguished Scientist Award to S.K.

[2]This article refers to supplementary materials, which are designated by Table W1 and Figures W1 to W6 and are available online at www.neoplasia.com.

Received 16 September 2008; Revised 22 October 2008; Accepted 23 October 2008

DOI 10.1593/neo.81180

astrocytic tumor malignancy [6], CD81 is highly expressed on normal astrocytes and regulates neuron-induced astrocytic cell cycle arrest and differentiation [7]. Consequently, CD81 null mice in mixed genetic backgrounds have enlarged brains owing to more astrocytes [8]. Furthermore, CD9 affects epidermal growth factor receptor ligand binding activities of the membrane-bound forms of transforming growth factor α and heparin-binding EGF-like growth factor [9,10], two molecules that contribute to human malignant glioma cell growth, most likely through juxtacrine and autocrine mechanisms [6,11,12].

Tetraspanins such as CD9 and CD81 influence motility and proliferation of normal cells and the metastatic functions and tumorigenicity of malignant cells [13,14]. To accomplish these actions, they do not typically serve as cell surface receptors, but rather function, together with laterally associated partner proteins (e.g., EWI-2, integrins, other tetraspanins), in the context of tetraspanin-enriched microdomains (TEMs) [15] on the cell surface. Changes in the protein content of TEMs can be seen as cells differentiate and/or progress toward a malignant state [16,17]. EWI-2, a major protein partner for CD9 and CD81 tetraspanins, had not been shown previously to affect tumor behavior *in vivo*. Here, we show that EWI-2 is substantially downregulated on glioblastomas compared to normal brain. Furthermore, EWI-2 expression inhibits glioblastoma tumor growth *in vivo* while also inhibiting three-dimensional growth and invasion and migration *in vitro*. These inhibitory effects are accompanied by reorganization of tetraspanin-enriched membrane microdomain components (i.e., CD9 and CD81) as well as matrix metalloproteinases (i.e., MMP-2 and MT1-MMP) on the surface of glioblastoma cells.

Materials and Methods

Plasmids and Reagents

Monoclonal antibodies (mAbs) to CD9 (ALB6; Beckman Coulter, Hialeah, FL), CD63 (6H1), CD81 (M38), CD82 (M104), CD151 (5C11), MHC class I (W6/32), CD147 (8G6), and EWI-2 polyclonal antibody were referenced previously [3,4]. Anti–EWI-2 mAb 8A12 [18] was a gift from Dr. E. Rubinstein. The M2 anti-FLAG mAb, horseradish peroxidase–conjugated goat antimouse polyclonal antibody and nonimmune mouse IgG were from Sigma (St. Louis, MO). C-terminal FLAG-tagged EWI-2 and CD2 were described [2,3].

Gene Expression Data Analysis

Primary gene expression data were downloaded from the Gene Expression Omnibus Web site (http://www.ncbi.nlm.nih.gov/geo/) and used as is. From these data [19,20], notched box-and-whisker graphs were generated using the R graphics module (http://www.r-project.org/). The Henry Ford GEO Data Set (GSE4290, *top panel*) includes MAS5 signal intensities for nontumor and grades II to IV glioblastoma samples [20]. The Stanford GEO Data Set (GSE2223) is a $\log_2$ Cy5/Cy3 ratio for normal brain reference samples and grades II to IV glioblastoma samples [21,22]. For genes with multiple probes, data from all probes are included. Dashed lines indicate the median of all probes across all samples in each data set. Notches indicate 95% confidence intervals surrounding the median (dark line). The boxes denote the 25th to 75th percentiles, and the whiskers extend to 1.5 times the interquartile range of the data. Outliers are indicated as open circles. Significance was calculated by 2-tailed Welch's *T*-test.

Cell Culture and Retroviral Transduction

The human glioblastoma cell lines T98G and U87-MG (American Type Culture Collection (ATCC), Manassas, VA) and FNX-ampho packaging cells (ATCC) were maintained in Dulbecco's modified Eagle's medium (DMEM) with 10% fetal bovine serum (Invitrogen, Carlsbad, CA). Transient transfection of FNX-ampho cells and retroviral infection of T98G and U87-MG cells were performed as described [23]. Stable infectants were selected in a medium containing 200 μg/ml zeocin (Invitrogen) and were maintained as a polyclonal cell population. The U87-MG cells expressing luciferase-neomycin phosphotransferase (*neo*) fusion protein (U87-LucNeo cells) were previously described [24].

Metabolic Labeling, Immunoprecipitation, Immunoblot Analysis, and Zymography

For [^{3}H]palmitate labeling, U87-LucNeo cells at 80% to 90% confluence were serum-starved for 2 hours and then pulsed for 2 hours in medium containing 0.2 mCi/ml [^{3}H]palmitic acid (NEN Bioscience, Boston, MA) and 5% dialyzed FBS (Invitrogen). Metabolic labeling with [^{3}H]palmitate is an effective means of analyzing TEMs, which are palmitate-enriched [25]. Cells were then lysed in 1% Brij 99, and immunoprecipitations were carried out as described [3]. Proteins resolved by SDS-PAGE were transferred to polyvinylidene fluoride membrane (BioRad Laboratories, Hercules, CA) and exposed to BioMax MS film (Kodak, Rochester, NY) at −80°C with an intensifying screen, to detect [^{3}H]labeling. Nonradioactive samples were transferred to nitrocellulose membrane and immunoblotted as described [3]. A phosphoimager machine (Storm 860; Molecular Dynamics, Co., Sunnyvale, CA) together with ImageQuant v.1.2. program was used for densitometric scanning of selected protein bands.

For gelatin zymography, serum-free conditioned media from U87-LucNeo cells or washed beads containing purified protein complexes were mixed with SDS sample buffer and separated on 10% SDS-PAGE copolymerized with 1 mg/ml gelatin (Sigma). Zymograms were then washed twice in 50 mM Tris-HCl, 5 mM $CaCl_2$, pH 8.0, and 2.5% Triton X-100 for 1 hour and then incubated in 50 mM Tris-HCl, pH 7.5, 5 mM $CaCl_2$ overnight at 37°C. Gels were stained with Coomassie brilliant blue, and densitometry was performed on inverted (black on white) images as mentioned in the previous paragraph.

Cell Proliferation, Chemotactic Migration, and Matrigel Invasion Assays

To assess proliferation, cells (5×10^4) were plated in triplicate wells of 24-well plates and then, at various times, were fixed and stained with methylene blue, extracted, and quantitated at OD of 650 nm. For migration and Matrigel invasion assays, BD BioCoat growth factor reduced Matrigel invasion chambers (BD Biosciences, Bedford, MA) were used according to the manufacturers' instructions. Briefly, the transwell membrane filter inserts (6.5 mm in diameter, 8-μm pore size, 10-nm-thick polycarbonate membrane), either coated with Matrigel (invasion assays) or uncoated (migration assays), were placed in a 24-well tissue culture plates. Cells (3×10^4) suspended in serum-free DMEM containing 0.1% heat-inactivated BSA, were added to top chambers in triplicate, and DMEM containing 10% FBS was added to each bottom chamber. After an overnight incubation at 37°C, nonmigrating cells were removed from the upper face of the filter using cotton swabs, and cells on the lower filter surface were fixed and stained with Diff-Quick (Baxter Healthcare Corp., McGraw Park, IL). The number of cells per field was counted under a light microscope.

Soft Agar and In Vivo *Tumor Growth Assays*

T98G and U87-MG cells were plated, in six-well plates, in 0.35% agar in complete medium over a solid underlay of 0.55% agar. Colonies were counted after 3 to 4 weeks at 37°C in humidified conditions. To assess ectopic growth, T98G cells (4×10^6 cells per flank in 1:1 mixture of RPMI media were injected subcutaneously into both flanks of irradiated (4.5 Gy of total body radiation) male nude mice (Taconic, Germantown, NY). Tumors were monitored for 3 months and measured with calipers weekly.

Intracranial orthotopic xenografts were established by implanting 50,000 U87-LucNeo cells (± EWI-2) as described [24]. At 6- to 8-day intervals, mice were anesthetized, injected with D-luciferin and imaged with the IVIS Imaging System (Xenogen, Alameda, CA), as described [24]. All animal procedures were approved by the Dana-Farber Cancer Institute Animal Care and Use Committee.

Immunohistochemistry of Xenograft and Human Brain Samples

Primary human glioblastoma tumors (BT34, BT70, BT74, and BT79) were propagated in SCID mice in the brain and subcutaneously as described elsewhere [26]. These xenografts have the same genetic and immunohistochemical characteristics of the original tumor as reported in the literature [26,27] and confirmed in our own laboratory (S.K., unpublished results). Histologic screening of xenograft tumors (both primary and U87-MG cell lines) was performed by serial analysis of hematoxylin and eosin coronal sections taken at ~5-mm intervals along the entire brain. Normal brain samples were obtained from autopsy cases at Brigham and Women's Hospital. Collection and use of fresh and discarded human tumor tissue was approved through Brigham and Women's Hospital Institutional Review Board. Immunohistochemistry was performed according to standard protocols [28]. Rabbit anti–EWI-2 polyclonal antibody was incubated at 1:10,000 dilution for ~10 hours at 4°C. After incubation with peroxidase-conjugated secondary antibody for 45 minutes, peroxidase substrate (diaminobenzidine) was added for 5 minutes, and slides were counterstained with Mayer's hematoxylin for 2 minutes.

Statistics

Unless otherwise indicated, graphs show means ± SD and significance was calculated by 2-tailed Student's *T*-test, with unequal variance.

Results

EWI-2 Is Present in Normal Brain But Lost in Human Gliomas

In two independent human data sets, EWI-2 (IGSF8) mRNA was considerably diminished in grade II, grade III astrocytic tumors, and most significantly in grade IV astrocytoma, compared to normal brain (Figure 1*A*, *top and bottom panels*). Conversely, another member of the EWI protein family, EWI-F, was elevated in each type of astrocytoma, with the effect most obvious in grade IV glioblastoma (Figure 1*A*). In the same data sets, two other members of the EWI protein family (EWI-3 and EWI-101) and tetraspanin proteins (CD9 and CD81) were increased only slightly in high-grade astrocytic tumors compared to normal brain tissue (Figure W1). Another tetraspanin protein, CD151, which can associate indirectly with EWI-2 [4], was substantially increased in grade IV glioblastoma (Figure W1). In other experiments, EWI-2 mRNA was highly expressed throughout adult human brain (Figure W2), and abundant EWI-2 protein was stained in normal human brain (Figure 1*B*, *e*), especially in the cortex (c) more so than in white matter (w). By contrast, primary human glioblastoma tumors, propagated in mouse brains, showed minimal staining for EWI-2 (Figure 1*B*, *c* and *f*). Tissue sections in subpanels *c* and *f* of Figure 1*B* are representative of results from four different human glioblastoma tumors and subpanel *e* is representative of three different normal human brain samples. In control experiments, U87 tumors in mouse brain did not stain for EWI-2 (Figure 1*B*, *a*), whereas EWI-2–transfected U87 tumors were strongly positive (Figure 1*B*, *d*). Background staining with negative control antibody is shown for normal human brain (Figure 1*B*, *b*). Furthermore, EWI-2 protein, detected using anti–EWI-2 antibodies, is well expressed in normal human astrocytes in culture within total lysate (Figure W3*A*) and on the cell surface (Figure W3*B*). EWI-2 protein is also abundant in normal brain cortex, hippocampus, and cerebellum, as shown elsewhere [29–31]. Conversely, EWI-2 protein expression was undetectable in total cell lysate from glioblastoma cell lines U87 and T98G, unless cells had been transfected (Figure W3*C*). Similarly, EWI-2 protein was minimally detected on the surface of four different glioblastoma cell lines (Figure W4*A*) but could be seen on other cell types (Figure W4*B*). A summary of EWI-2 expression results (Table W1) indicates that EWI-2 RNA and protein is abundant in normal brain and in normal astrocytes. Conversely, EWI-2 RNA and protein is essentially absent from glioblastoma tumors and cell lines. From these results, we hypothesized that EWI-2 may inhibit astrocytoma growth *in vivo*. As an initial test of this hypothesis, Kaplan-Meier survival curves were generated from a combined grade III and grade IV glioblastoma patient data set. As indicated (Figure 1*C*), patients with low EWI-2 expression showed significantly diminished survival. Similar trends were seen when grade III and grade IV data sets were analyzed separately, although statistical significance was not achieved owing to the smaller numbers in each group (Figure W5).

EWI-2 Reexpression Inhibits Astrocytoma Growth In Vivo

To test more directly for possible *in vivo* antitumor effects of EWI-2, we expressed EWI-2 in T98G glioblastoma cells at a moderate level comparable that naturally occurring in HeLa cells (Figure W4*B*). Control and EWI-2–transfected cells were then injected subcutaneously into nude mice. Cells expressing CD2 or vector control formed tumors in ~50% of the mice, within 45 days. However, no tumors were observed (in eight mice), even after 90 days, when EWI-2 was present (Figure 2*A*). Having observed EWI-2 inhibition of glioblastoma growth in this preliminary subcutaneous xenograft model, we then proceeded to test EWI-2 effects in an orthotopic tumor growth model. U87-LucNeo cells expressing either control vector, or EWI-2, were injected intracranially, and tumor growth was quantified over time by noninvasive imaging of tumor-associated bioluminescence. Bioluminescence imaging is rapid, nonlethal, noninvasive, and closely correlated with volumetric measurements [24]. Every control mouse showed detectable tumor growth, as recorded by *in vivo* imaging (Figure 2*B*). By contrast, few tumors were seen in mice injected with U87-LucNeo/EWI-2 cells, and those seen were generally smaller (Figure 2*B*). Quantitation of results from three independent experiments confirmed that EWI-2, during a 20- to 40-day period, markedly suppressed orthotopic tumor formation by U87-LucNeo cells in mice

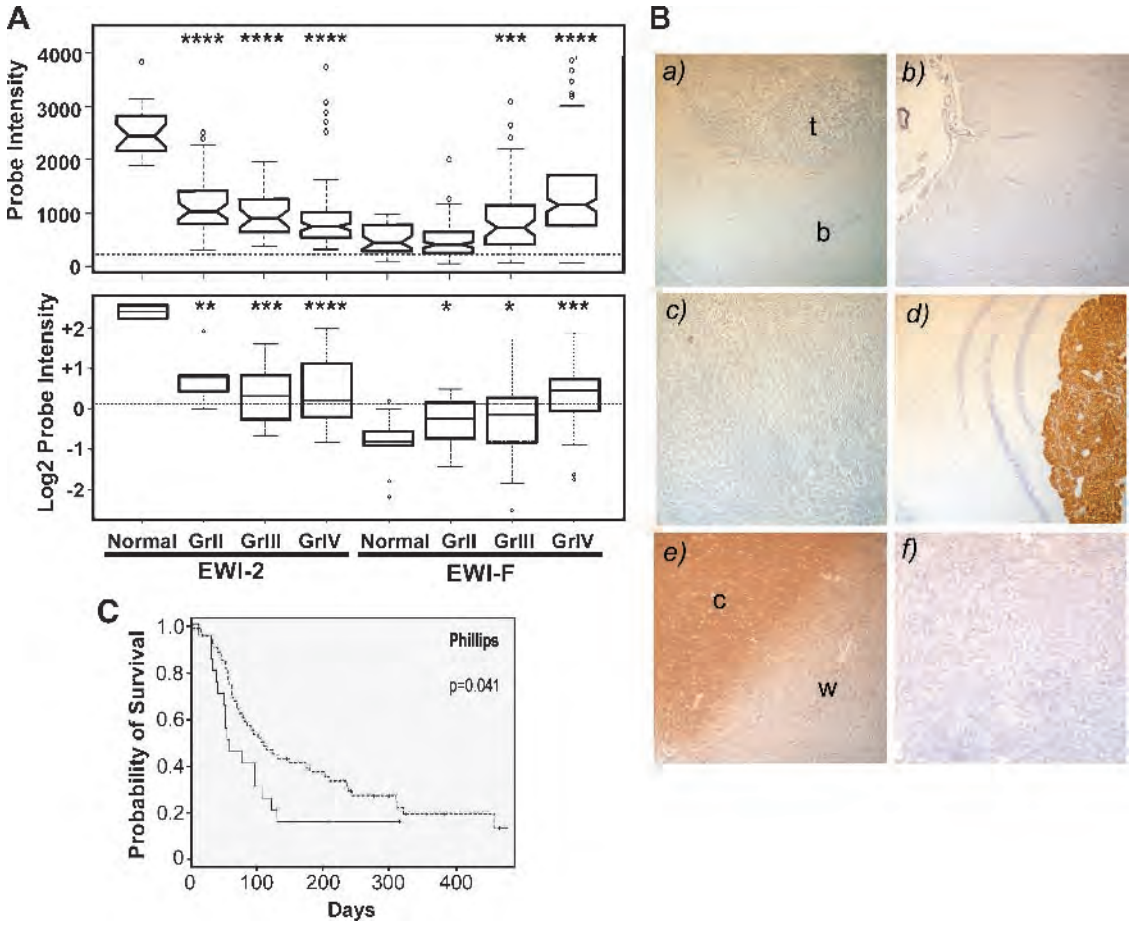

Figure 1. EWI-2 expression in human astrocytoma and normal brain. (A) EWI gene expression in normal human brain and astrocytoma (grades II, III, IV) samples. The Henry Ford GEO Data Set (GSE4290, top panel) includes 23 nontumor, 42 grade II, 31 grade III, and 77 grade IV glioblastoma samples. The Stanford GEO Data Set (GSE2223, bottom panel) includes 4 normal brain, 5 grade II, 9 grade III, and 27 grade IV glioblastoma samples. Molecules analyzed are EWI-2 (IGSF8, PGRL) and EWI-F (PTGFRN, CD9P-1, FPRP, CD315). (B) EWI-2 protein expression is shown in sections of (c) and (f) human glioblastoma tumors (representative of samples from four different tumors) and (e) normal human brain: c indicates cortex; w, white matter (representative of samples from three different brains). Control experiments show absence of EWI-2 staining in (a) U87 tumor = t, implanted in mouse brain = b; and presence of EWI-2 in (d) U87–EWI-2–transfected cells implanted in mouse brain; (b) negative control antibodies are used to show background staining in normal human brain. (C) *EWI-2* gene expression correlates with glioma patient survival. The Phillips data (GEO DataSet GSE4271) are MAS5 signal intensities for 77 grade III and grade IV glioblastomas [60]. The Phillips data were divided based on EWI-2 MAS5 expression values (probe set 225025_at) into above (n = 57, dashed line) or below (n = 20, solid line) first quartile groups. Censored data are indicated by vertical ticks. P value is the log rank test probability. Note: MAS5 is a statistical algorithm developed by Affymetrix, Inc. to estimate gene expression from array data, as described in a documentation available from Affymetrix.com.

(Figure 2*C*). Analysis of tissue slices from injected mice confirmed the bioluminescence imaging results. For example, in Figure 2*C*, experiment 3, tumors were present in 10 of 10 brains injected with control U87-LucNeo cells, whereas only 8 of 15 brains showed tumors on U87-LucNeo/EWI-2 injection, and those tumors were smaller. Representative brain sections from eight mice are shown in Figure W6. As indicated in Figure 2*D*, EWI-2 was expressed on the cell surface of U87-LucNeo cells at a level only 4.3-fold greater than endogenous EWI-2. Hence, excessive overexpression does not explain the effects of EWI-2 on orthotopic U87-LucNeo cell growth.

EWI-2 Inhibition of Glioblastoma Cell Functions In Vitro

To gain insight into how EWI-2 might be functioning *in vivo*, we carried out relevant *in vitro* assays using glioblastoma-derived cell lines T98G and U87-MG (or U87-LucNeo). Compared to controls, EWI-2 did not affect U87-LucNeo cell proliferation *in vitro* during a 2- to 6-day interval (Figure 3*A*). However, anchorage-independent growth in soft agar is typically seen as an assay more relevant to the *in vivo* behavior of transformed cells. In soft agar, both T98G and U87-MG cells showed significantly reduced colony formation on expression of EWI-2 but not vector or CD2 control protein (Figure 3*B*). Hence, EWI-2 can at least partially affect anchorage-independent growth of glioblastoma cells. Cell invasion and migration is also relevant to the progression of glioblastoma *in vivo* [32]. In this regard, expression of EWI-2 significantly diminished U87-LucNeo cell invasion and chemotactic migration 45% and 30%, respectively (Figure 3*C*). Hence, combined effects of EWI-2 on both anchorage-independent growth and tumor invasion/migration may explain glioblastoma inhibition *in vivo*.

EWI-2 Causes Reorganization of Its Associated Cell Surface Protein Complexes

Next, we sought to identify relevant molecular mechanisms to help explain EWI-2 function. Initially, we focused on tetraspanins CD9 and CD81 because 1) these molecules themselves may play critical roles during gliomagenesis (see the introduction), 2) they associate closely with EWI-2, and 3) they are known to regulate cell growth, migration, and invasion (see the introduction). For these studies, we focused on plasma membrane organization of CD9 and CD81 because this has been previously linked to EWI-2 function [3,4] and correlated with tumor cell malignancy [17]. Immunoprecipitation of either CD9 or CD81 from surface biotin-labeled U87-LucNeo cells yielded EWI-2 (Figure 4*A*). Hence, tetraspanin–EWI-2 complexes are present on the cell surface. Furthermore, the presence of EWI-2 caused staining with anti-CD9 mAb C9BB to decrease by ~70% relative to total CD9, stained by mAb MM2/57 (Figure 4*B*). The mAb C9BB preferentially recognizes homoclustered CD9 [17]. Consequently, EWI-2 is causing CD9 to become reorganized into heteroclusters, as seen previously in other cell types [17]. Tetraspanin reorganization could also be seen in immunoprecipitation experiments. Recoveries of CD81 (on CD9 immunoprecipitation) and CD9 (on CD81 immunoprecipitation) were markedly increased when EWI-2 was present in U87-LucNeo cells (Figure 4*C*). For example, as indicated by densitometric scanning (Figure 4*D*), approximately three-fold more CD81 associated with CD9, and approximately three-fold more CD9 associated with CD81 when EWI-2 was present (compare lanes 2 and 4 with lanes 1 and 3). Thus, the molecular organization of CD9 and CD81, with respect to neighboring proteins, is substantially affected by the presence of EWI-2 in these cells. In other experiments, we found that EWI-2 expression did not trigger any detectable shedding of either CD9 or CD81-containing complexes from intact cells into the growth media. In addition, EWI-2 expression did not affect tetraspanin internalization, during a 1- to 3-hour period, as assessed by monitoring the disappearance of cell surface–bound antibodies.

For further mechanistic insight into EWI-2 effects on glioblastoma, we focused on MMP-2 because 1) pericellular proteolysis, involving proteases such as MMP-2, plays a key role during glioblastoma invasion and survival [33–35] and 2) MMP-2 activation is supported by tetraspanins CD9 and CD81 (M.L. et al., manuscript submitted). On EWI-2 expression, there were no obvious changes in secreted MMP-2 levels, from U87-MG cells, at three different time points in a gelatin zymogram assay (Figure 5*A*). However, tetraspanin-associated MMP-2 was changed. Immunoprecipitation

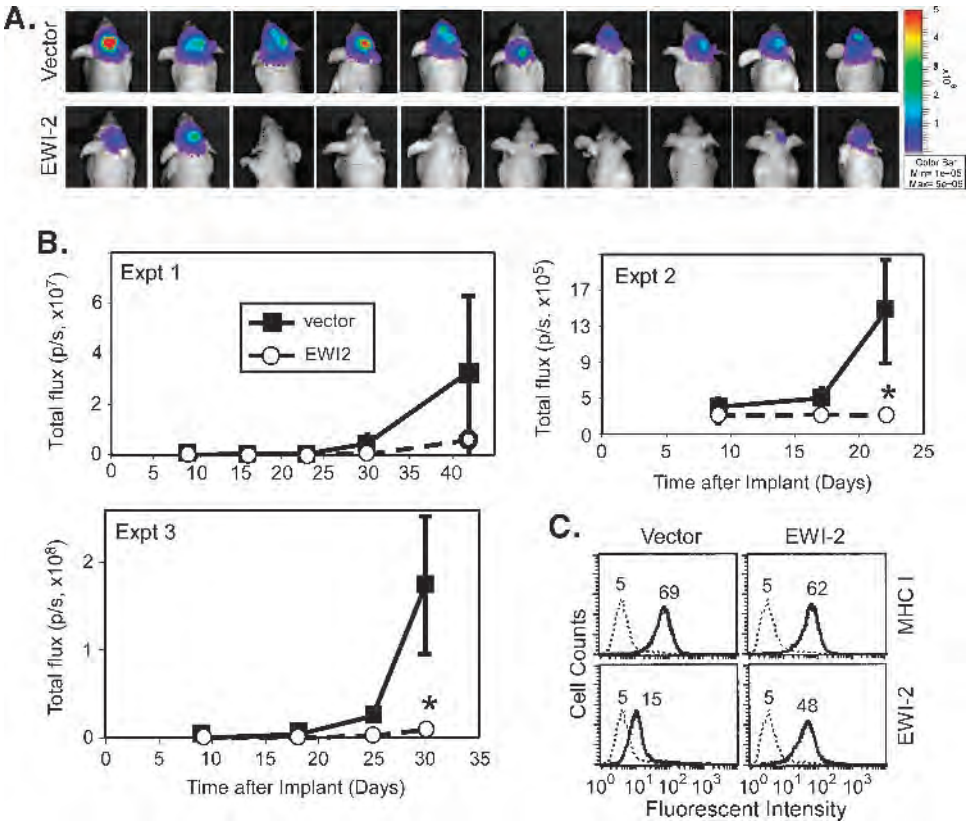

Figure 2. *In vivo* tumor formation. (A) T98G cells (4×10^6 cells) were injected subcutaneously into nude mice (in two flanks, four mice per cell line), and tumor sizes, (*l*)(*w*)(*h*)(0.52), were determined after 90 days. *$P < .05$ when EWI-2 samples are compared with vector control results. $P < .02$ when EWI-2 samples are compared with pooled control experiments (vector control plus CD2 control), according to Fisher exact test. (B) U87-LucNeo and U87-LucNeo/EWI-2 cells (50,000) were each injected intracranially into 10 nude mice and then imaged after 14 days. (C) Three independent experiments were carried out as in (B), and tumor size was quantitated by *in vivo* bioluminescence imaging (*$P < .05$). Note that tumors were observed in 100% of vector control mice. The arbitrary units representing photon flux values (*y*-axes) show interexperimental variability that may arise owing to the use of different stocks of luciferin, altered imaging parameters, altered size of the imaging area, or other variables. However, these parameters were carefully controlled intraexperimentally. (D) Cell surface expression of EWI-2 and control MHC class I in U87-LucNeo cells.

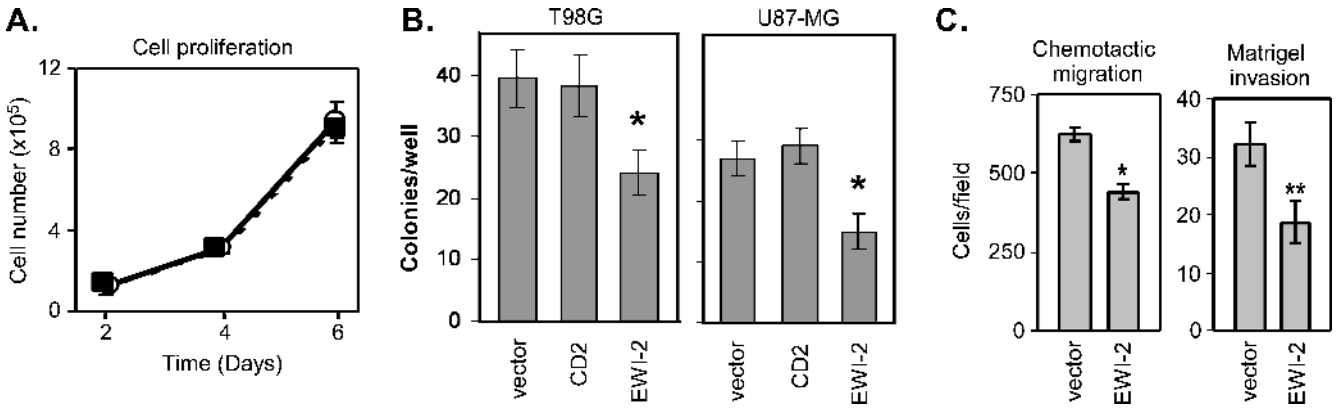

Figure 3. EWI-2 effects on proliferation, soft agar colony formation invasion and migration. (A) Cell numbers were measured for U87-LucNeo cells stably transduced with vector (open circles), or EWI-2 (closed squares). (B) The indicated cell lines expressing vector alone, CD2 (another cell surface IgSF protein), or EWI-2 were plated (600 cells per well) in soft agar for 3 weeks, and then colonies were counted (*$P < .01$ *vs* vector control cells). (C) U87-LucNeo cells, transduced with vector or EWI-2, were measured for chemotactic migration and cell invasion (*$P < .01$; **$P < .001$).

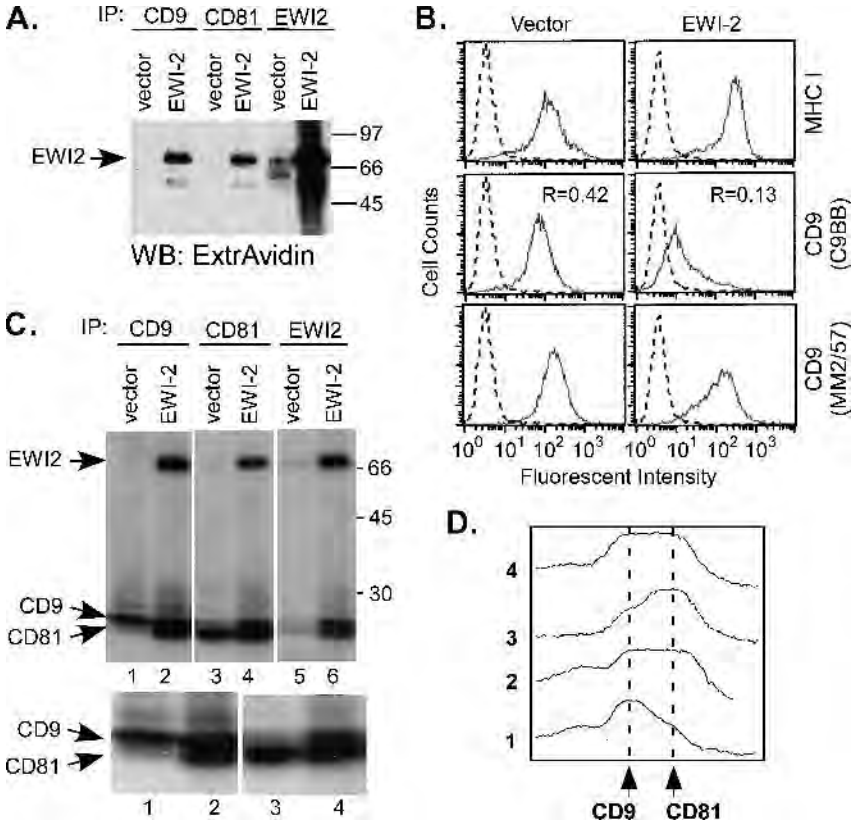

Figure 4. EWI-2 affects cell surface molecular organization of CD9 and CD81. (A) Intact U87-LucNeo cells (expressing wild type EWI-2 or vector control) were labeled with biotin and were then lysed. CD9, CD81, and EWI-2 were immunoprecipitated, and cell surface proteins were visualized by blot analysis with ExtrAvidin. Note: EWI-2–associated CD9 and CD81 themselves do not label very well with biotin because associated proteins limit accessibility (e.g., see Kolesnikova et al. [3]). (B) U87-LucNeo cells, expressing vector alone or EWI-2, were incubated with mAb W6/32 (to MHC-I), mAb C9BB (which preferentially recognizes oligomerized CD9 [18], or mAb MM2/57 (which recognizes total CD9). After washing, bound antibodies were visualized using fluorescein isothiocyanate–rabbit antimouse second antibody, and quantitated by flow cytometry. R = ratio of mean fluorescence intensities for C9BB divided by MM2/57. (C) U87-LucNeo cells, expressing vector alone or EWI-2, were labeled with ^{3}H-palmitate, lysed, and then CD9, CD81, and EWI-2 were immunoprecipitated. Lower panels show an enlarged view of key regions from the top panel. The palmitoylation of EWI-2 on membrane proximal cysteines will be described in more detail elsewhere. (D) Densitometric scans of lanes 1 to 4 are shown. Quantitation reveals increases of approximately three-fold in recovery of CD9 (in lane 4 *vs* 3) and CD81 (in lane 2 *vs* 1). Note: These results provide the first definitive demonstration that EWI-2 is palmitoylated.

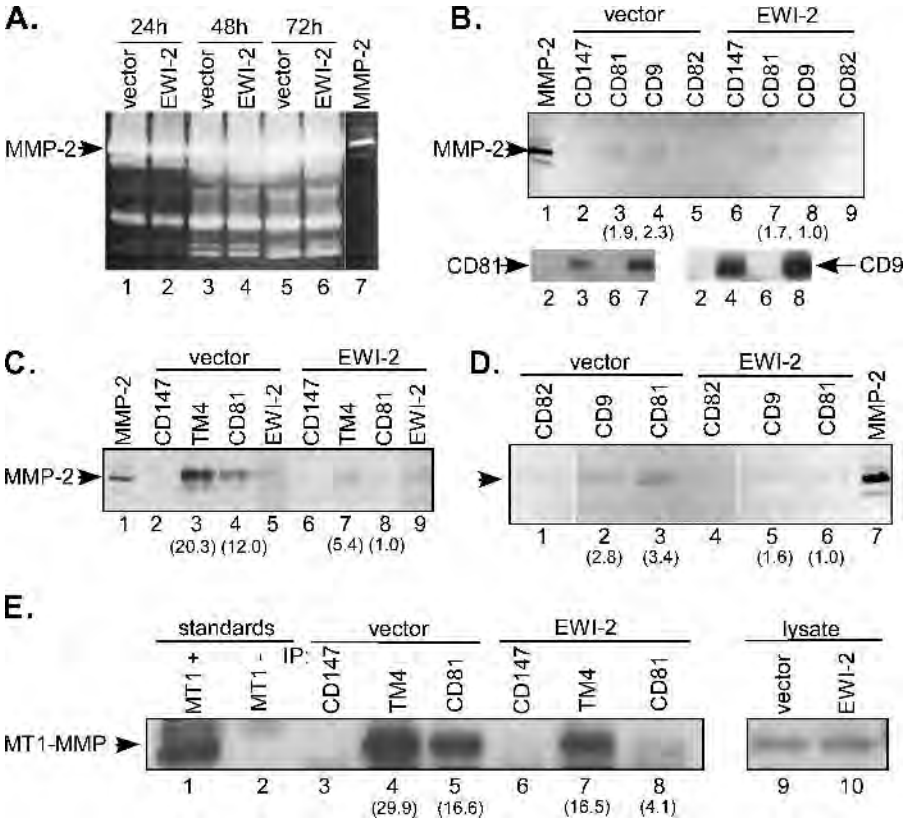

Figure 5. EWI-2 affects the molecular organization of MMP-2 and MT1-MMP. (A) Conditioned media were collected from U87-LucNeo cells (± EWI-2) and assayed for MMP-2 levels using gelatin zymography. (B, C) U87-LucNeo cells (± EWI-2) were lysed, protein complexes were immunoprecipitated, and associated MMP-2 levels were determined using gelatin zymography. TM4 = mixture of CD9, CD63, CD81, CD82, and CD151. Numbers in parentheses indicate relative amounts of MMP-2 in corresponding lanes. Selected samples (in B) were also analyzed for the presence of CD81 and CD9, as determined by Western blot analysis with M38 (CD81) and ALB6 (CD9) antibodies (lower panels). (D) T98G cells (± EWI-2) were lysed and analyzed as in (B, C). Note: Zymograms in (B–D) are inverted to show black on a white background. (E) U87-LucNeo cells (± EWI-2) were lysed, protein complexes were immunoprecipitated, and associated MT1-MMP levels were determined by immunoblot analysis of the active form of MT1-MMP. MT1-MMP in total lysates was also blotted. TM4 = mixture of CD9, CD63, CD81, CD82, and CD151. Numbers in parentheses indicate the relative amounts of MT1-MMP in the corresponding lanes. MT1-MMP standards are from MCF-7 cell lysates with or without MT1-MMP expression.

of pooled tetraspanins (Figure 5*C*, *lane 3*) or CD81 alone (*lane 4*) from mild detergent lysates of U87-LucNeo cells yielded MMP-2 gelatinolytic activity. Recovery of this activity was diminished by 70% to 90% when EWI-2 was present (Figure 5*C*, *lanes 7 and 8*). In additional experiments, MMP-2 activity associated with CD81 and CD9 was reduced by 13% to 57% in U87 cells (Figure 5*B*, *compare lanes 3 and 4 with 7 and 8*) and by 43% to 71% in T98G cells (Figure 5*D*, *compare lanes 2 and 3 with 5 and 6*) when EWI-2 was present. Diminished MMP-2 activity was not caused by the decreased immunoprecipitation of CD9 or CD81. In fact, recovery of CD9 and CD81 was typically increased when EWI-2 was present, as seen by immunoblot analysis (Figure 5*B*, *lower panels*; Figure 5*D*, not shown). Minimal amounts of MMP-2 were recovered on immunoprecipitation of CD147, an abundant cell surface protein that does not associate with TEMs (Figure 5, *B* and *C*, *lanes 2 and 6*), or of CD82, a tetraspanin that associates poorly with EWI-2 (Figure 5*B*, *lanes 5 and 9*; Figure 5*D*, *lanes 1 and 4*).

We suspected that a subset of total MMP-2 may be linked to tetraspanins through membrane-bound protease MT1-MMP because 1) MT1-MMP can associate with CD9 and CD81 (M.L. et al., manuscript submitted) and 2) MMP-2 is known to form a complex with MT1-MMP during MMP-2 activation [36]. Immunoprecipitation of pooled tetraspanins (Figure 5*E*, *lane 4*) or CD81 alone (Figure 5*E*, *lane 5*) yielded MT1-MMP protein. However, when EWI-2 was present in U87 cells, association of MT1-MMP with pooled tetraspanins was decreased by 45% (compare lane 4 with lane 7) and association with CD81 was decreased by 75% (compare lane 5 with lane 8). Meanwhile, in U87 cells, there was no decrease in either the amount of total MT1-MMP (Figure 5*E*, *lanes 9 and 10*) or in the amount of tetraspanin proteins (e.g., Figure 5*B*, *lower panels*).

In conclusion, results in this section show that EWI-2 markedly reorganizes multiple molecules (CD9, CD81, MMP-2, MT1-MMP) of likely importance during glioblastoma invasion and growth.

Discussion

EWI-2 protein and gene transcripts are abundant in normal brain tissue and in primary astrocyte cultures. However, EWI-2 protein is reduced in all glioblastoma tumors and cell lines analyzed, and EWI-2 transcripts are markedly reduced in glioblastoma and other gliomas, as seen from the analysis of two independent human data sets. By contrast, transcripts corresponding to other EWI protein family members are either strongly (EWI-F) or moderately (EWI-101, EWI-3) increased in human glioma data sets, compared to normal brain. Loss of EWI-2 expression is accompanied by diminished survival for grade

III and grade IV glioma patients. Furthermore, EWI-2 reexpression abolished T98G ectopic (subcutaneous) tumor growth *in vivo*, and considerably impaired intracranial U87-MG tumor growth *in vivo*, in nude mice. EWI-2 expression in glioblastoma cell lines also inhibited soft agar growth, invasion, and migration. These studies demonstrate that EWI-2 may have tumor suppressor–like properties in preclinical glioma models. However, the prognostic and clinical significance of EWI-2 loss of function still needs to be evaluated prospectively.

The *EWI-2* gene, which maps to 1q23.1, is not known to be specifically mutated or deleted in gliomas. Of possible relevance, partial or complete 1q monosomies have been observed in a few adult astrocytomas [37], and 1q21-41 trisomy is associated with a worse prognosis in pediatric anaplastic astrocytoma [37,38]. However, although chromosome 1q alterations appear only in a minority of cases, EWI-2 expression is markedly diminished in most adult gliomas. Hence, another mode of regulation, e.g., at the level of transcription, possibly through promoter methylation, may play a major role. As a cell surface transmembrane protein, EWI-2 is quite distinct from known glioblastoma tumor suppressors, which typically are intracellular molecules involved in signaling or cell cycle regulation [39]. One other transmembrane protein that could serve as a glioma tumor suppressor is coxsackie and adenovirus receptor (CAR). The expression of CAR is markedly reduced in high-grade astrocytomas, and CAR diminishes the size of U87-MG tumor xenografts [40].

Our *in vitro* studies provide several insights into the mechanism of EWI-2 action. First, although EWI-2 did not inhibit glioblastoma cell proliferation in two-dimensional culture, it significantly inhibited soft agar growth, consistent with EWI-2 being antitumorigenic. Second, EWI-2 caused a decrease in cell invasion and migration. This helps to explain how EWI-2 could affect *in vivo* glioblastoma progression, which is a highly invasive process [34,35]. Rodent glioblastoma xenograft models are sometimes criticized for not recapitulating invasive pathologic features of human glioblastoma multiforme (GBM) [41]. However, GBM arising from implanted U87 cells does show histopathologic features compatible with tumor invasion into nonneoplastic brain parenchyma [42]. EWI-2 inhibition of glioblastoma cell invasion and migration is consistent with previously observed inhibitory effects on motility, spreading, and ruffling in carcinoma and leukemia cell lines [3–5].

Our biochemical studies provide mechanistic insights into EWI-2 functions *in vivo* and *in vitro*. We focused on molecules that 1) directly or indirectly associate with EWI-2 and 2) are known to affect relevant functions of astrocytes and/or glioblastoma cells. Initially, we focused on tetraspanin proteins CD9 and CD81. For CD9 and CD81, EWI-2 (and EWI-F) are the most robust protein partners yet described [2,43–45], and CD9 and/or CD81 are required for EWI-2 cell surface expression and maturation [4]. EWI-2 associated with tetraspanins CD9 and CD81 on the surface of glioblastoma cells, thereby disrupting CD9 homo-oligomers and enhancing formation of CD9–CD81–EWI-2 complexes. Similar results have been seen on the expression of EWI-2 in other cell types [3,4,17]. Such changes could affect glioblastoma cell invasion and growth in multiple ways: 1) EWI-2 can cause redistribution of CD9 and CD81 to filopodia [4]. If a similar change occurs in glioblastoma, CD81 and CD9 would be well positioned to modulate tumor cell expansion into brain parenchyma, especially because CD9 can affect the dynamics of filopodia formation [46]. 2) Reorganization and redistribution of CD9 could potentially be accompanied by rearrangement of CD9 partner molecules, such as transforming growth factor α and heparin-binding EGF-like growth factor, which play major roles during glioblastoma tumor progression [6,11,12]. 3) Redistribution of CD9 and CD81 could lead to altered localization and function of CD9 and CD81-associated signaling molecules, such as protein kinase C [47] and PI 4-kinase [48]. 4) Alterations in CD9 and CD81 organization could affect the subcellular positioning and functions of integrins and other relevant molecules. For example, EWI-2 can markedly affect CD9 and CD81 colocalization with $\alpha_3\beta_1$ integrin in filopodia [4]. In this regard, $\alpha_3\beta_1$ integrin also plays an important role during glioblastoma invasion [49]. Also, other tetraspanin proteins such as CD151 [4] can associate with EWI-2–CD9–CD81 complexes, and CD151 is upregulated on glioblastoma cells (Figure W1 and [22]) and can stimulate glioblastoma motility and invasion [50]. Hence, CD151 could play an opposing role during inhibition of glioblastoma functions by overexpressed EWI-2. Several additional genes have been shown to be differentially expressed in correlation with GBM occurrence (e.g., [51]) and patient survival (e.g., [52]). It remains to be seen whether any of these gene products act in coordination with EWI-2.

We also analyzed the effects of EWI-2 expression on key proteases MMP-2 and MT1-MMP. Both are known to be involved in glioblastoma cell invasion, survival, and growth [33,35,53]. MT1-MMP promotes tumor growth by disrupting three-dimensional matrix growth control exerted on tumors [54]. On expression of EWI-2, total protein levels of MMP-2 and MT1-MMP were unaltered. However, there was a substantial decrease in both the amount of MMP-2 activity and the amount of MT1-MMP protein recovered in association with tetraspanin complexes. We show elsewhere that MT1-MMP can associate with tetraspanins CD9 and CD81 (M.L. et al., manuscript submitted). Although tetraspanin CD151 was not a prominent partner for MT1-MMP on glioblastoma cells (M.L. et al., manuscript submitted), CD151–MT1-MMP association was seen on endothelial cells [55]. During MMP-2 activation, it forms a complex with MT1-MMP and TIMP-2 [36]. The existence of this complex helps to explain the parallel dissociation of MMP-2 and MT1-MMP from tetraspanins on EWI-2 expression. Our current model is that MMP-2–MT1-MMP complexes associate preferentially with homo-oligomeric CD9 and/or CD81. When EWI-2 is present, there is a shift toward hetero-oligomeric complexes [17], accompanied by MMP dissociation (as shown here). If EWI-2 is disrupting MMP complexes, while driving CD81 and CD9 into the filopodia [4], this would likely influence glioblastoma invasion, survival, and/or growth. However, it remains to be determined whether EWI-2 causes reorganization of MMPs within filopodia.

Another possibility is that EWI-2 inhibition of glioblastoma depends on EWI-2 interaction with a counter-receptor. So far, we have failed to identify potential counter-receptor activity, or specific counter-receptors, on astrocytoma cells. Nonetheless, a possible contribution by a counter-receptor cannot be ruled out.

In conclusion, we find that EWI-2 levels are considerably diminished in human glioblastoma samples in association with diminished patient survival. Furthermore, reexpression of EWI-2 in glioblastoma cell lines leads to impaired tumor growth *in vivo*, in both ectopic and orthotopic models. EWI-2 seems to function, at least in part, by extensively reorganizing CD9 and CD81 protein complexes. This is likely accompanied by concurrent reorganization of additional other CD9 and CD81 partner proteins (e.g., proteases, adhesion receptors, signaling molecules), thus leading to suboptimal glioblastoma growth, invasion, and motility. Finally, we speculate that the tumor suppressor effects of CD9 observed on several non–glioma tumor

types [56–58] could, to a large extent, involve inhibitory effects of EWI-2, which is CD9's major partner protein.

Acknowledgments

The authors thank Renee D. Wright for technical assistance with animal studies.

References

[1] *Brain Tumor Invasion. Biological, Clinical, and Therapeutic Considerations.* In T Mikkelsen, R Bjerkvig, OD Laerum, ML Rosenblum (Eds). ISBN: 978-0-471-15452-5.

[2] Stipp CS, Kolesnikova TV, and Hemler ME (2001). EWI-2 is a major CD9 and CD81 partner, and member of a novel Ig protein subfamily. *J Biol Chem* **276**, 40545–40554.

[3] Kolesnikova TV, Stipp CS, Rao RM, Lane WS, Luscinskas FW, and Hemler ME (2004). EWI-2 modulates lymphocyte integrin alpha4beta1 functions. *Blood* **103**, 3013–3019.

[4] Stipp CS, Kolesnikova TV, and Hemler ME (2003). EWI-2 regulates {alpha}3{beta}1 integrin-dependent cell functions on laminin-5. *J Cell Biol* **163**, 1167–1177.

[5] Zhang XA, Lane WS, Charrin S, Rubinstein E, and Liu L (2003). EWI2/PGRL associates with the metastasis suppressor KAI1/CD82 and inhibits the migration of prostate cancer cells. *Cancer Res* **63**, 2665–2674.

[6] Kawashima M, Doh-ura K, Mekada E, Fukui M, and Iwaki T (2002). CD9 expression in solid non-neuroepithelial tumors and infiltrative astrocytic tumors. *J Histochem Cytochem* **50**, 1195–1203.

[7] Kelic S, Levy S, Suarez C, and Weinstein DE (2001). CD81 regulates neuron-induced astrocyte cell-cycle exit. *Mol Cell Neurosci* **17**, 551–560.

[8] Geisert EE Jr, Williams RW, Geisert GR, Fan L, Asbury AM, Maecker HT, Deng J, and Levy S (2002). Increased brain size and glial cell number in CD81-null mice. *J Comp Neurol* **453**, 22–32.

[9] Nakamura K, Iwamoto R, and Mekada E (1995). Membrane-anchored heparin-binding EGF-like growth factor (HB-EGF) and diptheria toxin receptor–associated protein (DRAP27)/CD9 form a complex with integrin $\alpha_3\beta_1$ at cell-cell contact sites. *J Cell Biol* **129**, 1691–1705.

[10] Shi W, Fan H, Shum L, and Derynck R (2000). The tetraspanin CD9 associates with transmembrane TGF-alpha and regulates TGF-alpha–induced EGF receptor activation and cell proliferation. *J Cell Biol* **148**, 591–602.

[11] Mishima K, Higashiyama S, Asai A, Yamaoka K, Nagashima Y, Taniguchi N, Kitanaka C, Kirino T, and Kuchino Y (1998). Heparin-binding epidermal growth factor–like growth factor stimulates mitogenic signaling and is highly expressed in human malignant gliomas. *Acta Neuropathol* **96**, 322–328.

[12] Rubenstein M, Glick R, Lichtor T, Mirochnik Y, Chou P, and Guinan P (2001). Treatment of the T98G glioblastoma cell line with antisense oligonucleotides directed toward mRNA encoding transforming growth factor-alpha and the epidermal growth factor receptor. *Med Oncol* **18**, 121–130.

[13] Hemler ME (2003). Tetraspanin proteins mediate cellular penetration, invasion and fusion events, and define a novel type of membrane microdomain. *Ann Rev Cell Dev Biol* **19**, 397–422.

[14] Maecker HT, Todd SC, and Levy S (1997). The tetraspanin superfamily: molecular facilitators. *FASEB J* **11**, 428–442.

[15] Hemler ME (2005). Tetraspanin functions and associated microdomains. *Nat Rev Mol Cell Biol* **6**, 801–811.

[16] Le Naour F, Andre M, Greco C, Billard M, Sordat B, Emile JF, Lanza F, Boucheix C, and Rubinstein E (2006). Profiling of the tetraspanin web of human colon cancer cells. *Mol Cell Proteomics* **5**, 845–857.

[17] Yang XH, Kovalenko OV, Kolesnikova TV, Andzelm MM, Rubinstein E, Strominger JL, and Hemler ME (2006). Contrasting effects of EWI proteins, integrins, and protein palmitoylation on cell surface CD9 organization. *J Biol Chem* **281**, 12976–12985.

[18] Charrin S, Le Naour F, Labas V, Billard M, Le Caer JP, Emile JF, Petit MA, Boucheix C, and Rubinstein E (2003). EWI-2 is a new component of the tetraspanin web in hepatocytes and lymphoid cells. *Biochem J* **373** (Pt 2), 409–421.

[19] Liang Y, Diehn M, Watson N, Bollen AW, Aldape KD, Nicholas MK, Lamborn KR, Berger MS, Botstein D, Brown PO, et al. (2005). Gene expression profiling reveals molecularly and clinically distinct subtypes of glioblastoma multiforme. *Proc Natl Acad Sci USA* **102**, 5814–5819.

[20] Sun L, Hui AM, Su Q, Vortmeyer A, Kotliarov Y, Pastorino S, Passaniti A, Menon J, Walling J, Bailey R, et al. (2006). Neuronal and glioma-derived stem cell factor induces angiogenesis within the brain. *Cancer Cell* **9**, 287–300.

[21] Bredel M, Bredel C, Juric D, Duran GE, Yu RX, Harsh GR, Vogel H, Recht LD, Scheck AC, and Sikic BI (2006). Tumor necrosis factor-alpha–induced protein 3 as a putative regulator of nuclear factor-kappaB–mediated resistance to O^6-alkylating agents in human glioblastomas. *J Clin Oncol* **24**, 274–287.

[22] Bredel M, Bredel C, Juric D, Harsh GR, Vogel H, Recht LD, and Sikic BI (2005). Functional network analysis reveals extended gliomagenesis pathway maps and three novel MYC-interacting genes in human gliomas. *Cancer Res* **65**, 8679–8689.

[23] Pear W, Nolan G, Scott M, and Baltimore D (1993). Production of high-titer helper-free retroviruses by transient transfection. *Proc Natl Acad Sci USA* **90**, 8392–8396.

[24] Rubin JB, Kung AL, Klein RS, Chan JA, Sun Y, Schmidt K, Kieran MW, Luster AD, and Segal RA (2003). A small-molecule antagonist of CXCR4 inhibits intracranial growth of primary brain tumors. *Proc Natl Acad Sci USA* **100**, 13513–13518.

[25] Yang X, Kovalenko OV, Tang W, Claas C, Stipp CS, and Hemler ME (2004). Palmitoylation supports assembly and function of integrin-tetraspanin complexes. *J Cell Biol* **167**, 1231–1240.

[26] Giannini C, Sarkaria JN, Saito A, Uhm JH, Galanis E, Carlson BL, Schroeder MA, and James CD (2005). Patient tumor *EGFR* and *PDGFRA* gene amplifications retained in an invasive intracranial xenograft model of glioblastoma multiforme. *Neuro Oncol* **7**, 164–176.

[27] Singh SK, Hawkins C, Clarke ID, Squire JA, Bayani J, Hide T, Henkelman RM, Cusimano MD, and Dirks PB (2004). Identification of human brain tumour initiating cells. *Nature* **432**, 396–401.

[28] Ligon KL, Huillard E, Mehta S, Kesari S, Liu H, Alberta JA, Bachoo RM, Kane M, Louis DN, DePinho RA, et al. (2007). Olig2-regulated lineage-restricted pathway controls replication competence in neural stem cells and malignant glioma. *Neuron* **53**, 503–517.

[29] Murdoch J, Doudney K, Gerrelli D, Wartham N, Patermott C, Stanier P, and Copp A (2003). Genomic organization and embryonic expression of Igsf8, an immunoglobulin superfamily member implicated in development of the nervous system and organ epithelia. *Mol Cell Neurosci* **22**, 62–74.

[30] Olsen JV, Nielsen PA, Andersen JR, Mann M, and Wisniewski JR (2007). Quantitative proteomic profiling of membrane proteins from the mouse brain cortex, hippocampus, and cerebellum using the HysTag reagent: mapping of neurotransmitter receptors and ion channels. *Brain Res* **1134**, 95–106.

[31] Yamada O, Tamura K, Yagihara H, Isotani M, Washizu T, and Bonkobara M (2006). Neuronal expression of keratinocyte-associated transmembrane protein-4, KCT-4, in mouse brain and its up-regulation by neurite outgrowth of Neuro-2a cells. *Neurosci Lett* **392**, 226–230.

[32] Nakada M, Nakada S, Demuth T, Tran NL, Hoelzinger DB, and Berens ME (2007). Molecular targets of glioma invasion. *Cell Mol Life Sci* **64**, 458–478.

[33] Belkaid A, Fortier S, Cao J, and Annabi B (2007). Necrosis induction in glioblastoma cells reveals a new "bioswitch" function for the MT1-MMP/G6PT signaling axis in proMMP-2 activation *versus* cell death decision. *Neoplasia* **9**, 332–340.

[34] Lakka SS, Gondi CS, and Rao JS (2005). Proteases and glioma angiogenesis. *Brain Pathol* **15**, 327–341.

[35] Tysnes BB and Mahesparan R (2001). Biological mechanisms of glioma invasion and potential therapeutic targets. *J Neurooncol* **53**, 129–147.

[36] Seiki M (1999). Membrane-type matrix metalloproteinases. *APMIS* **107**, 137–143.

[37] Thiel G, Lozanova T, Vogel S, Kintzel D, Janisch W, and Witkowski R (1993). Age-related nonrandom chromosomal abnormalities in human low-grade astrocytomas. *Hum Genet* **91**, 547–550.

[38] Rickert CH, Strater R, Kaatsch P, Wassmann H, Jurgens H, Dockhorn-Dworniczak B, and Paulus W (2001). Pediatric high-grade astrocytomas show chromosomal imbalances distinct from adult cases. *Am J Pathol* **158**, 1525–1532.

[39] Ohgaki H (2005). Genetic pathways to glioblastomas. *Neuropathology* **25**, 1–7.

[40] Huang KC, Altinoz M, Wosik K, Larochelle N, Koty Z, Zhu L, Holland PC, and Nalbantoglu J (2005). Impact of the coxsackie and adenovirus receptor (CAR) on glioma cell growth and invasion: requirement for the C-terminal domain. *Int J Cancer* **113**, 738–745.

[41] Gutmann DH, Maher EA, and Van Dyke T (2006). Mouse models of human cancers consortium workshop on nervous system tumors. *Cancer Res* **66**, 10–13.

[42] Candolfi M, Curtin JF, Nichols WS, Muhammad AG, King GD, Pluhar GE, McNiel EA, Ohlfest JR, Freese AB, Moore PF, et al. (2007). Intracranial glioblastoma models in preclinical neuro-oncology: neuropathological characterization and tumor progression. *J Neurooncol* **85**, 133–148.

[43] Charrin S, Le Naour F, Oualid M, Billard M, Faure G, Hanash SM, Boucheix C, and Rubinstein E (2001). The major CD9 and CD81 molecular partner. Identification and characterization of the complexes. *J Biol Chem* **276**, 14329–14337.

[44] Clark KL, Zeng Z, Langford AL, Bowen SM, and Todd SC (2001). Pgrl is a major CD81-associated protein on lymphocytes and distinguishes a new family of cell surface proteins. *J Immunol* **167**, 5115–5121.

[45] Stipp CS, Orlicky D, and Hemler ME (2001). FPRP: a major, highly stoichiometric, highly specific CD81 and CD9-associated protein. *J Biol Chem* **276**, 4853–4862.

[46] Runge KE, Evans JE, He ZY, Gupta S, McDonald KL, Stahlberg H, Primakoff P, and Myles DG (2007). Oocyte CD9 is enriched on the microvillar membrane and required for normal microvillar shape and distribution. *Dev Biol* **304**, 317–325.

[47] Zhang XA, Bontrager AL, and Hemler ME (2001). TM4SF proteins associate with activated PKC and link PKC to specific beta1 integrins. *J Biol Chem* **276**, 25005–25013.

[48] Yauch RL and Hemler ME (2000). Specific interactions among transmembrane 4 superfamily (TM4SF) proteins and phosphatidylinositol 4-kinase. *Biochem J* **351**, 629–637.

[49] Chintala SK, Sawaya R, Gokaslan ZL, and Rao JS (1996). Modulation of matrix metalloproteinase-2 and invasion in human glioma cells by $\alpha_3\beta_1$ integrin. *Cancer Lett* **103**, 201–208.

[50] Kohno M, Hasegawa H, Miyake M, Yamamoto T, and Fujita S (2002). CD151 enhances cell motility and metastasis of cancer cells in the presence of focal adhesion kinase. *Int J Cancer* **97**, 336–343.

[51] Scrideli CA, Carlotti CG Jr, Okamoto OK, Andrade VS, Cortez MA, Motta FJ, Lucio-Eterovic AK, Neder L, Rosemberg S, Oba-Shinjo SM, et al. (2008). Gene expression profile analysis of primary glioblastomas and non-neoplastic brain tissue: identification of potential target genes by oligonucleotide microarray and real-time quantitative PCR. *J Neurooncol* **88**, 281–291.

[52] Marko NF, Toms SA, Barnett GH, and Weil R (2008). Genomic expression patterns distinguish long-term from short-term glioblastoma survivors: a preliminary feasibility study. *Genomics* **91**, 395–406.

[53] Nakada M, Okada Y, and Yamashita J (2003). The role of matrix metalloproteinases in glioma invasion. *Front Biosci* **8**, e261–e269.

[54] Hotary K, Li XY, Allen E, Stevens SL, and Weiss SJ (2006). A cancer cell metalloprotease triad regulates the basement membrane transmigration program. *Genes Dev* **20**, 2673–2686.

[55] Yanez-Mo M, Barreiro O, Gonzalo P, Batista A, Megias D, Genis L, Sachs N, Sala-Valdes M, Alonso MA, Montoya MC, et al. (2008). MT1-MMP collagenolytic activity is regulated through association with tetraspanin CD151 in primary endothelial cells. *Blood* **112**, 3217–3226.

[56] Huang CL, Liu D, Masuya D, Kameyama K, Nakashima T, Yokomise H, Ueno M, and Miyake M (2004). MRP-1/CD9 gene transduction downregulates Wnt signal pathways. *Oncogene* **23**, 7475–7483.

[57] Ovalle S, Gutierrez-Lopez MD, Olmo N, Turnay J, Lizarbe MA, Majano P, Molina-Jimenez F, Lopez-Cabrera M, Yanez-Mo M, Sanchez-Madrid F, et al. (2007). The tetraspanin CD9 inhibits the proliferation and tumorigenicity of human colon carcinoma cells. *Int J Cancer* **121**, 2140–2152.

[58] Miyake M, Nakano K, Ieki Y, Adachi M, Huang C-L, Itoi S, Koh T, and Taki T (1995). Motility related protein 1 (MRP-1/CD9) expression: inverse correlation with metastases in breast cancer. *Cancer Res* **55**, 4127–4131.

[59] Phillips HS, Kharbanda S, Chen R, Forrest WF, Soriano RH, Wu TD, Misra A, Nigro JM, Colman H, Soroceanu L, et al. (2006). Molecular subclasses of high-grade glioma predict prognosis, delineate a pattern of disease progression, and resemble stages in neurogenesis. *Cancer Cell* **9**, 157–173.

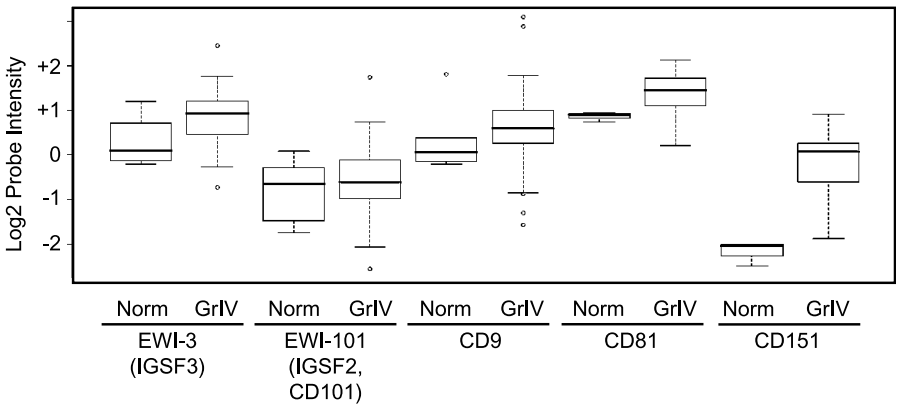

Figure W1. Expression of EWI proteins and tetraspanins in normal brain and in grade IV astrocytoma. Data shown are from the Stanford GEO DataSet GSE2223, analyzed as in Figure 1*A*, *bottom panel*. Molecules analyzed are EWI-3 (IGSF3), EWI-101 (CD101), CD9, CD81, and CD151. Similar results were obtained on analysis of these same molecules in the Henry Ford GEO Data Set (GSE4290, used in Figure 1*A*, *top panel*; not shown).

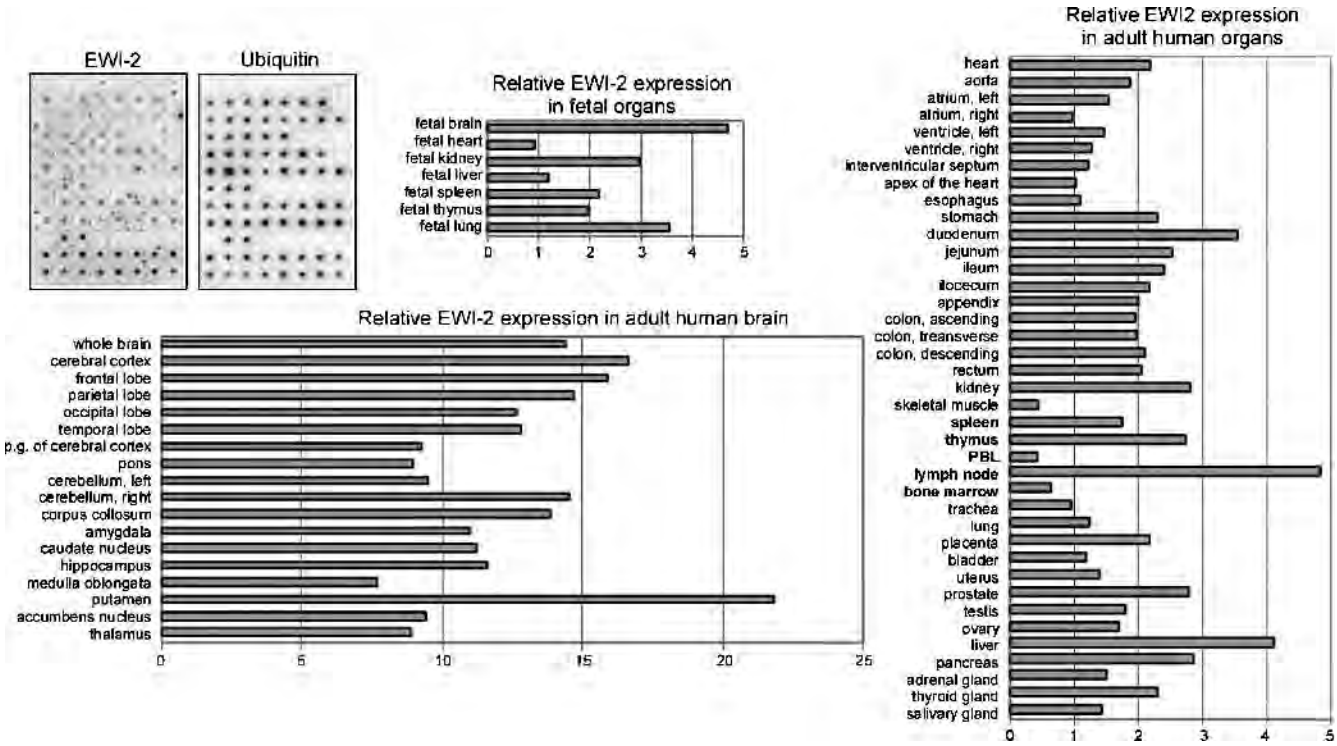

Figure W2. EWI-2 expression in diverse human tissues and organs. Multiple tissue expression array (Clontech, Mountain View, CA) was hybridized with EWI-2 probe or ubiquitin probe. Relative expression level of EWI-2 after normalization for ubiquitin probe is shown.

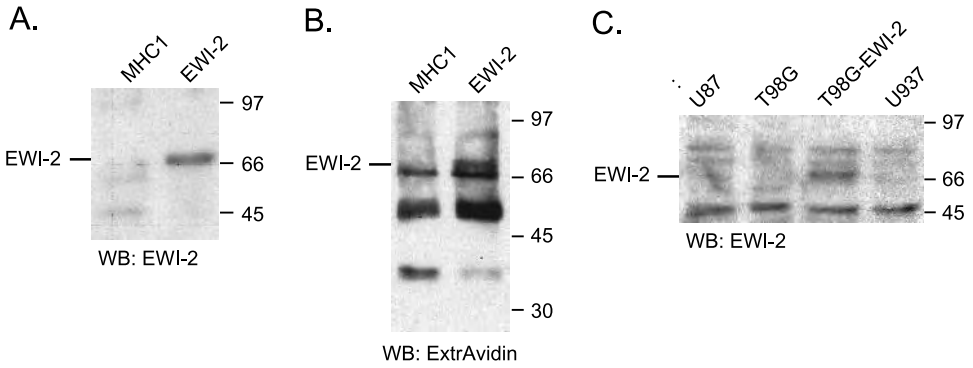

Figure W3. EWI-2 expression by normal human astrocytes. Normal human astrocytes (Lonza, Walkersville, Inc) were cell surface–labeled with biotin, lysed in 1% NP-40 and then MHC I (mAb W6/32) and EWI-2 (polyclonal antibody) were immunoprecipitated. Proteins were resolved by 10% SDS-PAGE and then blotted (A) using anti–EWI-2 mAb 8A12 to detect total immunoprecipitated EWI-2 or (B) ExtrAvidin to detect surface-biotinylated EWI-2. (C) Control cell lysates from U87, T98G, T98G−EWI-2, and U937 cells were blotted using anti–EWI-2 mAb 8A12.

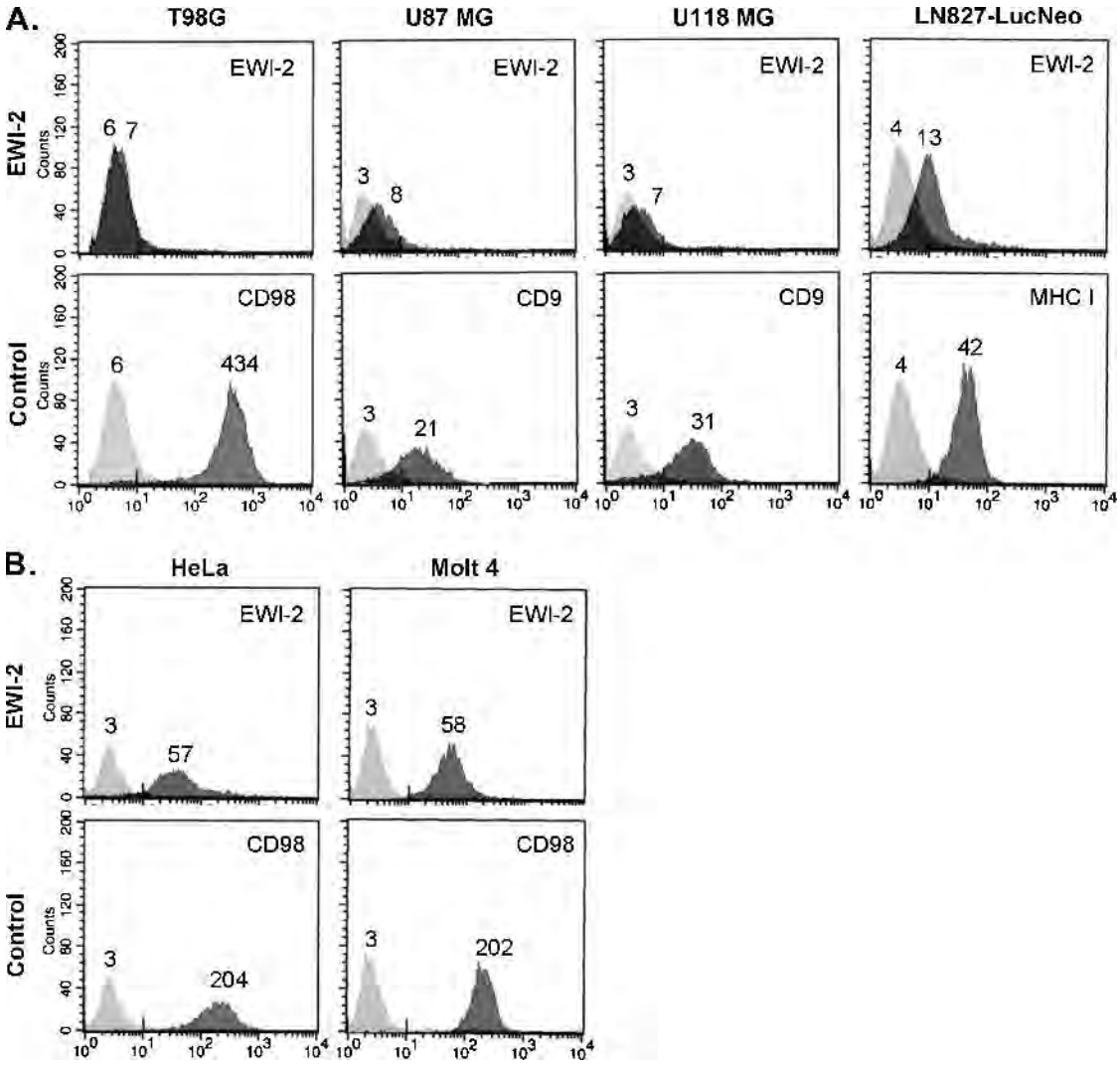

Figure W4. Cell surface expression of EWI-2 and control cell surface antigens (CD98, MHC class I, or CD9) in glioblastoma (A) and other cell lines (B). Cell lines used were glioblastoma cell lines T98G, U87 MG, U118 MG, and LN827-LucNeo, as well as Molt 4 (T cell leukemic cell line) and HeLa (ovarian carcinoma). Numbers next to peaks indicate mean fluorescence intensities.

Table W1. Summary of EWI-2 Expression Data.

Experiment	Normal Brain	Glioblastoma
RNA expression (Henry Ford GEO Data Set; Figure 1*A*, *top panel*)	++	–
RNA expression (Stanford GEO Data Set; Figure 1*A*, *bottom panel*)	++	–
RNA expression (Figure W2)	++	ND
RNA in developing mouse brain [29]	++	ND
RNA in adult mouse brain [31]	++	ND
Protein staining (IHC; Figure 1*B*)	++ (n = 3)	– (n = 4)
Protein on surface of human GBM cell lines (Figure W4)	ND	– (n = 4)
Protein in human GBM cell lysates (Figure W3*C*)	ND	– (n = 2)
Protein in primary human astrocytes (Figure W3, *A* and *B*)	++	ND
Protein in mouse brain [30]	++	ND

IHC indicates immunohistochemistry; ND, Not Determined

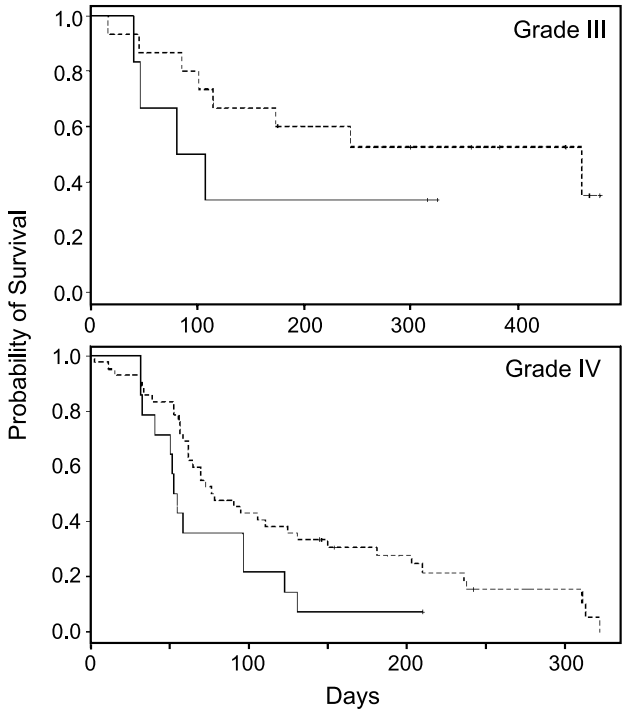

Figure W5. EWI-2 expression correlates with patient survival for both Grade III and grade IV glioblastomas. Data are analyzed exactly as in Figure 1*C*, except that grade III and grade IV glioblastomas are now analyzed separately, instead of being pooled. For grade III results, $P = .27$; for grade IV, $P = .057$. As indicated in Figure 1*C* for pooled results, $P = .041$.

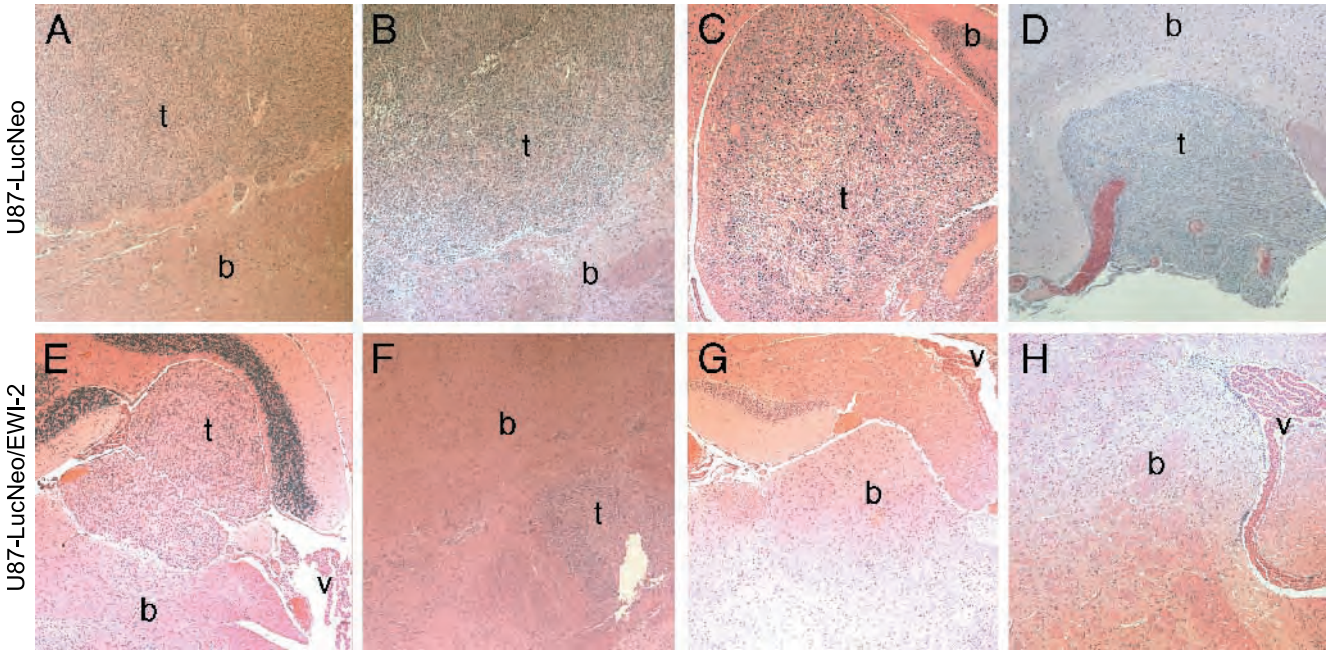

Figure W6. U87-LucNeo (A–D) and U87-LucNeo/EWI-2 (E–H) cells were injected intracranially as in Figure 1*C*. After 35 days, serial brain sections were obtained, starting from the injection point. All images show hematoxylin and eosin staining at 4× magnification. Sections are shown from four representative mice injected with U87-LucNeo control cells (top row) and four representative mice injected with U87-LucNeo/EWI-2 cells (bottom row). b indicates brain; t, tumor; v, ventricle.

Tetraspanin12 regulates ADAM10-dependent cleavage of amyloid precursor protein

Daosong Xu, Chandan Sharma, and Martin E. Hemler[1]

Department of Cancer Immunology and AIDS, Dana-Farber Cancer Institute and Harvard Medical School, Boston, Massachusetts, USA

ABSTRACT **Using mass spectrometry, we identified ADAM10 (a membrane-associated metalloproteinase) as a partner for TSPAN12, a tetraspanin protein. TSPAN12-ADAM10 interaction was confirmed by reciprocal coimmunoprecipitation in multiple tumor cell lines. TSPAN12, to a greater extent than other tetraspanins (CD81, CD151, CD9, and CD82), associated with ADAM10 but not with ADAM17. Overexpression of TSPAN12 enhanced ADAM10-dependent shedding of amyloid precursor protein (APP) in MCF7 (breast cancer) and SH-SY5Y (neuroblastoma) cell lines. Conversely, siRNA ablation of endogenous TSPAN12 markedly diminished APP proteolysis in both cell lines. Furthermore, TSPAN12 overexpression enhanced ADAM10 prodomain maturation, whereas TSPAN12 ablation diminished ADAM10 maturation. A palmitoylation-deficient TSPAN12 mutant failed to associate with ADAM10, inhibited ADAM10-dependent proteolysis of APP, and inhibited ADAM10 maturation, most likely by interfering with endogenous wild-type TSPAN12. In conclusion, TSPAN12 serves as a novel and robust partner for ADAM10 and promotes ADAM10 maturation, thereby facilitating ADAM10-dependent proteolysis of APP. This novel mode of regulating APP cleavage is of relevance to Alzheimer's disease therapy.—Xu, D., Sharma, C., Hemler, M. E. Tetraspanin12 regulates ADAM10-dependent cleavage of amyloid precursor protein. *FASEB J.* 23, 3674–3681 (2009). www.fasebj.org**

Key Words: Alzheimer's disease · α-secretase · pericellular proteolysis

ADAM10 (kuzbanian; kuz) is a member of the ADAM (a disintegrin and metalloproteinase) family of membrane-bound zinc-dependent metalloproteinases (1). ADAM10 causes shedding of amyloid precursor protein (APP) and more than 20 other membrane-bound proteins, including pro EGF, ephrin A2, E-cadherin, CD44, and Notch (2, 3). ADAM10-deficient mice die early in embryogenesis due to deficient Notch signaling (4). During maturation, proprotein convertases (*e.g.*, PC7 and furin) cleave the N-terminal prodomain to yield active ADAM10 (5). ADAM10 association with tetraspanin proteins (CD9, CD81, and CD82) was suggested to inhibit ADAM10 proteolysis of epidermal growth factor (EGF) and/or TNF-α (6).

APP is a type I transmembrane protein, which can be processed to yield Aβ peptide, a triggering factor in Alzheimer's disease (7). To produce Aβ peptide, full-length APP is first cut by β-secretase, yielding a fragment, then further cut by γ-secretase (8). Alternatively, full-length APP is cleaved by α-secretase, releasing a soluble fragment (sAPPα) with neuroprotective properties (9). Major goals of Alzheimer's disease research are to inhibit β- and γ-secretase processing of APP (10, 11) and to enhance α-secretase activity (12). Among ADAM proteinases with α-secretase activity, ADAM10 may have the most neuroprotective potential, and strategies to enhance ADAM10 activity are being developed (9, 12, 13). Moderate neuronal overexpression of ADAM10 in transgenic mice yielded a therapeutically beneficial increase in α-secretase activity (13).

The tetraspanin protein family, containing 33 mammalian members, is defined by characteristic conserved amino acids and specific structural features, including 4 transmembrane domains (14, 15). Widely expressed tetraspanin proteins regulate immune-cell and platelet functions, fertilization, and development in brain, skin, kidney, and nervous system (15–18). Tetraspanins and protein partners function within complexes called tetraspanin-enriched microdomains (TEMs) (14, 15, 19). Tetraspanin TSPAN12 (NET2) has an atypically long C-terminal cytoplasmic tail (~60 aa) and is widely expressed on many cell and tissue types (20). TSPAN12, acting together with other tetraspanin proteins, has an incremental positive effect on the cell-surface expression and function of MT1-MMP (21). Nothing else is known regarding TSPAN12 functions. To provide insight into TSPAN12 functions, we first sought to identify its transmembrane protein partners. Using mass spectrometry, we identified ADAM10 among several putative TSPAN12 partners. Then we showed that TSPAN12 associates with mature ADAM10, promotes ADAM10 maturation, and enhances ADAM10 dependent cleavage of APP.

[1] Correspondence: Dana-Farber Cancer Institute and Department of Pathology, Harvard Medical School, Boston, Massachusetts 02115; E-mail: martin_hemler@dfci.harvard.edu

doi: 10.1096/fj.09-133462

 0892-6638/09/0023-3674 © FASEB

MATERIALS AND METHODS

Cells and antibodies

Cell lines from American Type Culture Collection (Manassas, VA, USA) were maintained as described previously (22). Antibodies to ADAM10 (mAb MAB1427; R&D Systems, Minneapolis, MN, USA; polyclonal Ab1997; Abcam, Cambridge, MA, USA) and ADAM17 (mAb 111633; R&D) recognize both pro and active forms. Anti-FLAG antibodies were mAb M2, M2-agarose, and pAb F7425 (Sigma, St. Louis, MO, USA). Other antibodies were mAbs 6E10 and 22C11 (Chemicon, Temecula, CA, USA) to APP; mAb Tub2.1 (Sigma) to β-tubulin; pAb 632460 (Clontech, Palo Alto, CA, USA) to GFP; mAb 5C11 (23) to CD151, and mAb 8G6 (22) to CD147. Antibodies to tetraspanins CD9, CD81, and CD82 were as described previously (23). Despite several attempts, no useful anti-TSPAN12 antibodies have been produced.

cDNAs

cDNA for human TSPAN12 was amplified using reverse transcriptase (Promega, Madison, WI, USA) and Pfu polymerase (Stratagene, La Jolla, CA, USA). Total RNA was purified from HT1080 cells (RNeasy kit; Qiagen, Valencia, CA, USA). RT primers were sense: 5′-GGG AGT AGG ATG TGG TGA AAG GA-3′; antisense: GTA CAT ACT ATG TGT TTCAGA AAT ATG. PCR primers were sense: 5′-CCG CTC GAG GGC ACC ATG GCC AGA GAA GAT TCC GTG AAG (with *Xho*I at the 5′ end); antisense: 5′-CCG GAT CCT CAC TTG TCA TCG TCA TCC TTG TAA TC*G CCC CC*G CCT AAC TCC TCC ATC TCA AAG TGT GTA-3′ (with *Bam*H I at 5′ end; one FLAG-tag at C-terminus). The PCR fragment for TSPAN12 and cDNAs for CD81, CD9, CD151, CD82, SDFR1, and CD147 were inserted into retrovirus vector pLXIZ (*Xho*I/*Bam*H I), and some also were inserted into plasmid AcGFP1 (Clontech) with C-terminal GFP. Cysteines 9, 12, and 83 [in TSPAN12(Pal$^-$)] and 9, 227 and 228 [in CD81(Pal$^-$)] were changed to serine. Stable cell lines were established as described previously (22).

LC-MS/MS

HT1080 cells stably expressing human TSPAN12-FLAG and CD81-FLAG (FLAGs at C terminus) were lysed. Proteins were purified using anti-FLAG beads and resolved by SDS-PAGE (0.5 cm in length). Then the entire area was in-gel digested, and proteins were identified using LC-MS/MS as described previously (22), at the Taplin Biological Mass Spectrometry Facility (Harvard Medical School).

Immunoprecipitation, Western blotting and [^{3}H]palmitate labeling

Cultured cells were lysed at 0°C (25 mM HEPES, pH 7.5; 150 mM NaCl; and 2.5 mM EDTA) with either 1% Brij 96 (Fluka AG, Buchs, Switzerland), or 0.5 or 1% Brij 97 (Sigma) or 1% Triton X-100 (Roche Applied Science, Indianapolis, IN, USA) plus proteinase inhibitor cocktail (Roche Applied Science). Immunoprecipitation, Western blotting, and DSP cross-linking were as described previously (22). [^{3}H]palmitate labeling and detection was as described previously (24). Relative band densities were quantitated using ImageQuant TL software (GE Healthcare, Piscataway, NJ, USA).

SiRNA-mediated gene silencing

SiRNA duplexes, transfected using Lipofactamine 2000 (Invitrogen, Carlsbad, CA, USA), were used to knock down human TSPAN12 (Dharmacon Inc., Chicago, IL, USA; catalog no. M-012466-00 for NM_012338) and ADAM10 (Dharmacon; M-004503-01 for NM_001110). Tetraspanins CD151, CD81, and CD9 were depleted as described previously (21, 25). For TSPAN12, siRNA transfection (of 30–40% confluent cells) was at d 0 and again at d 3, and experiments were done at d 5 and 6. For ADAM10, experiments were performed 3 d after transfection. Silencing efficiency was evaluated using RT-PCR and/or Western blotting.

Immunofluorescence localization of TSPAN12-GFP

After culture for 24–48 h on slide chambers (BD Falcon; BD Biosciences, Franklin Lakes, NJ, USA), subconfluent cells were washed with PBS and fixed (3.7% PFA, 15 min). After blocking (1 h in PBS containing 1% BSA and 2% goat serum at 25°C) and washing (3 times with PBS), primary antibody (1:50–100 dilution in 1% BSA in PBS) was added for 1 h at room temperature. Then, after 3 washes, secondary antibodies were added at 1:100 (goat anti-rabbit IgG Alexa 594 or Alexa Fluor 488 goat anti-mouse in 1% BSA in PBS) for 1 h at 25°C. After 3 PBS washes, coverslips were air-dried and mounted (in solution containing DAPI; Vector Laboratories, Burlingame, CA, USA). Fluorescence images were acquired at 1-μm depth intervals, by confocal microscopy (Zeiss LMS510; Carl Zeiss, Oberkochen, Germany) at Harvard NeuroDiscovery Center. Staining was repeated ≥3 times.

APP detection

Cells were washed 3 times in PBS and incubated in serum-free medium (3–4 h). Then medium was concentrated 2-fold (Microcon filter; Millipore, Bedford, MA, USA; 10-kD cutoff). Samples were run on 4–20% precast gradient gel (Invitrogen) before APP blotting. To confirm cell equivalency, cells were lysed (1% Triton X-100 buffer), and proteins were quantified using a DC Protein Assay kit (Bio-Rad, Hercules, CA, USA).

RESULTS

TSPAN12 interacts with ADAM10 and other transmembrane proteins

Putative TSPAN12 partners (**Table 1**; identified by LC-MS/MS) include TSPAN12 itself and ADAM10. MMP14 (MT1-MMP) association is consistent with prior results (21). Other possible TSPAN12 partners (CD44, CD29, and CD49c) were shown previously to associate with other tetraspanin proteins (26–29), but TSPAN12 association still needs to be confirmed. Coimmunoprecipitation experiments did not confirm TSPAN12 associations with CD13, CD71, ADAM17, and EGFR. Associations with EphA2, CA08, LRP10, CAV1, and TR10B remain to be confirmed. TSPAN12 and CD81 partners (Table 1) are almost completely nonoverlapping, indicating specificity.

Confirming TSPAN12-ADAM10 association, TSPAN12 immunoprecipitation from HT1080 and MDA231 cells readily yielded endogenous ADAM10 (**Fig. 1*A*, *B***; lane 3).

TABLE 1. *Membrane protein complexes with TSPAN12 and CD81*

Name (protein ID)	TSPAN12	CD81
TSPAN12 (O95859)[a]	5	0
MMP14 (P50281)[b]	10	0
CD29 (P05556) (integrin β1)[c]	6	0
CD49c (P26006) (integrin α3)[c]	3	0
ADAM10 (O14672)[c]	4	0
CD44 (P16070)[d]	9	0
CD13 (P15144)[e,g]	3	1
CD71 (P02786)[e]	5	0
ADAM17 (P78536)[e]	3	0
EGFR (P00533)[e]	2	0
EphA2 (P29317)[f]	6	0
CA08 (Q9bxs4)[f]	3	0
LRP 10 (Q7z4f1)[f]	3	0
CAV1 (Q03135) (caveolin 1)[f]	2	0
TR10B (O14763)[f]	2	0
CD81 (P60033)[a]	0	1
EWIF/FPRP (Q9P2B2)[h]	0	12

Values represent number of distinct peptides. Complete peptide information is given in Supplemental Table S1. [a]As expected, TSPAN12 and CD81 yield TSPAN12 and CD81 peptides. [b]Association with MMP14 (MT1-MMP) has been seen elsewhere (21). [c]Association has been confirmed by coimmunoprecipitation. [d]TSPAN12-CD44 association is consistent with CD44 associating with other tetraspanins (47) and being a substrate for ADAM10 (48). [e]Coimmunoprecipitation experiments did not confirm interactions with TSPAN12. [f]These TSPAN12 interactions have not been tested further. [g]Interactions of CD13 with CD81 have been confirmed by coimmunoprecipitation. [h]EWIF/FPRP interaction with CD81 has been seen previously (49, 50).

Despite comparable expression (bottom panels), tetraspanin CD81 yielded much less ADAM10 (Fig. 1*A*, lane 6; *B*, lane 4), while tetraspanin CD82 (Fig. 1*B*, lane 5) and transmembrane protein SDFR1 (Fig. 1*A*, lane 5) yielded no detectable ADAM10. Tetraspanins CD9 and CD151 also did not associate with ADAM10 (not shown). Pro-ADAM10 (~98 kDa) was abundant in whole-cell lysates (Fig. 1*A*, *B*; lane 1), and both pro- and mature ADAM10 could be readily immunoprecipitated using anti-ADAM10 antibody (Fig. 1*C*). However, only mature ADAM10 (~68 kDa) associated with TSPAN12 (Fig. 1*A*, *B*; top panels). In reciprocal experiments, immunoprecipitation of ADAM10 endogenously expressed in HT1080 cells yielded abundant TSPAN12, lesser CD81, and no SDFR1 (Fig. 1*D*). By RT-PCR, overexpressed TSPAN12 was only ~2-fold greater than endogenous TSPAN12 in HT1080 cells (Supplemental Fig. S1) and in other cell lines (not shown).

For use in functional studies, we sought to identify minimally mutated TSPAN12, no longer associating with ADAM10. TSPAN12 C-terminal deletion mutants (Δ267 and Δ261), and CD81(N′-LEL)/TSPAN12 lost ADAM10 association (**Fig. 2*A***, lanes 4, 5, 8). Other TSPAN12 mutants [CD81(N′-SEL/TSPAN12) and TSPAN12(R88E)], partially lost ADAM10 association (Fig. 2*A*, lanes 7, 9). Palmitoylation-deficient [TSPAN12(Pal$^-$)] was prepared by mutating membrane-proximal cysteines 9, 12, and 83 to serine. TSPAN12(Pal$^-$) showed minimal ADAM10 association (Figs. 1*A*, lane 4, and 2*A*, lane 6). Anti-FLAG immunoblotting confirmed the presence of mutants in HT1080 lysate (Fig. 2*A*, bottom panel). ADAM10 association results are summarized in Fig. 2*B*. Also, all mutants are indicated schematically in Fig. 2*B* and described in more detail in Supplemental Table S2. Because TSPAN12(Pal$^-$) showed maximal loss of ADAM10 association with minimal change to the native tetraspanin protein, it was chosen for further study. TSPAN12, but not TSPAN12(Pal$^-$), incorporated [^{3}H]palmitate (Supplemental Fig. S2*A*, lanes 1, 4). Following biotinylation of intact cells, we determined that TSPAN12(Pal$^-$) expression on the cell surface was ~64% reduced, compared to TSPAN12 (Supplemental Fig. S2*B*, lanes 1, 2), with both abundantly expressed in total cell lysate (Supplemental Fig. S2*C*, lanes 1, 2).

TSPAN12 affects ADAM10 function

To assess function, we focused on ADAM10-dependent APP shedding, which releases a fragment of ~110–120

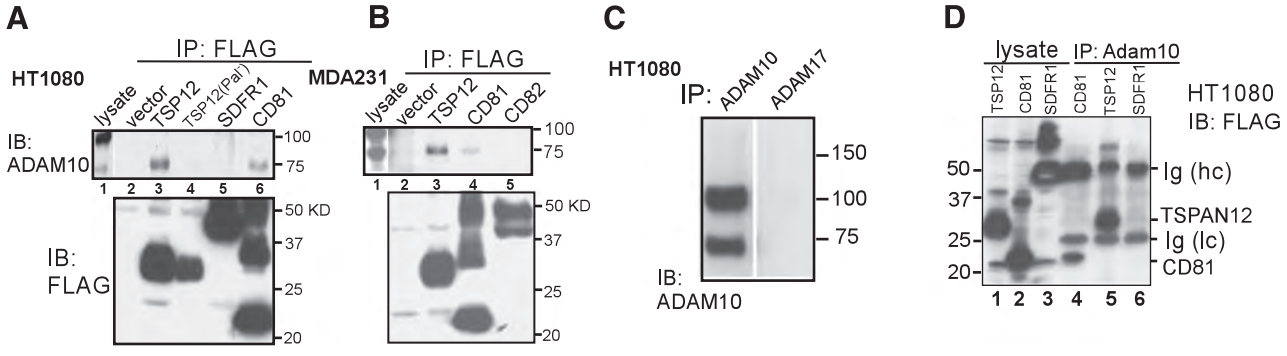

Figure 1. Confirmation of ADAM10-TSPAN12 association. *A*, *B*) Indicated FLAG-tagged proteins were immunoprecipitated from HT1080 (*A*) and MDA231 cells (*B*). ADAM10 (top panel) and FLAG-tagged proteins (bottom panel) were detected by immunoblotting. Pro-ADAM10, 95 kDa; mature ADAM10, ~68 kDa. *C*) Endogenously expressed ADAM10 (MAB1427) and ADAM17 were immunoprecipitated from HT1080 cells, after cells were lysed in 0.5% Brij 97. Resulting proteins were detected using anti-ADAM10 polyclonal antibody. Presence of ADAM17 was confirmed using anti-ADAM17 polyclonal antibody (not shown). *D*) HT1080 cells stably expressing the indicated FLAG-tagged proteins were lysed in 0.5% Brij 97. Anti-FLAG immunoblotting was used to detect proteins in lysates (lanes 1–3) and in complexes after ADAM10 was immunoprecipitated using mAb MAB1427 (lanes 4–6). CD81 appears as dimer and monomer, as described previously (32). Ig(hc), immunoglobulin heavy chain; Ig(lc), immunoglobulin light chain.

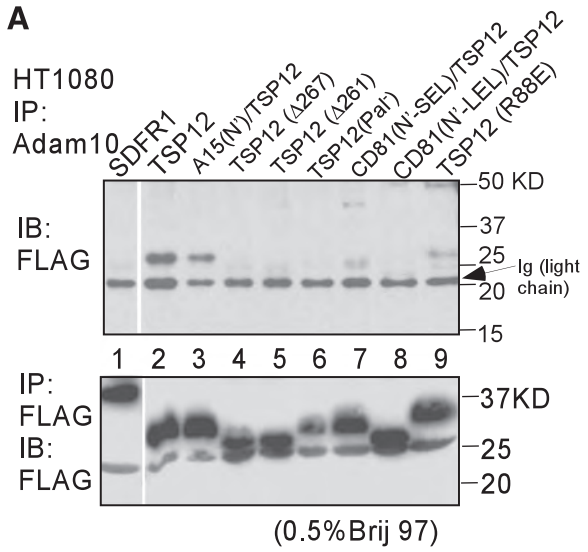

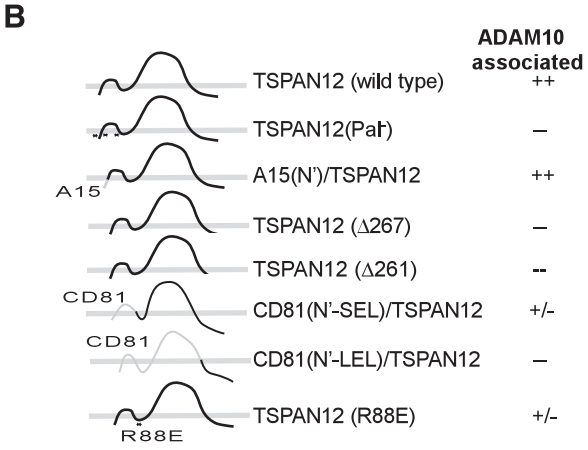

Figure 2. TSPAN12 mutations variably disrupt ADAM10 association. *A*) HT1080 cells stably expressing FLAG-tagged proteins were lysed (0.5% Brij 97), and then ADAM10 (top panel) and FLAG-tagged proteins (bottom panel) were immunoprecipitated. Proteins were then detected by anti-FLAG immunoblotting (both panels). *B*) ADAM10 association is summarized for TSPAN12 mutants. SEL, small extracellular loop; LEL, large extracellular loop. Additional mutant information is in Supplemental Table S2.

kDa (30, 31). Anti-FLAG immunoblotting confirmed stable expression of TSPAN12-FLAG and control FLAG in MCF7 (breast cancer) and SH-SY5Y (neuroblastoma) cell lines (not shown). TSPAN12 overexpression stimulated, by 120–160%, release of APP fragments of ~110 kDa (**Fig. 3*A***, lane 2). By contrast, TSPAN12(Pal$^-$) inhibited APP shedding (32–36% of control cells) in both MCF7 and SH-SY5Ycell lines (Fig. 3*A*, lane 3, both panels). Palmitoylation-deficient CD81 [CD81(Pal$^-$)], CD81, and CD9 had only marginal effects on APP shedding (Fig. 3*A*).

Ablation of endogenous ADAM10 (by>95%; Supplemental Fig. S3*A*) from SH-SY5Y and MCF7 cells reduced APP shedding to 13–21% of control levels (Fig. 3*B*). Knockdown of endogenous TSPAN12 (Supplemental Fig. S4) also reduced APP shedding (Fig. 3*B*; 32–43% of control), whereas knockdown of tetraspanins CD81 and CD82 (by 90–95%; refs. 21, 25) had less of an inhibitory effect (Fig. 3*B*). Reduced APP shedding due to ADAM10 and TSPAN12 knockdown was confirmed (Supplemental Fig. S5) using siRNAs with sequences distinct from those used in Fig. 3*B*). In summary, on multiple cell lines, ADAM10-dependent APP shedding is markedly affected by TSPAN12, to a greater extent than by other tetraspanin proteins.

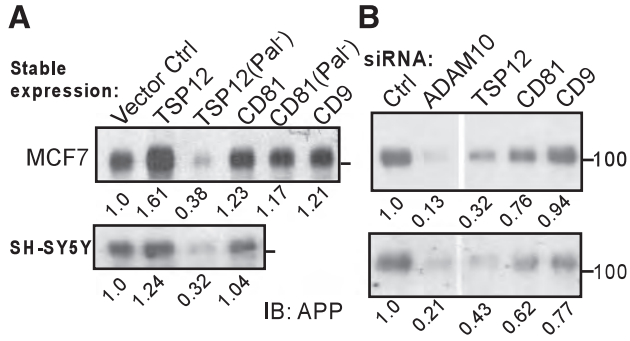

Figure 3. TSPAN12 expression influences ADAM10-dependent proteolysis of APP. *A*) Indicated FLAG-tagged proteins were expressed stably in MCF7 and SH-SY5Y cells; shed APP was detected by immunoblotting. *B*) Endogenous ADAM10 (siRNA = ADAM10–3), TSPAN12 (siRNA-1), CD81 (21) and CD9 (25) were knocked down, and shed APP was detected. Numbers below panels represent protein density scanning results.

TSPAN12 affects ADAM10 maturation

Not only did TSPAN12 associate preferentially with active ADAM10 (Figs. 1, 2), but also it promoted ADAM10 maturation (**Fig. 4*A***). Expression of additional TSPAN12 in MCF7 cells increased the ratio of mature/precursor ADAM10 from ~3.5 to ~5.4, as detected in cell lysates. Conversely, TSPAN12(Pal$^-$)

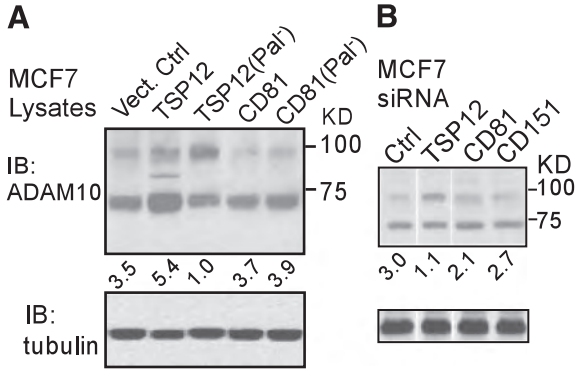

Figure 4. TSPAN12 expression influences ADAM10 maturation. *A*) MCF7 cells expressing the indicated FLAG-tagged proteins were lysed (0.5% Brij 97), and ADAM10 and tubulin were detected by immunoblotting. The ~85-kDa protein in the TSPAN12 lane likely represents an atypical form of ADAM10 that has been intermediately processed. *B*) MCF7 cells were treated with siRNAs (as in Fig. 3*B*), and then lysed and immunoblotted as in *A*. Numbers below panels represent ADAM10 active/prodomain ratios.

decreased the maturation ratio (from ~3.5 to ~0.96), while control proteins [CD81 and CD81(Pal$^-$)] had minimal effect on ADAM10 processing (Fig. 4*A*). Similar results were seen in 1% Brij 97 (Fig. 4*A*) and Triton X-114 (not shown) detergent lysates. Conversely, siRNA-mediated knockdown of endogenous TSPAN12 diminished ADAM10 maturation (from ~3.0 to ~1.1), while knockdown of tetraspanins CD81 and CD151 had much less of an effect (Fig. 4*B*). Overexpression, knockdown, or mutation of TSPAN12 did not affect the subcellular distribution of ADAM10 (Supplemental Fig. S6). Also, these manipulations of TSPAN12 minimally affected ADAM10 cell-surface levels (Supplemental Table S3 and Supplemental Fig. S3*B*).

TSPAN12(Pal$^-$) interferes with TSPAN12

Despite not associating with ADAM10, TSPAN12(Pal$^-$) markedly decreased ADAM10 function (APP shedding) and maturation. Since tetraspanins homooligomerize (32), we suspected that TSPAN12(Pal$^-$) might directly associate with endogenous TSPAN12, perturb its function, and thereby indirectly affect ADAM10. Indeed, we did observe direct association of TSPAN12(Pal)-GFP with TSPAN12-FLAG in MCF7 cells. Following DSP crosslinking, immunoprecipitation of TSPAN12-FLAG yielded TSPAN12(Pal$^-$)-GFP (~65 kD), under reducing conditions (**Fig. 5*A***, lane 8). The sharp band corresponding to TSPAN12(Pal$^-$)-GFP was not seen under the following conditions: DSP treatment was omitted (Fig. 5, lane 3); TSPAN12-FLAG was replaced with SDFR1-FLAG (Fig. 5, lanes 9, 4); TSPAN12-FLAG was replaced with vector alone (Fig. 5, lanes 10, 5); TSPAN12(Pal$^-$)-GFP was replaced with CD81(Pal$^-$)-GFP (Fig. 5, lanes 6, 11).

In addition, we showed that non-GFP TSPAN12(Pal$^-$) alters the distribution of TSPAN12-GFP. TSPAN12-GFP is mostly membrane-proximal in fixed MCF7 cells (Fig. 5*Ba*). However, expression of TSPAN12(Pal$^-$)-FLAG (Fig. 5*Bc*), but not control (SDFR1-FLAG; Fig. 5*Bb*), caused TSPAN12-GFP redistribution into a punctate pattern. When TSPAN12(Pal$^-$) was itself GFP tagged, it showed punctate distribution (Fig. 5*Bd*). Hence, TSPAN12(Pal$^-$) associates with wild-type TSPAN12 and dominantly affects its subcellular localization.

DISCUSSION

ADAM10, a cell surface metalloproteinase, cleaves >20 different membrane proteins, including growth factors, growth factor receptors, adhesion molecules, and various other signaling molecules (3). ADAM10 plays critical roles during human embryonic development (4), cancer (3), diabetes (33), and Alzheimer's disease (13). Here we show that ADAM10 associates preferentially with TSPAN12, a tetraspanin protein. In addition, we used three different molecular approaches (TSPAN12 overexpression, knockdown, and mutation), to show that TSPAN12 enhances ADAM10 maturation and promotes ADAM10-dependent cleavage of APP, a key contributor to Alzheimer's disease.

Cell surface association

ADAM10-TSPAN12 association, first demonstrated in a mass spectrometry search for TSPAN12 partners, was confirmed in multiple cell lines, by reciprocal coimmunoprecipitation. ADAM10-TSPAN12 association was specific, as other tetraspanins (CD81, CD9, and CD151)

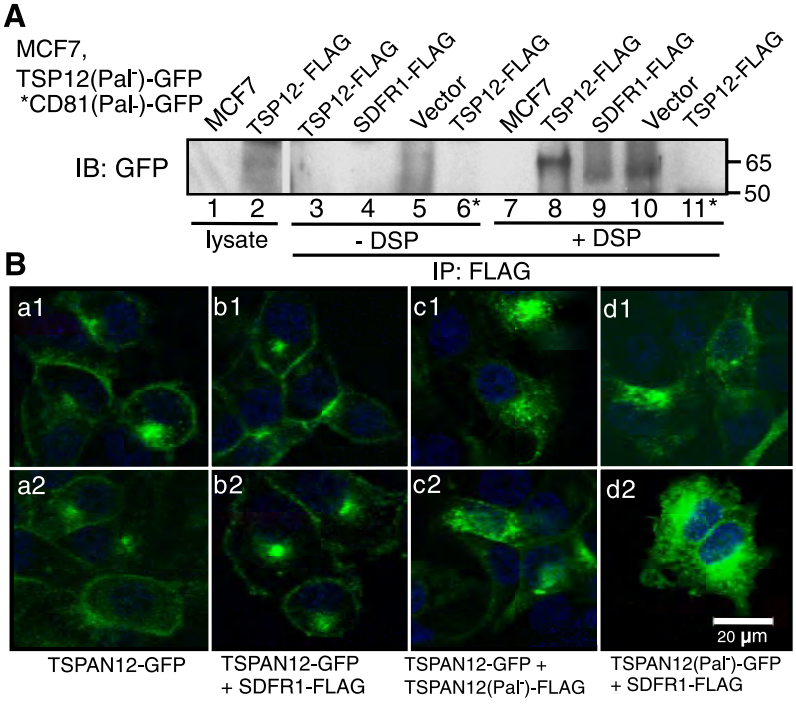

Figure 5. TSPAN12(Pal$^-$) mutant associates with wild-type TSPAN12 and perturbs its subcellular distribution. *A*) TSPAN12(Pal$^-$)-GFP (lanes 2–5, 7–10) or CD81(Pal$^-$)-GFP (lanes 6, 11) were expressed in MCF7 cells, together with vector-FLAG (lanes 5, 10) or other FLAG-tagged proteins (lanes 2–4, 6, 8, 9, 11). Lanes 1 and 7 are from untransfected MCF7 (no GFP or FLAG proteins). After lysis (1% Triton X-100) MCF7 cells were treated with (lanes 7–11) or without (lanes 1–6) covalent cross-linker DSP. After anti-FLAG immunoprecipitations, reduction of the dithiol cross-link, and SDS-PAGE, proteins were detected by GFP immunoblotting. Diffuse proteins of 50–60 kDa in lanes 5, 9, and 10 likely represent background proteins, immunoprecipitated by anti-FLAG antibody (even when no FLAG proteins are present, as in lanes 5, 10), which also weakly cross-react with anti-GFP antibody. *B*) Either TSPAN12-GFP (*a–c*) or TSPAN12(Pal$^-$)-GFP (*d*) was expressed in MCF7 cells, together with indicated FLAG-tagged proteins. FLAG- and GFP-tagged tetraspanins were expressed at comparable levels, as seen by immunoblotting (not shown).

did not associate to the same extent as TSPAN12. However, in Brij 97 lysates elsewhere (6), ADAM10 did associate with other tetraspanins (CD9, CD53, CD63, CD81, and CD151). This discrepancy may be explained by our lysates having minimal divalent cation levels, which can limit the range of tetraspanin protein associations (34). ADAM17, which is more structurally and functionally similar to ADAM10 than any other ADAM protein (1, 35), appeared in Table 1 as a possible TSPAN12 partner. However, further experiments by us (not shown) and by others (6) did not confirm ADAM17-tetraspanin association. TSPAN12 association with CD13 and CD71 was likewise not confirmed. TSPAN12 association with MMP14 (MT1-MMP) was confirmed elsewhere (21). Other TSPAN12 associations in Table 1 remain to be confirmed.

The TSPAN12 large extracellular loop, intracellular C-terminal tail, and palmitoylation sites all contributed to ADAM10 association. Large extracellular loop and C-terminal tail contributions are consistent with tetraspanin proteins having a rod-like structure (36), with extracellular and intracellular sites contacting partner proteins (18). Interactions occurring within TEMs are stabilized by tetraspanin palmitoylation (14, 19, 34, 37). The contribution of TSPAN12 palmitoylation to ADAM10 association indicates that TSPAN12-ADAM10 complexes likely occur within the context of TEMs.

TSPAN12 promotes ADAM10 function

APP, which is widely expressed on most cell and tissue types (http://www.genecards.org), undergoes ADAM10-dependent shedding (38), as confirmed here by siRNA knockdown of endogenous ADAM10. ADAM10-dependent APP proteolysis was promoted by TSPAN12 overexpression and inhibited by knockdown of endogenous TSPAN12, indicating that TSPAN12-ADAM10 complexes are functionally important. The TSPAN12(Pal$^-$) mutant, which does not associate with ADAM10, did not stimulate function. Instead, TSPAN12(Pal$^-$) inhibited function, through a dominant negative-like effect on endogenous TSPAN12.

In a prior study, tetraspanins CD9, CD81, and CD82 were suggested to have a negative effect on ADAM10-dependent proteolysis of TNF-α and HB-EGF, which was overcome by anti-tetraspanin antibodies (6). In another case, CD9 suppressed proteolysis of transmembrane TNF-α, mediated by an unspecified protease (39). Here we observed only positive effects of TSPAN12 on ADAM10 function. Hence, compared to other tetraspanin proteins, TSPAN12 not only associates more proximally with ADAM10, but also exerts a different functional effect. We predict that TSPAN12 will promote ADAM10-dependent proteolysis of many, if not all, of its other membrane protein substrates (3). In this regard, another ADAM10 substrate, CD44 (40), may also associate with TSPAN12 (Table 1). Furthermore, shedding of ADAM10 substrate L1 (41), a cell-surface adhesion molecule, is supported by TSPAN12 (unpublished results). We confirmed that TSPAN12 is present at moderate levels in 7 of 7 different cell lines tested (by RT-PCR, not shown). The wide cell distributions of TSPAN12 and ADAM10 (see http://www.genecards.org) are consistent with functional interactions in multiple settings. TSPAN12 also supported functions of another protease (MMP14/MT1-MMP), although in that case, the incremental positive role of TSPAN12 depended on substantial augmentation by other tetraspanins (21).

Mechanistic insights

TSPAN12 manipulation (overexpression, knockdown, and mutation) did not affect total ADAM10 levels in the cell, or on the cell surface. However, TSPAN12 associated selectively with mature, processed ADAM10, and promoted maturation. ADAM10 matures in the trans-Golgi network, with maturation leading to increased APP shedding (5). Hence, TSPAN12 must promote ADAM10 function in a post-Golgi compartment. We suspect that TSPAN12 stabilizes active ADAM10 and/or accelerates ADAM10 activation by prodomain convertase. TSPAN12(Pal$^-$) inhibited both ADAM10 function and maturation, even though TSPAN12(Pal$^-$) failed to associate with ADAM10. Instead, TSPAN(Pal$^-$), which itself is mostly not at the cell surface, associated directly with wild-type TSPAN12, and partly diverted it from the plasma membrane. Hence, TSPAN(Pal$^-$) appears to impair ADAM10 maturation and function indirectly, by a dominant negative-like effect on endogenous TSPAN12. In the case of MT1-MMP, TSPAN12 and other tetraspanins protected newly synthesized protein (both pro and active) from degradation, thereby increasing total cell surface levels, without accelerating maturation (21). Although tetraspanins promote biosynthetic maturation of partner proteins, such as CD19 (42), and EWI-2 (43), we could find no other examples of tetraspanins promoting prodomain processing.

Therapeutic implications

ADAM10 is a major α-secretase, responsible for nonamyloidogenic processing of APP. Hence, amplification of ADAM10 function should lead to therapeutically desirable reduction in brain β-amyloid deposits (12). Strategies for amplifying ADAM10 α-secretase activity thus far include ADAM10 overexpression (13), overexpression of PC7 or furin to accelerate ADAM10 maturation (5), and retinoic acid induction of the ADAM10 promoter (31). Because TSPAN12 promotes ADAM10 α-secretase activity, agents stimulating TSPAN12 function or promoting TSPAN12-ADAM10 association should be therapeutically beneficial. As seen for other tetraspanins, soluble large loops and antitetraspanin antibodies can have agonistic effects (18). It remains to be seen whether TSPAN12 works together with other proteins supporting ADAM10 α-secretase activity, such as the intracellular neuronal protein SAP97 (44), and several G protein coupled receptors (31, 45).

In some cases, such as on tumor cells, it may be desirable to inhibit ADAM10 activity (3). This can be

achieved using soluble ADAM10 prodomain (30), dominant-negative ADAM10 (38), and hydroxamate-based metalloproteinase inhibitors (46). As shown here, targeting TSPAN12 should also diminish ADAM10 activity. This could be achieved by expression of an inhibitory TSPAN12 mutant [*e.g.*, TSPAN12(Pal$^-$)], or by RNAi knockdown, inhibitory antibodies, or inhibitory tetraspanin soluble large loop protein, such as seen for other tetraspanins (18).

CONCLUSIONS

We describe here an atypical tetraspanin protein, TSPAN12, which associates selectively with ADAM10, leading to accelerated ADAM10 activation and enhanced nonamyloidogenic shedding of APP. These results, together with others (6), indicate that ADAM10 functions in the context of TEMs. Promotion of TSPAN12-ADAM10-dependent functions should be therapeutically beneficial in Alzheimer's disease, whereas inhibition of TSPAN12-ADAM functions may be beneficial in cancer. FJ

This work was supported by National Institutes of Health grants GM38903 and CA102034 to M.E.H.

REFERENCES

1. Stone, A. L., Kroeger, M., and Sang, Q. X. (1999) Structure-function analysis of the ADAM family of disintegrin-like and metalloproteinase-containing proteins (review). *J. Protein Chem.* **18,** 447–465
2. White, J. M. (2003) ADAMs: modulators of cell-cell and cell-matrix interactions. *Curr. Opin. Cell Biol.* **15,** 598–606
3. Moss, M. L., Stoeck, A., Yan, W., and Dempsey, P. J. (2008) ADAM10 as a target for anti-cancer therapy. *Curr. Pharm. Biotechnol.* **9,** 2–8
4. Hartmann, D., De Strooper, B., Serneels, L., Craessaerts, K., Herreman, A., Annaert, W., Umans, L., Lubke, T., Lena, I. A., von Figura, K., and Saftig, P. (2002) The disintegrin/metalloprotease ADAM 10 is essential for Notch signalling but not for alpha-secretase activity in fibroblasts. *Hum. Mol. Genet.* **11**, 2615–2624
5. Anders, A., Gilbert, S., Garten, W., Postina, R., and Fahrenholz, F. (2001) Regulation of the alpha-secretase ADAM10 by its prodomain and proprotein convertases. *FASEB J.* **15,** 1837–1839
6. Arduise, C., Abache, T., Li, L., Billard, M., Chabanon, A., Ludwig, A., Mauduit, P., Boucheix, C., Rubinstein, E., and Le Naour, F. (2008) Tetraspanins regulate ADAM10-mediated cleavage of TNF-alpha and epidermal growth factor. *J. Immunol.* **181,** 7002–7013
7. LaFerla, F. M., Green, K. N., and Oddo, S. (2007) Intracellular amyloid-beta in Alzheimer's disease. *Nat. Rev. Neurosci.* **8,** 499–509
8. Wolfe, M. S., and Guenette, S. Y. (2007) APP at a glance. *J. Cell Sci.* **120,** 3157–3161
9. Allinson, T. M., Parkin, E. T., Turner, A. J., and Hooper, N. M. (2003) ADAMs family members as amyloid precursor protein alpha-secretases. *J. Neurosci. Res.* **74,** 342–352
10. Vassar, R. (2004) BACE1: the beta-secretase enzyme in Alzheimer's disease. *J. Mol. Neurosci.* **23,** 105–114
11. Imbimbo, B. P. (2008) Therapeutic potential of gamma-secretase inhibitors and modulators. *Curr. Top. Med. Chem.* **8,** 54–61
12. Fahrenholz, F., and Postina, R. (2006) Alpha-secretase activation–an approach to Alzheimer's disease therapy. *Neurodegener. Dis.* **3,** 255–261
13. Postina, R., Schroeder, A., Dewachter, I., Bohl, J., Schmitt, U., Kojro, E., Prinzen, C., Endres, K., Hiemke, C., Blessing, M., Flamez, P., Dequenne, A., Godaux, E., van Leuven, F., and Fahrenholz, F. (2004) A disintegrin-metalloproteinase prevents amyloid plaque formation and hippocampal defects in an Alzheimer disease mouse model. *J. Clin. Invest.* **113,** 1456–1464
14. Hemler, M. E. (2005) Tetraspanin functions and associated microdomains. *Nat. Rev. Mol. Cell. Biol.* **6,** 801–811
15. Levy, S., and Shoham, T. (2005) The tetraspanin web modulates immune-signalling complexes. *Nat. Rev. Immunol.* **5,** 136–148
16. Rubinstein, E., Ziyyat, A., Wolf, J. P., Le Naour, F., and Boucheix, C. (2006) The molecular players of sperm-egg fusion in mammals. *Semin. Cell. Dev. Biol.* **17,** 254–263
17. Berditchevski, F., and Odintsova, E. (2007) Tetraspanins as regulators of protein trafficking. *Traffic* **8,** 89–96
18. Hemler, M. E. (2008) Targeting of tetraspanin proteins—potential benefits and strategies. *Nat. Rev. Drug Discov.* **7,** 747–758
19. Hemler, M. E. (2003) Tetraspanin proteins mediate cellular penetration, invasion and fusion events, and define a novel type of membrane microdomain. *Ann. Rev. Cell. Dev. Biol.* **19,** 397–422
20. Serru, V., Dessen, P., Boucheix, C., and Rubinstein, E. (2000) Sequence and expression of seven new tetraspans. *Biochim. Biophys. Acta* **1478,** 159–163
21. Lafleur, M. A., Xu, D., and Hemler, M. E. (2009) Tetraspanin proteins facilitate MT1-MMP-dependent tumor cell invasion. *Mol. Biol. Cell* **20,** 2030–2040
22. Xu, D., and Hemler, M. E. (2005) Metabolic activation-related CD147-CD98 complex. *Mol. Cell. Proteomics* **4,** 1061–1071
23. Yauch, R. L., Berditchevski, F., Harler, M. B., Reichner, J., and Hemler, M. E. (1998) Highly stoichiometric, stable and specific association of integrin α3β1 with CD151 provides a major link to phosphatidylinositol 4-kinase and may regulate cell migration. *Mol. Biol. Cell* **9,** 2751–2765
24. Yang, X., Claas, C., Kraeft, S. K., Chen, L. B., Wang, Z., Kreidberg, J. A., and Hemler, M. E. (2002) Palmitoylation of tetraspanin proteins: modulation of CD151 lateral interactions, subcellular distribution, and integrin-dependent cell morphology. *Mol. Biol. Cell* **13,** 767–781
25. Yang, X. H., Richardson, A. L., Torres-Arzayus, M. I., Zhou, P., Sharma, C., Kazarov, A. R., Andzelm, M. M., Strominger, J. L., Brown, M., and Hemler, M. E. (2008) CD151 accelerates breast cancer by regulating α6 integrin functions, signaling, and molecular organization. *Cancer Res.* **68,** 3204–3213
26. Herlevsen, M., Schmidt, D. S., Miyazaki, K., and Zoller, M. (2003) The association of the tetraspanin D6.1A with the alpha6beta4 integrin supports cell motility and liver metastasis formation. *J. Cell Sci.* **116,** 4373–4390
27. Rubinstein, E., Le Naour, F., Billard, M., Prenant, M., and Boucheix, C. (1994) CD9 antigen is an accessory subunit of the VLA integrin complexes. *Eur. J. Immunol.* **24,** 3005–3013
28. Tachibana, I., Bodorova, J., Berditchevski, F., Zutter, M. M., and Hemler, M. E. (1997) NAG-2, a novel transmembrane-4 superfamily (TM4SF) protein that complexes with integrins and other TM4SF proteins. *J. Biol. Chem.* **272,** 29181–29189
29. Hemler, M. E., Mannion, B. A., and Berditchevski, F. (1996) Association of TM4SF proteins with integrins: relevance to cancer. *Biochim. Biophys. Acta* **1287,** 67–71
30. Moss, M. L., Bomar, M., Liu, Q., Sage, H., Dempsey, P., Lenhart, P. M., Gillispie, P. A., Stoeck, A., Wildeboer, D., Bartsch, J. W., Palmisano, R., and Zhou, P. (2007) The ADAM10 prodomain is a specific inhibitor of ADAM10 proteolytic activity and inhibits cellular shedding events. *J. Biol. Chem.* **282,** 35712–35721
31. Fahrenholz, F. (2007) Alpha-secretase as a therapeutic target. *Curr. Alzheimer. Res.* **4,** 412–417
32. Kovalenko, O. V., Yang, X., Kolesnikova, T. V., and Hemler, M. E. (2004) Evidence for specific tetraspanin homodimers: inhibition of palmitoylation makes cysteine residues available for cross-linking. *Biochem. J.* **377,** 407–417
33. Zhang, L., Bukulin, M., Kojro, E., Roth, A., Metz, V. V., Fahrenholz, F., Nawroth, P. P., Bierhaus, A., and Postina, R. (2008) Receptor for advanced glycation end products is subjected to protein ectodomain shedding by metalloproteinases. *J. Biol. Chem.* **283,** 35507–35516
34. Charrin, S., Manie, S., Oualid, M., Billard, M., Boucheix, C., and Rubinstein, E. (2002) Differential stability of tetraspanin/tet-

raspanin interactions: role of palmitoylation. *FEBS Lett.* **516,** 139–144
35. Le Gall, S. M., Bobe, P., Reiss, K., Horiuchi, K., Niu, X. D., Lundell, D., Gibb, D. R., Conrad, D., Saftig, P., and Blobel, C. P. (2009) ADAMs 10 and 17 represent differentially regulated components of a general shedding machinery for membrane proteins such as transforming growth factor alpha, L-selectin, and tumor necrosis factor alpha. *Mol. Biol. Cell* **20,** 1785–1794
36. Min, G., Wang, H., Sun, T. T., and Kong, X. P. (2006) Structural basis for tetraspanin functions as revealed by the cryo-EM structure of uroplakin complexes at 6-A resolution. *J. Cell Biol.* **173,** 975–983
37. Berditchevski, F., Odintsova, E., Sawada, S., and Gilbert, E. (2002) Expression of the palmitoylation-deficient CD151 weakens the association of alpha 3 beta 1 integrin with the tetraspanin-enriched microdomains and affects integrin-dependent signalling. *J. Biol. Chem.* **277,** 36991–37000
38. Lammich, S., Kojro, E., Postina, R., Gilbert, S., Pfeiffer, R., Jasionowski, M., Haass, C., and Fahrenholz, F. (1999) Constitutive and regulated alpha-secretase cleavage of Alzheimer's amyloid precursor protein by a disintegrin metalloprotease. *Proc. Natl. Acad. Sci. U. S. A.* **96,** 3922–3927
39. Shi, W., Fan, H., Shum, L., and Derynck, R. (2000) The tetraspanin CD9 associates with transmembrane TGF-alpha and regulates TGF-alpha-induced EGF receptor activation and cell proliferation. *J. Cell Biol.* **148,** 591–602
40. Murai, T., Miyazaki, Y., Nishinakamura, H., Sugahara, K. N., Miyauchi, T., Sako, Y., Yanagida, T., and Miyasaka, M. (2004) Engagement of CD44 promotes Rac activation and CD44 cleavage during tumor cell migration. *J. Biol. Chem.* **279,** 4541–4550
41. Gutwein, P., Stoeck, A., Riedle, S., Gast, D., Runz, S., Condon, T. P., Marme, A., Phong, M. C., Linderkamp, O., Skorokhod, A., and Altevogt, P. (2005) Cleavage of L1 in exosomes and apoptotic membrane vesicles released from ovarian carcinoma cells. *Clin. Cancer Res.* **11,** 2492–2501
42. Shoham, T., Rajapaksa, R., Boucheix, C., Rubinstein, E., Poe, J. C., Tedder, T. F., and Levy, S. (2003) The tetraspanin CD81 regulates the expression of CD19 during B cell development in a postendoplasmic reticulum compartment. *J. Immunol.* **171,** 4062–4072
43. Stipp, C. S., Kolesnikova, T. V., and Hemler, M. E. (2003) EWI-2 regulates {alpha}3{beta}1 integrin-dependent cell functions on laminin-5. *J. Cell Biol.* **163,** 1167–1177
44. Marcello, E., Gardoni, F., Mauceri, D., Romorini, S., Jeromin, A., Epis, R., Borroni, B., Cattabeni, F., Sala, C., Padovani, A., and Di Luca, M. (2007) Synapse-associated protein-97 mediates alpha-secretase ADAM10 trafficking and promotes its activity. *J. Neurosci.* **27,** 1682–1691
45. Camden, J. M., Schrader, A. M., Camden, R. E., Gonzalez, F. A., Erb, L., Seye, C. I., and Weisman, G. A. (2005) P2Y2 nucleotide receptors enhance alpha-secretase-dependent amyloid precursor protein processing. *J. Biol. Chem.* **280,** 18696–18702
46. Ludwig, A., Hundhausen, C., Lambert, M. H., Broadway, N., Andrews, R. C., Bickett, D. M., Leesnitzer, M. A., and Becherer, J. D. (2005) Metalloproteinase inhibitors for the disintegrin-like metalloproteinases ADAM10 and ADAM17 that differentially block constitutive and phorbol ester-inducible shedding of cell surface molecules. *Comb. Chem. High Throughput Screen.* **8,** 161–171
47. Kuhn, S., Koch, M., Nubel, T., Ladwein, M., Antolovic, D., Klingbeil, P., Hildebrand, D., Moldenhauer, G., Langbein, L., Franke, W. W., Weitz, J., and Zoller, M. (2007) A complex of EpCAM, claudin-7, CD44 variant isoforms, and tetraspanins promotes colorectal cancer progression. *Mol. Cancer Res.* **5,** 553–567
48. Anderegg, U., Eichenberg, T., Parthaune, T., Haiduk, C., Saalbach, A., Milkova, L., Ludwig, A., Grosche, J., Averbeck, M., Gebhardt, C., Voelcker, V., Sleeman, J. P., and Simon, J. C. (2008) ADAM10 is the constitutive functional sheddase of CD44 in human melanoma cells. *J. Invest Dermatol.* **129,** 1471–1482
49. Stipp, C. S., Orlicky, D., and Hemler, M. E. (2001) FPRP: A major, highly stoichiometric, highly specific CD81 and CD9-associated protein. *J. Biol. Chem.* **276,** 4853–4862
50. Charrin, S., Le Naour, F., Oualid, M., Billard, M., Faure, G., Hanash, S. M., Boucheix, C., and Rubinstein, E. (2001) The major CD9 and CD81 molecular partner. Identification and characterization of the complexes. *J. Biol. Chem.* **276,** 14329–14337

Received for publication March 10, 2009.
Accepted for publication June 11, 2009.

The C-terminal tail of tetraspanin protein CD9 contributes to its function and molecular organization

Hong-Xing Wang[1,*], Tatiana V. Kolesnikova[1,*], Carilee Denison[2], Steven P. Gygi[2] and Martin E. Hemler[1,‡]

[1]Department of Cancer Immunology and AIDS, Dana-Farber Cancer Institute and Department of Pathology, Harvard Medical School, Boston, MA 02115, USA
[2]Department of Cell Biology, Harvard Medical School, Boston, MA 02115, USA

*These authors contributed equally to this work
‡Author for correspondence (martin_hemler@dfci.harvard.edu)

Accepted 1 April 2011
Journal of Cell Science 124, 2702-2710

doi:10.1242/jcs.085449

Summary

Tetraspanin protein CD9 supports sperm–egg fusion, and regulates cell adhesion, motility, metastasis, proliferation and signaling. The large extracellular loop and transmembrane domains of CD9 engage in functionally important interactions with partner proteins. However, neither functional nor biochemical roles have been shown for the CD9 C-terminal tail, despite it being highly conserved throughout vertebrate species. To gain new insight into the CD9 tail, three C-terminal amino acids (Glu-Met-Val) were replaced with residues corresponding to C-terminal amino acids from tetraspanin protein CD82 (Pro-Lys-Tyr). Wild-type and mutant CD9 were then stably expressed in MOLT-4, K562, U937, RD and HT1080 cells. Whereas wild-type CD9 inhibited cell adhesion and spreading on fibronectin, mutant CD9 did not. Wild-type CD9 also promoted homotypic cell–cell aggregation and microvilli formation, whereas mutant CD9 did not. Protein interactions of wild-type and mutant CD9 were compared quantitatively using stable isotope labeling with amino acids in cell culture (SILAC) in conjunction with liquid-chromatography–tandem mass spectrometry (LC-MS/MS) technology. SILAC results showed that, despite wild-type and mutant CD9 having identical expression levels, mutant CD9 and its major transmembrane interacting partners were recovered in substantially reduced amounts from 1% Brij 96 lysates. Immunoprecipitation experiments confirmed that mutant CD9 recovery was decreased in Brij 96, but not in more stringent Triton X-100 detergent. Additionally, compared with wild-type CD9 complexes, mutant CD9 complexes were larger and more oligomerized in Brij 96 detergent, consistent with decreased Brij 96 solubility, perhaps due to more membrane domains packing more tightly together. In conclusion, multiple CD9 functions depend on its C-terminal tail, which affects the molecular organization of CD9 complexes, as manifested by their altered solubilization in Brij 96 and organization on the cell surface.

Key words: CD9, Tetraspanin, SILAC, Microvilli, Cell adhesion, Cell spreading

Introduction

The tetraspanin protein family contains 33 distinct members, each with four transmembrane domains, short N- and C-terminal cytoplasmic domains, a small intracellular loop and two extracellular loops (Berditchevski, 2001; Boucheix and Rubinstein, 2001; Hemler, 2003). The larger extracellular loop contains CCG and PXSC motifs, which are hallmarks of the tetraspanin family (Seigneuret et al., 2001). Through the large extracellular loop, tetraspanins interact with themselves and with other proteins, including membrane-bound growth factors, immunoglobulin (Ig) superfamily proteins, signaling enzymes and integrins (Berditchevski, 2001; Levy and Shoham, 2005). These protein–protein interactions underlie the assembly of structural and functional units called tetraspanin-enriched microdomains (TEMs) (Espenel et al., 2008; Hemler, 2005; Nydegger et al., 2006; Yanez-Mo et al., 2009). Within TEMs, tetraspanins can modulate the functions of associated proteins, thereby regulating many physiological and pathological processes, such as fertilization, cell adhesion, motility, tumor invasion and transendothelial migration (Barreiro et al., 2005; Berditchevski and Odintsova, 1999; Miyado et al., 2000; Ono et al., 1999; Zoller, 2009).

CD9, a member of the tetraspanin family, is expressed in multiple cell types, including hematopoietic cells, endothelial cells, epithelial cells, smooth muscle cells, pre-B cells and many tumor cell lines (Boucheix and Rubinstein, 2001; Hemler, 2003). Oocytes lacking CD9 are deficient in sperm–egg fusion (Kaji et al., 2000; Le Naour et al., 2000; Miyado et al., 2000), at least partly due to alterations in microvilli on the oocyte surface (Runge et al., 2007). CD9 also regulates myoblast (Tachibana and Hemler, 1999) and monocyte (Takeda et al., 2003) fusion, and HIV-induced syncytia formation (Gordon-Alonso et al., 2006). CD9 has tumor- suppressor-like functions in many tumor cell types, and can inhibit cell invasion and metastasis (Ikeyama et al., 1993; Zoller, 2009). CD9 also contributes to cell signaling (Huang et al., 2004), and can regulate cell adhesion (Masellis-Smith and Shaw, 1994), migration (Anton et al., 1995), apoptosis (Murayama et al., 2004), membrane protein shedding (Shi et al., 2000) and diphtheria toxin binding (Iwamoto et al., 1994). To assist in these diverse functions, CD9 interacts directly with transmembrane proteins EWI-2 (Charrin et al., 2003; Stipp et al., 2001a) and EWI-F (also called CD9P-1 and FPRP) (Charrin et al., 2001; Stipp et al., 2001b). CD9 also interacts with other proteins, including other tetraspanins, a subset of integrins, other adhesion molecules, membrane proteases, choline receptors and G proteins (Le Naour et al., 2006).

Whereas the functional importance of tetraspanin large extracellular loops (EC2) is well recognized, the C-terminal tails have received less attention. The C-terminal tail of tetraspanin CD63 binds to AP-3 adaptor subunit μ3 (Rous et al., 2002) and to

a PDZ domain in syntenin-1 (Latysheva et al., 2006), which affects CD63 distribution and trafficking. The CD81 C-terminal tail was suggested to associate directly with ezrin-radixin-moesin (ERM) proteins (Sala-Valdes et al., 2006), whereas a YRSL sequence in the CD151 cytoplasmic domain might determine intracellular trafficking and function (Liu et al., 2007). In addition, the short C-terminal tail of CD151 supports integrin-α6β1-dependent cellular cable formation and adhesion strengthening (Lammerding et al., 2003; Yang et al., 2002). As in other tetraspanins, CD9 contains a C-terminal tail that is short (only eight residues) and highly conserved across several animal species, suggesting functional importance. However, essentially nothing is known about the function and biochemistry of the CD9 C-terminal tail. Here, we have mutated the CD9 C-terminal tail and examined the functional consequences. In addition, we have used a differential mass spectrometry technology called SILAC [stable isotope labeling of amino acids in cell culture (Ong et al., 2002)], together with immunoprecipitation, gel filtration and flow cytometry, to examine the effects of CD9 tail mutation on the molecular organization of CD9 complexes in detergent lysates and on the cell surface. To establish the generality of the conclusions, functional and biochemical studies were carried out using four to five different cell lines, including both adherent and non-adherent types.

Results

Expression and distribution of CD9 and CD9 mutant in different cell lines

The short C-terminal tail of CD9 (eight residues) is well conserved among seven different vertebrate species (Fig. 1A). To address the functional and biochemical importance of the CD9 tail, the C-terminal EMV motif was replaced with PKY, which corresponds to the C-terminal amino acids of CD82 (Fig. 1B). This particular conservative strategy was chosen because: the C-terminal EMV motif in CD9 partly resembles the functionally important PDZ-domain-interacting C-terminal EVM site in CD63 (Latysheva et al., 2006); more radical CD9 C-tail mutations lead to loss of cell-surface expression (e.g. Ryu et al., 2000); CD9 and CD82 are the two tetraspanins most known for having tumor suppressor functions (Cajot et al., 1997; Huang et al., 1998; Miranti, 2009; Miyake et al., 1995); and various other CD9–CD82 chimeras have been effectively utilized in prior studies (Charrin et al., 2003; Gutierrez-Lopez et al., 2003). Several CD9-deficient cell lines (MOLT-4, K562, RD, HT1080 and U937) were stably transfected with wild-type and mutant CD9, to yield similar total expression levels, as seen by immunoblotting of CD9 (supplementary material Fig. S1A and Fig. S1C, inset). Cell-surface expression was also comparable, as seen by flow cytometry (supplementary material Fig. S1B,C).

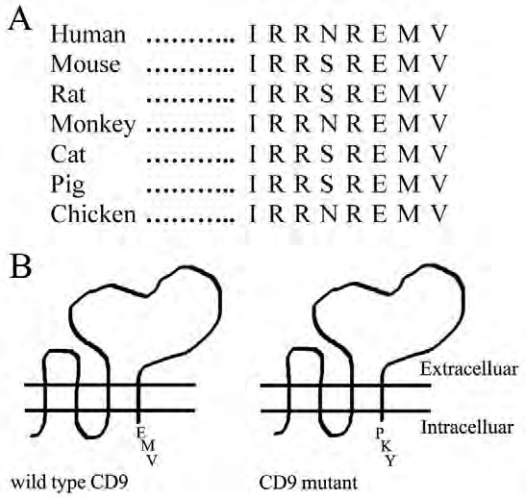

Fig. 1. CD9 C-terminal tail and mutagenesis. (**A**) CD9 C-terminal tail sequences from seven different animal species. (**B**) The three C-terminal amino acids (glutamic acid-methionine-valine, EMV) of wild-type CD9 were changed to proline-lysine-tyrosine (PKY) to yield mutant CD9.

CD9 but not CD9 mutant inhibits cell adhesion and cell spreading

CD9 might regulate integrin-dependent cell adhesion and spreading (Berditchevski, 2001; Deng et al., 2000; Hemler, 2003). Hence, we analyzed cell adhesion and spreading for K562 cells transfected to express wild-type and mutant CD9. Diminished adhesion to fibronectin was seen for wild-type CD9 cells (Fig. 2A) compared to mutant CD9 cells (Fig. 2B) and control K562 cells (Fig. 2C). Quantification (Fig. 2D) confirmed that adhesion was diminished upon expression of wild-type CD9, but not mutant CD9, at both 30 minutes and 2 hours after plating. CD9 also inhibited spreading of both MOLT-4 and K562 cells on fibronectin, as seen in photos (Fig. 3A) and after quantification (Fig. 3B,C). Unlike CD9, mutant CD9 failed to inhibit spreading after 6 hours (Fig. 3), and also after 1 and 3 hours (supplementary material Fig. S2A,B). Likewise, wild-type CD9, but not mutant CD9, inhibited spreading of RD cells at multiple time points after plating (supplementary material Fig. S2C–E).

CD9 but not CD9 mutant promotes cell aggregation

CD9 has been associated with cell–cell aggregation (Letarte et al., 1993; Masellis-Smith et al., 1990). Indeed, expression of wild-type CD9 promoted MOLT-4 cell–cell aggregation when cells were plated for 2 hours on collagen I (Fig. 4A) or on laminin-5 (Fig. 4B), or in the presence of 10% fetal bovine serum (FBS) (Fig. 4C).

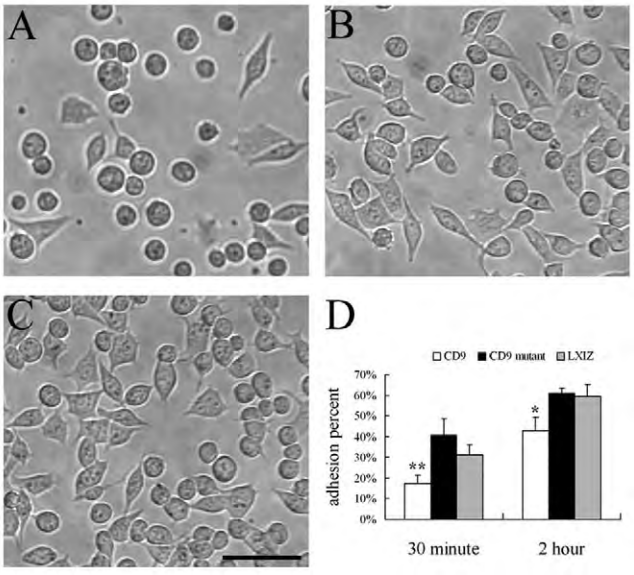

Fig. 2. CD9 mutation affects K562 cell adhesion to fibronectin. K562 cells expressing (**A**) wild-type CD9, (**B**) mutant CD9 or (**C**) LXIZ control vector were allowed to adhere to fibronectin for 2 hours, and then photographed. Scale bar: 50 μm. (**D**) Quantification of K562 cell adhesion results. Error bars indicate means ± s.d. **P*<0.05; ***P*<0.01.

Expression of mutant CD9 had a minimal pro-aggregation effect (Fig. 4A–C). Non-coated plastic with no serum yielded no aggregation, regardless of CD9 expression (Fig. 4D). CD9 promotion of MOLT-4 cell aggregation in the presence of collagen I, laminin-5 or FBS (which contains fibronectin) is consistent with a role for β1 integrins (Letarte et al., 1993; Ziyyat et al., 2006).

CD9 but not CD9 mutant promotes microvilli formation

CD9 was previously observed within filopodia and microvilli, in proximity to F-actin (Kaji et al., 2001; Runge et al., 2007; Stipp et al., 2003). To gain clues regarding functional differences between wild-type and mutant CD9, we analyzed staining patterns on adherent cell lines RD (Fig. 5) and HT1080 (supplementary material Fig. S3). In both cell types, wild-type CD9 expression correlated with formation of abundant filopodia and microvilli-like projections, with CD9 within the projections (Fig. 5A, arrows) colocalized with F-actin (Fig. 5A; supplementary material Fig. S3A). By contrast, RD and HT1080 cells transfected with mutant CD9 did not show microvilli-like projections (Fig. 5A, arrows), as seen by staining of either CD9 or F-actin. The density and lengths of microvilli-like structures in CD9 mutant cells closely resembled those in cells transfected with control vector (Fig. 5A; supplementary material Fig. S3A). Quantification of the number of microvilli per cell confirmed that microvilli formation was promoted by CD9, but not by mutant CD9 (Fig. 5B; supplementary material Fig. S3B).

CD9 mutation alters sensitivity to Brij 96 detergent

To compare wild-type and mutant CD9 with respect to molecular interactions, they were expressed in a U937 cell variant, which lacks both CD9 and CD81. Thus, we hoped to avoid indirect CD81-dependent interactions between various partner proteins and CD9. CD9 complexes then were analyzed using SILAC, a differential mass spectrometry quantification method (Ong et al., 2002). Wild-type and mutant CD9 were expressed at comparable levels in U937 cells, as demonstrated by cell surface flow cytometry (supplementary material Fig. S1C) and by immunoblotting from Triton X-100 whole-cell lysates (supplementary material Fig. S1C, inset). Wild-type CD9-transfected cells were then grown for 10 doublings in ^{13}C-leucine heavy isotope, whereas mutant CD9-transfected cells were grown in medium containing normal leucine (light isotope). Equal numbers of cells were mixed, lysed together in 1% Brij 96 and then CD9 complexes were recovered, using beads coated with anti-CD9 monoclonal antibody (mAb) ALB6. Mass spectrometry coupled with quantitative SILAC analysis showed that peptides from eight different proteins were co-immunoprecipitated in comparable amounts [heavy (H):light (L) ratios~1.0–1.4] with wild-type and mutant CD9 (Table 1, bottom). However, recovery of CD9 itself and six of its known partner binding proteins was notably amplified for wild-type CD9 compared with for mutant CD9 (H:L ratios=2.3–3.3; Table 1, top). Although recovery of the major CD9 partner protein EWI-2 was increased for wild-type CD9 compared with mutant CD9 (Table 1), cell surface expression of EWI-2 on U937 cells (data not shown), K562 and RD cells (supplementary material Fig. S4) was unaltered by CD9 tail mutation.

CD9 mutation changes protein solubilization and organization in Brij 96

Results obtained in Table 1 indicated that, even though wild-type and mutant CD9 were expressed at comparable levels on the surface of U937 cells and recovered at nearly identical levels in Triton X-100 lysates, recovery from Brij 96 lysates was diminished for complexes containing mutant CD9. Consistent with this interpretation, mutant CD9 was immunoprecipitated from RD and MOLT-4 Brij 96 lysates at levels that were 40–60% less than those

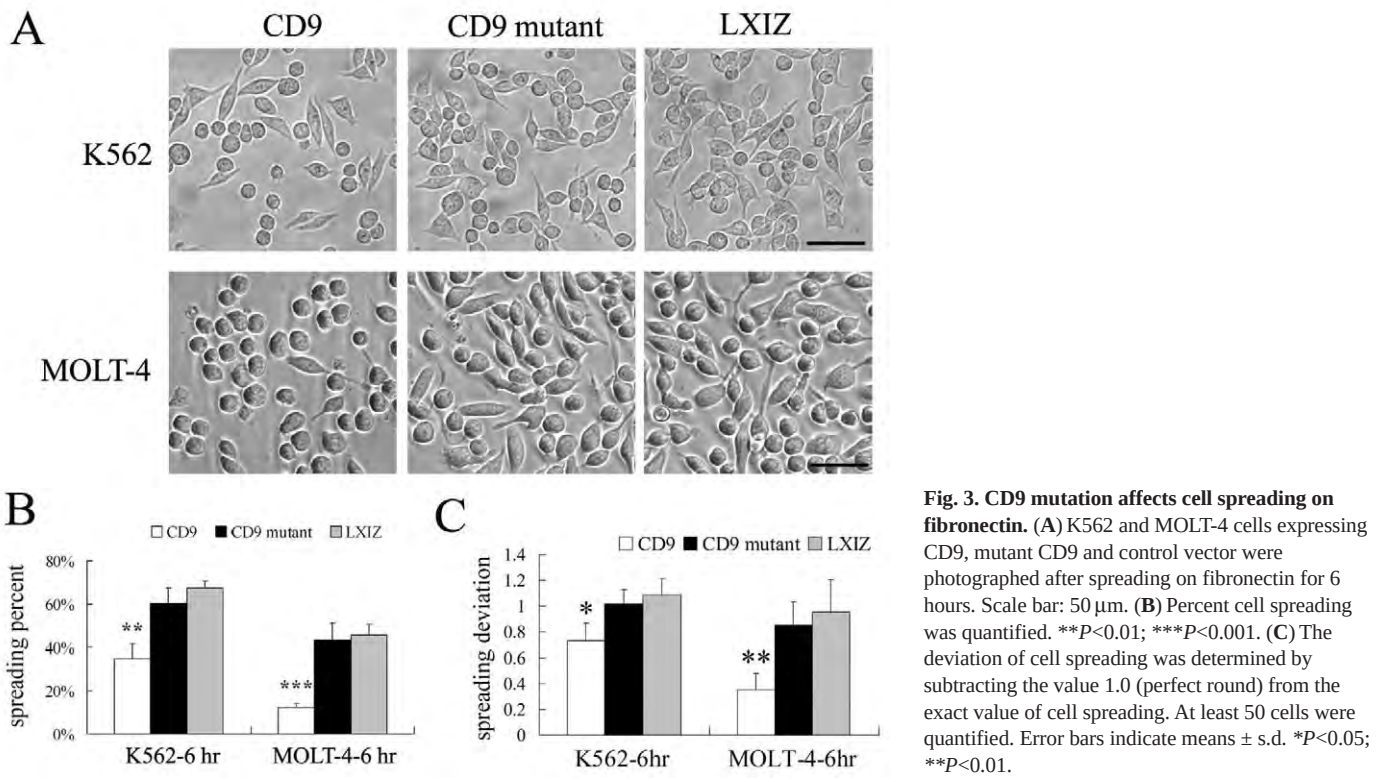

Fig. 3. CD9 mutation affects cell spreading on fibronectin. (**A**) K562 and MOLT-4 cells expressing CD9, mutant CD9 and control vector were photographed after spreading on fibronectin for 6 hours. Scale bar: 50 μm. (**B**) Percent cell spreading was quantified. ***P*<0.01; ****P*<0.001. (**C**) The deviation of cell spreading was determined by subtracting the value 1.0 (perfect round) from the exact value of cell spreading. At least 50 cells were quantified. Error bars indicate means ± s.d. **P*<0.05; ***P*<0.01.

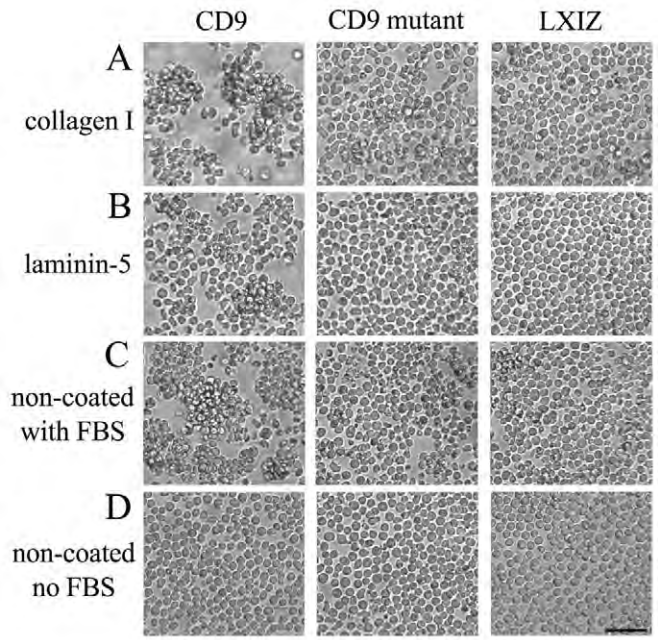

Fig. 4. CD9 and mutant CD9 effects on MOLT-4 cell aggregation. MOLT-4 cells stably expressing CD9, mutant CD9 or control vector were incubated on (**A**) collagen I, (**B**) laminin-5, (**C**) non-coated tissue culture plastic with FBS or (**D**) non-coated tissue culture plastic. Photos were obtained after 2 hours. Scale bar: 50 μm.

Table 1. SILAC results comparing CD9 (heavy isotope) and CD9 mutant (light isotope) ratios for coimmunoprecipitated proteins.

Protein	Peptides	H:L ratio*
CD9	2	2.5±0.5
CD82	4	2.9±0.6
TSPAN14	1	2.5
CD4	3	2.3±0.4
CTL1 (CD92)	7	3.3±1.0
CD224 (GGT)	3	3.2±0.4
EWI-2 (CD316)	3	2.5±1.0
GRP75	12	1.3±0.2
GRP78	2	1.3±0.01
HSP7C	2	1.3±0.2
Trim21	6	1.0±0.1
Tuba6	2	1.1±0.3
Tubb2c	3	1.4±0.3
Acta2	2	1.1±0.2
Q13707	2	1.3±0.2

*H:L ratios represent mean ± s.d. for results from multiple distinct peptides, except for TSPAN14 results, which are based on one peptide.

The top panel shows H:L ratio results=2.2–2.3. The bottom panel shows H:L ratio results=1.0–1.4.

of wild-type CD9 (Fig. 6A, left panels). By contrast, wild-type and mutant CD9 were recovered at nearly identical levels from Triton X-100 lysates (Fig. 6A, middle panels). Furthermore, when 1% Brij 96 cell lysates were subsequently supplemented, post lysis, to contain also 1% Triton X-100, the difference in CD9 recoveries disappeared (Fig. 6A, right panels). These results suggest that mutant CD9 was not simply left behind in the cell pellet, but rather was reorganized to become partially unavailable (i.e. less soluble) within the Brij 96 lysate.

In contrast to the recognition of total CD9 by high-affinity anti-CD9 mAb (i.e. MM2/57 and ALB6), low-affinity anti-CD9 mAb C9BB preferentially recognizes clustered CD9 (Yang et al., 2006). Whereas immunoprecipitation with anti-CD9 mAb MM2/57 typically yielded more wild-type CD9 (e.g. see Fig. 6A), immunoprecipitation with mAb C9BB consistently yielded more mutant CD9 from Brij 96 lysates (Fig. 6B, left panels). Hence, C9BB:MM2/57 recovery ratios (Fig. 6B, numbers below panels) were consistently higher for mutant CD9 relative to wild-type CD9. These ratios show that mAb C9BB, compared to MM2/57, has a 3–10-fold preference for mutant CD9 over wild-type CD9 in K562, RD and MOLT-4 cells. This result is consistent with mutant CD9 complexes being more clustered (Yang et al., 2006) and less well solubilized in Brij 96 detergent. Preferential recovery of mutant CD9 by mAb C9BB disappeared upon solubilization in Triton X-100 or upon post-lysis addition of Triton X-100 to lysates already containing Brij 96 (Fig. 6B; middle and right panels).

To assess further the differences between mutant and wild-type CD9 complexes in Brij 96 lysates, gel filtration experiments were carried out. Consistent with diminished mutant CD9 solubility in 1% Brij 96 and increased mutant CD9 clustering, a subset of surface biotin-labeled mutant CD9 complexes were distinctly larger than the largest wild-type CD9 complexes (Fig. 7A, fractions 3,4). The gel filtration size difference was not as obvious when cells were metabolically labeled with 3[H]-palmitate, largely because newly synthesized CD9 did not have time to assemble into larger complexes. Nonetheless, mutant CD9 complexes were still also a little larger than wild-type CD9 complexes, as particularly evident in column fractions 4–6 (Fig. 7B).

Results in Figs 6 and 7 suggest that our CD9 mutation might also alter the organization of CD9 complexes on the surface of intact cells. As shown in Fig. 8A, mutant CD9 again showed enhanced binding of mAb C9BB, a probe for homooligomerization (Yang et al., 2006). In a control experiment, surface expression of total CD9, assessed using mAb MM2/57, was not altered (Fig. 8B).

Discussion

A functional role for the CD9 C-terminal tail

To assess the functional role of the highly conserved CD9 C terminus, a chimeric protein was designed, replacing the CD9 C-terminal Glu-Met-Val with Pro-Lys-Tyr from CD82. Expression of wild-type CD9 (in cells otherwise lacking CD9) inhibited cell adhesion and spreading on fibronectin, but promoted homotypic aggregation and microvilli formation. By contrast, mutant CD9 did not inhibit adhesion or spreading, and did not promote homotypic aggregation and microvilli formation.

Involvement of CD9 in integrin-dependent adhesion, spreading and homotypic aggregation has previously been observed (Masellis-Smith et al., 1990; Masellis-Smith and Shaw, 1994; Shaw et al., 1995). CD9-dependent formation of microvilli has also been observed (Runge et al., 2007) and anti-CD9-antibody-induced microvilli ‘zippers’ might promote cell–cell associations, leading to homotypic aggregation (Singethan et al., 2008). We suggest that microvilli formation could interfere with cell adhesion and spreading, thus accounting for CD9 inhibition of these processes. Therefore, because mutant CD9 did not form microvilli, it was less able to promote homotypic aggregation and to inhibit adhesion and spreading. Our CD9 C-terminal mutation severely hindered each

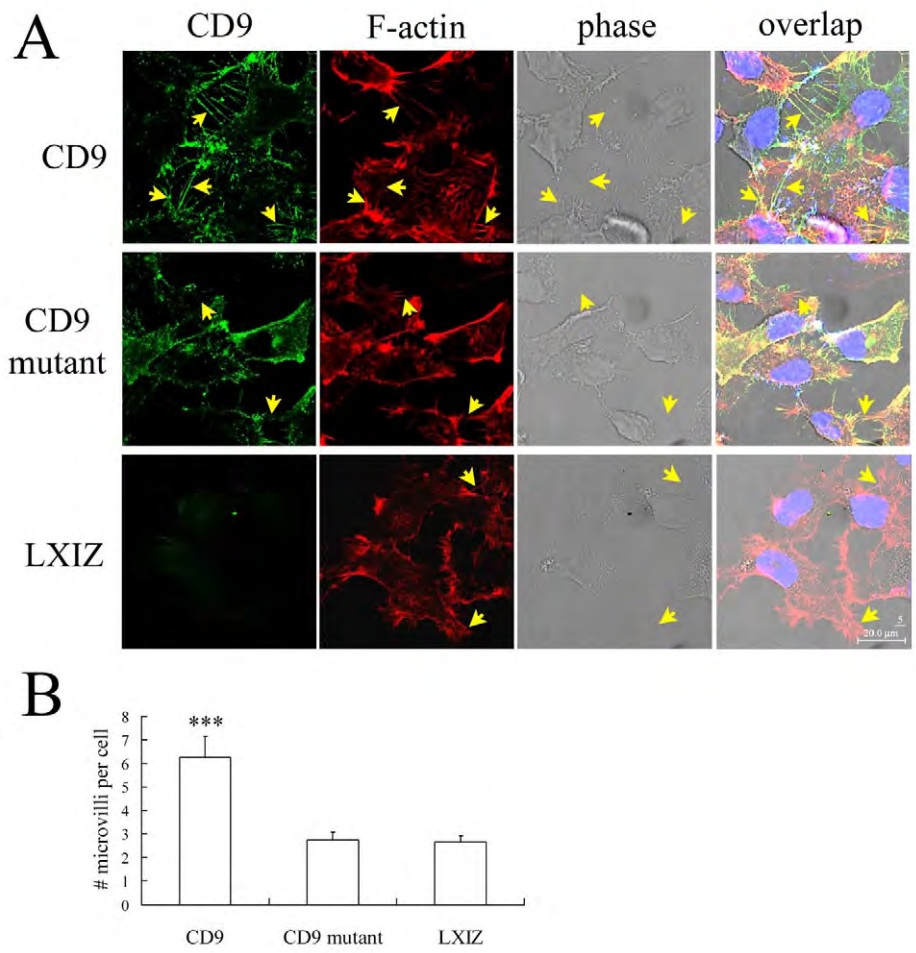

Fig. 5. CD9 and mutant CD9 effects on microvilli formation in RD cells. (**A**) RD cells were stained for CD9 using mAb MM2/57 labeled with AlexaFluor488 (green) and for F-actin using AlexaFluor594–phalloidin (red). Cell nuclei are stained with DAPI (blue). Microvilli-like structures are marked with arrows. Scale bar: 20 µm. (**B**) Counting of microvilli (greater than 5 µm) was completed using Scion Image software, with quantification for each cell type from 10 random photos, each containing multiple cells (counted by staining of nuclei). Error bars indicate means ± s.d. ***P<0.001.

of the four different CD9 functions tested, and these results were seen in four different cell lines (two adherent, two nonadherent). Hence, the C-terminal tail is also likely to be crucial for other CD9-dependent processes, including platelet functions (Goschnick and Jackson, 2007), tumor suppression (Cajot et al., 1997; Huang et al., 1998; Miyake et al., 1995), oocyte fertilization (Le Naour et al., 2000; Miyado et al., 2000), MHC protein organization (Kropshofer et al., 2002; Unternaehrer et al., 2007), cell–cell fusion (Tachibana and Hemler, 1999; Takeda et al., 2003), formation and/or maintenance of paranodal junctions (Ishibashi et al., 2004), HIV1-induced membrane fusion (Gordon-Alonso et al., 2006) and HIV1 cell–cell transmission (Krementsov et al., 2009).

Specific residues within the large extracellular loop of CD9 contribute to gamete fusion (Zhu et al., 2002) and to upregulation of diphtheria toxin binding (Hasuwa et al., 2001), and specific transmembrane residues contribute to CD9 homodimerization (Kovalenko et al., 2005). However, until now there was little, if any, evidence for the CD9 C-terminal tail being functionally important. Although a role for the CD9 C-terminal tail was not previously established, there is precedent for the C termini of other tetraspanins being functionally important. For example, the C-terminal tail of CD151 supports integrin-dependent adhesion strengthening, cell morphology (Lammerding et al., 2003; Zhang et al., 2002) and intracellular trafficking (Liu et al., 2007), and the C-terminal tail of CD63 regulates its internalization (Latysheva et al., 2006; Rous et al., 2002), together with a cell-surface partner protein (Duffield et al., 2003).

Biochemical consequences of CD9 C-terminal tail mutation

Tetraspanin CD63, with a C-terminal G-Y-E-V-M sequence, interacts with a PDZ domain in syntenin-1 (Latysheva et al., 2006), a transmembrane and cytoplasmic connector protein. However, CD9 does not directly interact with syntenin-1 (Latysheva et al., 2006), and the C-terminal R-N-R-E-M-V sequence of CD9 does not closely match any of 16 consensus PDZ-interaction motifs (Tonikian et al., 2008). The C-terminal tail of CD81, a tetraspanin similar to CD9, might interact directly with ERM proteins (Sala-Valdes et al., 2006). However, the C terminus of CD9 did not directly interact with ERM proteins (Sala-Valdes et al., 2006). To gain an unbiased assessment of CD9 protein associations affected by C-terminal tail mutation, we undertook a SILAC mass spectrometry approach, applying it to the study of multimolecular tetraspanin CD9 protein complexes. Although we mixed equal numbers of cells expressing equal amounts of wild-type CD9 (heavy-isotope labeled) and mutant CD9 (light-isotope labeled), we recovered 2.3–3.3-fold more wild-type CD9 and associated partner proteins from 1% Brij 96 lysates. Notably, CD9 and mutant CD9 were present in equal amounts both on the cell surface (as indicated by flow cytometry) and in the total cell lysate (as indicated by immunoblotting of Triton X-100 lysates). Furthermore, eight different background proteins, not known to be associated with CD9, were recovered at similar levels (H:L ratios=1.0–1.4). Hence, complexes containing mutant CD9 and six of its associated proteins (but not

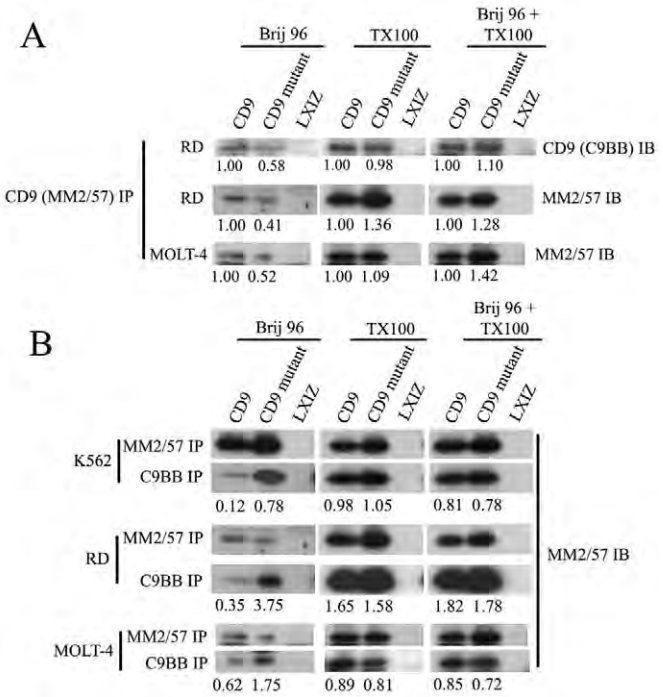

Fig. 6. CD9 mutation affects recovery of CD9 complexes in Brij 96 detergent. (**A**) RD and MOLT-4 cells were lysed in 1% Brij 96, 1% Triton X-100, or 1% Brij 96 subsequently supplemented to also contain 1% Triton X-100. After immunoprecipitation (IP) using anti-CD9 mAb MM2/57 and SDS-PAGE resolution, CD9 was detected by immunoblotting using mAb C9BB or MM2/57. Numbers indicate recovery of mutant CD9 relative to that of wild-type CD9. Note that the six lower panels are used again in B for a different purpose. (**B**) After detergent lysis as in A, immunoprecipitations were carried out using anti-CD9 mAb MM2/57 or C9BB as indicated. CD9 was then detected by immunoblotting using mAb MM2/57. Numbers indicate recovery of CD9 (wild type or mutant) using mAb C9BB relative to mAb MM2/57. Note that the third and fifth panel rows are identical to images used in the second and third rows of A.

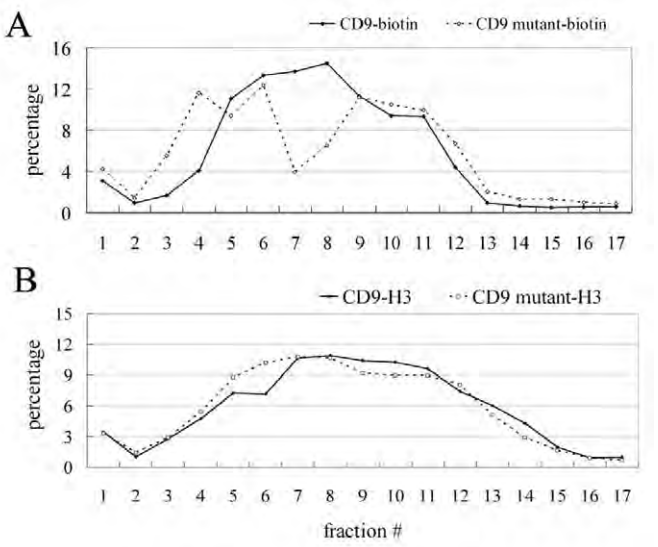

Fig. 7. Gel filtration analyses of CD9 and mutant CD9 complexes. (**A**) U937 cells stably expressing CD9 or mutant CD9 were surface labeled with biotin and then lysed in 1% Brij 96. Lysates were fractionated using a sepharose CL6B gel filtration column and biotin-labeled CD9 was detected as described in the Materials and Methods. (**B**) U937 cells were metabolically labeled using ^{3}H-palmitate, and then CD9 and mutant CD9 were fractionated and detected as described in the Materials and Methods. The sum of densitometry quantifications for each set of samples is 100%.

the eight background proteins) were selectively less available to the anti-CD9 mAb-coated beads used to retrieve CD9 complexes from 1% Brij 96 lysates. These results point to a selective decrease in Brij 96 solubility for complexes containing mutant CD9 from U937 cells. Reduced recovery of mutant CD9 from 1% Brij 96 lysates was seen in two additional cell lines (RD and MOLT-4), expressing CD9 and mutant CD9 at comparable levels on the cell surface and in Triton X-100 lysates.

The post-lysis addition of Triton X-100 to Brij 96 lysates restored CD9 and mutant CD9 to a state of equal recovery, thus establishing that mutant CD9 was not left in the Brij 96 insoluble pellet. Instead, mutant CD9 seems to be reorganized into larger complexes in Brij 96 lysates, with skewed mAb recognition profiles. This idea is reinforced by mutant CD9 in lysates showing selectively decreased recognition by anti-CD9 mAb such as MM2/57 and ALB6, and showing selectively enhanced recognition by mAb C9BB, which preferentially binds to oligomerized CD9 (Yang et al., 2006). Also, mutant CD9 seems to be larger than wild-type CD9, as seen by gel filtration of 1% Brij 96 lysates. Consistent with results seen in detergent lysates, mutant CD9 on the surface of intact cells again showed selectively enhanced mAb C9BB binding, indicative of increased homooligomerization. In a prior study, molecular alterations of tetraspanin CD81 complexes resulted in major size changes (as seen by gel filtration) and major differences in recognition by selected anti-CD81 antibodies, both on the cell surface and in detergent lysates, with the latter differences disappearing upon addition of Triton X-100 (Kolesnikova et al., 2004).

Regarding CD9 molecular organization, consistent results were seen in five different cell lines (two adherent, three nonadherent), each expressing CD9 and mutant CD9 at comparably moderate levels. Hence, conclusions seem to be generally applicable and not due to either excessive CD9 overexpression or specialized tetraspanin microdomain conditions only found in one or a few cell types.

We suggest that mutation of the CD9 tail leads to altered and/or unregulated assembly of CD9 complexes, with enhanced CD9 homooligomerization, such that transmembrane domain packing becomes more difficult to disrupt by the oleate sidechain of Brij 96. By contrast, wild-type CD9 probably engages in a specific (but not yet identified) interaction with the cytoskeleton, which leads to assembly of complexes that are less extensively organized in the lateral dimension and that seem more likely to contribute to assembly of microvilli.

CD9-associated proteins with high H:L ratios include CD82, TSPAN14, CD4, CTL1, CD224 and EWI-2. CD9 interactions with other tetraspanin proteins, including CD82 and TSPAN14, are well established (e.g. see Le Naour et al., 2006; Rubinstein et al., 1996). CD9 associations with CD4, CD224 (γ-glutamyl transferase) and CTL1 (a choline transporter) have also been previously noted (Le Naour et al., 2006; Toyo-Oka et al., 1999), but their functional implications are unknown. CD9 associates directly with EWI-2 (Charrin et al., 2003; Stipp et al., 2001a); EWI-2 might contribute

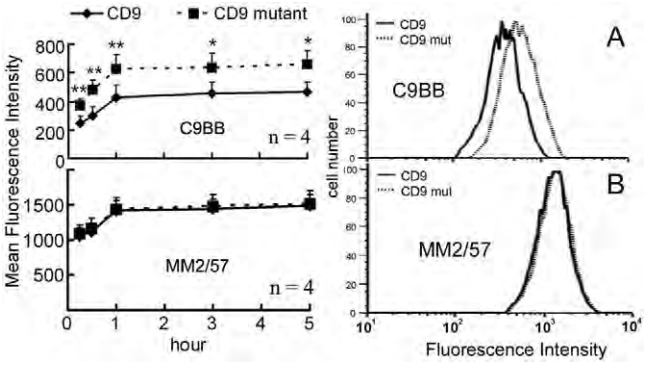

Fig. 8. CD9 mutation effects on cell-surface organization. RD cells expressing CD9 or mutant CD9 were incubated with 4.0 μg low-affinity anti-CD9 antibody (C9BB, **A**) or 1.0 μg high-affinity antibody (MM2/57, **B**) for the indicated times, and CD9 mean fluorescence intensities (MFIs) were plotted. Right panels show representative flow cytometry profiles from the 1 hour time point.

to CD9-dependent inhibition of cell migration and glioblastoma growth (Kolesnikova et al., 2008). A problem with classical protein mass spectrometry assessment of protein complexes is that it is sometimes difficult to distinguish 'real' from adventitious protein associations. In our study, the six CD9 partner proteins identified with high H:L ratios are all therefore at least partly dependent on the CD9 C-terminal tail for assembly into the complex and thus might be validated as 'real' CD9 partners. By contrast, eight other proteins, with H:L ratios close to 1.0, associate independent of the C-terminal tail, consistent with them being background proteins.

The C-terminal tail of CD9 and other tetraspanins has several times been covalently tagged for the purpose of studying subcellular distribution and/or tetraspanin dynamics. Findings shown in this paper indicate that such results need to be evaluated cautiously. We show that even a relatively small change to the C-terminal tail can have a major effect on a wide range of functions, while also altering the cell-surface organization of a tetraspanin and nearly all, if not all, of its transmembrane partners.

Materials and Methods

Antibodies, plasmids and cell culture

mAbs to tetraspanin CD9 (MM2/57, ALB6, C9BB), integrin β1 (TS2/16) and EWI-2 (rabbit polyclonal antibody) were referenced elsewhere (Yang et al., 2006). MOLT-4, K562 and U937 cells [American Type Culture Collection (ATCC), Manassas, VA] were cultured in RPMI 1640 medium with 10% FBS, 100 U/ml penicillin and 100 μg/ml streptomycin (Invitrogen). RD, HT1080 and ΦNX-ampho packaging cells (ATCC) were maintained in DMEM with 10% FBS plus antibiotics. In CD9 mutant plasmid, the last three amino acids of CD9 (EMV) were replaced by the last three amino acids of CD82 (PKY). CD9 and CD9 mutant were cloned in a C-terminal FLAG-tagged pLXIZ retroviral vector. CD9, CD9 mutant and pLXIZ were transiently transfected into ΦNX-ampho cells and retroviral infection of MOLT-4, K562, U937, RD and HT1080 cells was performed as previously described (Kolesnikova et al., 2004). Stable infectants were selected in medium containing 200 μg/ml zeocin (Invitrogen).

Cell adhesion, spreading and aggregation assays

For fibronectin coating, 12-well or 96-well plates were treated with 10 μg/ml human fibronectin (BD Biosciences, Bedford, MA) in PBS at 4°C overnight, and blocked with 1% BSA in PBS for 1 hour. For adhesion assays, K562 cells (1.0×10^5) were labeled with 5 μM Calcein AM (Vybrant Cell Adhesion Assay Kit, Invitrogen) for 30 minutes, then washed, resuspended in FBS-free medium and added to fibronectin-coated 12-well plates for 0.5 and 2 hours. Unattached cells were removed by two washes with culture medium. Fluorescence intensity was then measured using a Wallac 1420 workstation (PerkinElmer, Waltham, MA) to detect emission at 494 nm before and after washes. Adhesion percent is calculated as (adherent cell fluorescence – background)/(total cell fluorescence – background). The background is taken as fluorescence of cells without Calcein AM labeling.

For spreading assays, K562, MOLT-4 and RD cells (1.0×10^5) were plated on fibronectin for 0.5–6 hours, and then photographed. To quantify cell spreading, 'deviation from round' was calculated by dividing the theoretical maximum area for a given perimeter ($\text{perimeter}^2/4\pi$) by the observed pixel area (Zhang et al., 2001) obtained using Scion Image software (Scion Corp., Frederick, MD). Cells with values >1.2 were judged to be spread (1.0=value for a perfectly round cell). At least 50 cells from three independent experiments were evaluated for each data point presented.

For cell aggregation assays, 12-well plates were either non-coated or coated with 10 μg/ml collagen I (Santa Cruz) or laminin-5 (produced from human A431 cells). MOLT-4 cells (1.0×10^5) were dispersed, washed in FBS-free medium, incubated in 12-well plates and then photographed after 2 hours. Cell images were acquired with a monochrome CCD camera (Spot RT; Diagnostic Instruments, Sterling Heights, MI) on a microscope (Axiovert 135; Carl Zeiss MicroImaging, Thornwood, NY). Cell shape was evaluated by the Scion Image Software.

Flow cytometry

MOLT-4, K562, RD, U937 and HT1080 cells (1.0×10^5) were stained with 1.0 μg specific mAb for 1 hour on ice, followed by 30 minutes with FITC-conjugated secondary antibody (Biosource, Camarillo, CA) and then analyzed using a FACS Calibur (Becton Dickinson, Bedford, MA). At least 10,000 cells were counted per sample. Graphs were processed using FlowJo software (Tree Star, Ashland, OR).

Immunofluorescence

Cells grown on glass cover slips were fixed with 4% paraformaldehyde at 4°C for 15 minutes and permeabilized by 0.1% Triton X-100 in PBS for 5 minutes, and then rinsed with phosphate-buffered saline (PBS). Cells were then blocked (1 hour) with 3% BSA in PBS (w/v), immunolabeled with CD9 primary antibody (1 hour), followed by AlexaFluor488-conjugated goat anti-mouse IgG for 1 hour (Invitrogen). For double staining of CD9 and F-actin, cells were stained with AlexaFluor594–phalloidin (30 minutes) before incubation with CD9 antibody. Cells were then mounted [ProLong Gold antifade mounting media containing DAPI (Invitrogen)] and imaged using a Leica SP5X laser scanning confocal microscope (Leica Microsystems, Chicago, IL). Microvilli greater than 5 μm were counted using Scion Image software and the cells from 10 random pictures were quantified.

Immunoprecipitation and immunoblotting

K562 and RD cells were washed twice with PBS and lysed in buffer (20 mM HEPES pH 7.4, 150 mM NaCl, 2 mM $MgCl_2$, 2 mM $CaCl_2$) containing 1% Brij 96 or Triton X-100 (Sigma) and EDTA-free protease inhibitors. After 1 hour at 25°C, insoluble material was removed by centrifugation. For immunoprecipitation, lysates were precleared for 1 hour with protein G-sepharose beads (Pharmacia, Uppsala, Sweden). Specific antibodies (1–2 μg) were added to lysates of total protein (500 μg) and incubated at 4°C overnight. Antibody–protein complexes were captured using protein G-sepharose beads, washed three times with lysis buffer, and immune complexes were eluted in 2× Tris-glycine SDS sample buffer. For immunoblotting, samples were resolved by SDS-PAGE, transferred to nitrocellulose membrane (Whatman, Dassel, Germany), blocked with 5% nonfat milk blocking agent, incubated with specific antibody, followed by addition of peroxidase- or HRP-conjugated secondary antibody and chemiluminescence detection (SuperSignal West Pico Chemiluminescent Substrate, Thermo Scientific, Rockford, IL). For multiple blottings, membranes were stripped with Restore Western Blot Stripping Buffer (Pierce). Band intensities were quantified using Quantity One software (Bio-Rad, Hercules, CA), with non-CD9 band intensities calculated relative to CD9=1.00.

SILAC

U937.7C2 cells lacking CD81 and CD9 (a gift from S. Levy, Department of Medicine, Stanford University, Stanford, CA) were stably transduced to express wild-type CD9 or mutant CD9. U937-CD9 cells were labeled with isotopically heavy leucine (U-$^{13}C_6$-leucine; Cambridge Isotope Labs, Andover, MA) using RPMI labeling medium lacking L-leucine. Mutant CD9 cells were grown in isotopically light L-leucine (Sigma). All cells were maintained in labeling medium [also containing 10% dialyzed fetal calf serum (Hyclone) and penicillin-streptomycin (Invitrogen)] for 10 days to ensure complete labeling. Equal numbers (2×10^9 cells each) of U937-CD9 (heavy leucine) and U937-CD9 mutant (light leucine) were then mixed, washed three times with PBS and lysed together in lysis buffer (50 mM HEPES pH 7.5, 150 mM NaCl, 2 mM $MgCl_2$, 2 mM $CaCl_2$) supplemented with 1% Triton X-100 (Roche Applied Science) or 1% Brij 96 (Sigma), and protease inhibitor mixture (Roche Applied Science) at 4°C for 1 hour. Lysates were centrifuged for 30 minutes at 20,000 ***g*** and supernatants were pre-cleared stepwise with protein A-sepharose, protein G-sepharose and two irrelevant antibodies covalently coupled to protein A-agarose. After each pre-clearing, the lysates were centrifuged for 5 minutes at 20,000 ***g***. After final pre-clearing, the supernatants were mixed with CD9 antibody (ALB6) that had been covalently coupled to protein G-sepharose beads (using dimethylpilimidate; Sigma) and incubated for 16 hours at 4°C. Beads were then extensively washed with lysis buffer (100 ml), and proteins were eluted with 100 mM glycine, pH 2.5, and the eluted fractions were neutralized with 1.5 M Tris-HCl, pH 8.8. After polyacrylamide gel electrophoresis and silver staining, gel lanes (~2 cm long) were excised, proteins were in-gel digested with trypsin and then analyzed

by LC-MS/MS techniques (Haas et al., 2006). Identified peptides were quantified based on the area-under-the-curve ratios for co-eluting heavy and light forms of each peptide using the Vista algorithm (Bakalarski et al., 2008). These ratios are given in Table 1.

Gel filtration

Intact U937-CD9 cells and U937-CD9 mutant cells were each cell-surface labeled with sulfo-NHS-LC biotin (Pierce, Rockford, IL) as previously described (Kolesnikova et al., 2004) and then cells (each at 1×10^7) were lysed in 1% Brij 96. The same cells were also labeled metabolically, by growing for 16 hours in [^{3}H]-palmitate (NEN Bioscience, Boston, MA) and 10% dialyzed FBS, and then lysed in 1% Brij 96. Lysates were mixed (CD9 biotin + CD9 mutant [^{3}H]-palmitate; CD9 mutant biotin + CD9 [^{3}H]-palmitate) and then passed over a sepharose CL6B gel filtration column. CD9 was then immunoprecipitated from each fraction, using mAb ALB6. Eluted proteins were resolved by SDS-PAGE, transferred to PVDF membrane (BioRad Laboratories) and exposed to BioMax MS film (Kodak, Rochester, NY) at –80°C with an intensifying screen to detect [^{3}H] labeling. Biotin-labeled CD9 samples were transferred to nitrocellulose membrane and immunoblotted with ExtrAvidin-HRP (Sigma). A phosphoimager machine (Storm 860, Molecular Dynamics), together with ImageQuant version 1.2 program, was used for densitometric analysis. The sum of signals from each column fraction was set to equal 100%.

We thank C. E. Bakalarski for his help with the Vista algorithm. This work was supported by a grant from the National Institutes of Health (GM38903) to M.E.H. Deposited in PMC for release after 12 months.

Supplementary material available online at
http://jcs.biologists.org/cgi/content/full/124/16/2702/DC1

References

Anton, E. S., Hadjiargyrou, M., Patterson, P. H. and Matthew, W. D. (1995). CD9 plays a role in Schwann cell migration *in vitro*. *J. Neurosci.* **15**, 584-595.

Bakalarski, C. E., Elias, J. E., Villen, J., Haas, W., Gerber, S. A., Everley, P. A. and Gygi, S. P. (2008). The impact of peptide abundance and dynamic range on stable-isotope-based quantitative proteomic analyses. *J. Proteome Res.* **7**, 4756-4765.

Barreiro, O., Yanez-Mo, M., Sala-Valdes, M., Gutierrez-Lopez, M. D., Ovalle, S., Higginbottom, A., Monk, P. N., Cabanas, C. and Sanchez-Madrid, F. (2005). Endothelial tetraspanin microdomains regulate leukocyte firm adhesion during extravasation. *Blood* **105**, 2852-2861.

Berditchevski, F. (2001). Complexes of tetraspanins with integrins: more than meets the eye. *J. Cell Sci.* **114**, 4143-4151.

Berditchevski, F. and Odintsova, E. (1999). Characterization of integrin-tetraspanin adhesion complexes: role of tetraspanins in integrin signaling. *J. Cell Biol.* **146**, 477-492.

Boucheix, C. and Rubinstein, E. (2001). Tetraspanins. *Cell. Mol. Life Sci.* **58**, 1189-1205.

Cajot, J. F., Sordat, I., Silvestre, T. and Sordat, B. (1997). Differential display cloning identifies motility-related protein (MRP1/CD9) as highly expressed in primary compared to metastatic human colon carcinoma cells. *Cancer Res.* **57**, 2593-2597.

Charrin, S., Le Naour, F., Oualid, M., Billard, M., Faure, G., Hanash, S. M., Boucheix, C. and Rubinstein, E. (2001). The major CD9 and CD81 molecular partner. Identification and characterization of the complexes. *J. Biol. Chem.* **276**, 14329-14337.

Charrin, S., Le Naour, F., Labas, V., Billard, M., Le Caer, J. P., Emile, J. F., Petit, M. A., Boucheix, C. and Rubinstein, E. (2003). EWI-2 is a new component of the tetraspanin web in hepatocytes and lymphoid cells. *Biochem. J.* **373**, 409-421.

Deng, J., Yeung, V. P., Tsitoura, D., DeKruyff, R. H., Umetsu, D. T. and Levy, S. (2000). Allergen-induced airway hyperreactivity is diminished in CD81-deficient mice. *J. Immunol.* **165**, 5054-5061.

Duffield, A., Kamsteeg, E. J., Brown, A. N., Pagel, P. and Caplan, M. J. (2003). The tetraspanin CD63 enhances the internalization of the H,K-ATPase beta-subunit. *Proc. Natl. Acad. Sci. USA* **100**, 15560-15565.

Espenel, C., Margeat, E., Dosset, P., Arduise, C., Le Grimellec, C., Royer, C. A., Boucheix, C., Rubinstein, E. and Milhiet, P. E. (2008). Single-molecule analysis of CD9 dynamics and partitioning reveals multiple modes of interaction in the tetraspanin web. *J. Cell Biol.* **182**, 765-776.

Gordon-Alonso, M., Yanez-Mo, M., Barreiro, O., Alvarez, S., Munoz-Fernandez, M. A., Valenzuela-Fernandez, A. and Sanchez-Madrid, F. (2006). Tetraspanins CD9 and CD81 modulate HIV-1-induced membrane fusion. *J. Immunol.* **177**, 5129-5137.

Goschnick, M. W. and Jackson, D. E. (2007). Tetraspanins-structural and signalling scaffolds that regulate platelet function. *Mini Rev. Med. Chem.* **7**, 1248-1254.

Gutierrez-Lopez, M. D., Ovalle, S., Yanez-Mo, M., Sanchez-Sanchez, N., Rubinstein, E., Olmo, N., Lizarbe, M. A., Sanchez-Madrid, F. and Cabanas, C. (2003). A functionally relevant conformational epitope on the CD9 tetraspanin depends on the association with activated beta1 integrin. *J. Biol. Chem.* **278**, 208-218.

Haas, W., Faherty, B. K., Gerber, S. A., Elias, J. E., Beausoleil, S. A., Bakalarski, C. E., Li, X., Villen, J. and Gygi, S. P. (2006). Optimization and use of peptide mass measurement accuracy in shotgun proteomics. *Mol. Cell. Proteomics* **5**, 1326-1337.

Hasuwa, H., Shishido, Y., Yamazaki, A., Kobayashi, T., Yu, X. and Mekada, E. (2001). CD9 amino acids critical for upregulation of diphtheria toxin binding. *Biochem. Biophys. Res. Commun.* **289**, 782-790.

Hemler, M. E. (2003). Tetraspanin proteins mediate cellular penetration, invasion and fusion events, and define a novel type of membrane microdomain. *Annu. Rev. Cell Dev. Biol.* **19**, 397-422.

Hemler, M. E. (2005). Tetraspanin functions and associated microdomains. *Nat. Rev. Mol. Cell Biol.* **6**, 801-811.

Huang, C. I., Kohno, N., Ogawa, E., Adachi, M., Taki, T. and Miyake, M. (1998). Correlation of reduction in MRP-1/CD9 and KAI1/CD82 expression with recurrences in breast cancer patients. *Am. J. Pathol.* **153**, 973-983.

Huang, C. L., Liu, D., Masuya, D., Kameyama, K., Nakashima, T., Yokomise, H., Ueno, M. and Miyake, M. (2004). MRP-1/CD9 gene transduction downregulates Wnt signal pathways. *Oncogene* **23**, 7475-7483.

Ikeyama, S., Koyama, M., Yamaoko, M., Sasada, R. and Miyake, M. (1993). Suppression of cell motility and metastasis by transfection with human motility-related protein (MRP-1/CD9) DNA. *J. Exp. Med.* **177**, 1231-1237.

Ishibashi, T., Ding, L., Ikenaka, K., Inoue, Y., Miyado, K., Mekada, E. and Baba, H. (2004). Tetraspanin protein CD9 is a novel paranodal component regulating paranodal junctional formation. *J. Neurosci.* **24**, 96-102.

Iwamoto, R., Higashiyama, S., Mitamura, T., Taniguchi, N., Klagsbrun, M. and Mekada, E. (1994). Heparin-binding EGF-like growth factor, which acts as a diphtheria toxin receptor, forms a complex with membrane protein DRAP27/CD9, which upregulates functional receptors and diphtheria toxin sensitivity. *EMBO J.* **13**, 2322-2330.

Kaji, K., Oda, S., Shikano, T., Ohnuki, T., Uematsu, Y., Sakagami, J., Tada, N., Miyazaki, S. and Kudo, A. (2000). The gamete fusion process is defective in eggs of Cd9-deficient mice. *Nat. Genet.* **24**, 279-282.

Kaji, K., Takeshita, S., Miyake, K., Takai, T. and Kudo, A. (2001). Functional association of CD9 with the Fc gamma receptors in macrophages. *J. Immunol.* **166**, 3256-3265.

Kolesnikova, T. V., Stipp, C. S., Rao, R. M., Lane, W. S., Luscinskas, F. W. and Hemler, M. E. (2004). EWI-2 modulates lymphocyte integrin alpha4beta1 functions. *Blood* **103**, 3013-3019.

Kolesnikova, T. V., Kazarov, A. R., Lemieux, M., Lafleur, M. A., Kesari, S., Kung, A. L. and Hemler, M. E. (2008). Glioblastoma suppression by tetraspanin partner protein EWI-2 in vitro and in vivo. *Neoplasia* **11**, 77-86.

Kovalenko, O. V., Metcalf, D. G., DeGrado, W. F. and Hemler, M. E. (2005). Structural organization and interactions of transmembrane domains in tetraspanin proteins. *BMC Struct. Biol.* **5**, 11.

Krementsov, D. N., Weng, J., Lambele, M., Roy, N. H. and Thali, M. (2009). Tetraspanins regulate cell-to-cell transmission of HIV-1. *Retrovirology* **6**, 64.

Kropshofer, H., Spindeldreher, S., Rohn, T. A., Platania, N., Grygar, C., Daniel, N., Wolpl, A., Langen, H., Horejsi, V. and Vogt, A. B. (2002). Tetraspan microdomains distinct from lipid rafts enrich select peptide-MHC class II complexes. *Nat. Immunol.* **3**, 61-68.

Lammerding, J., Kazarov, A. R., Huang, H., Lee, R. T. and Hemler, M. E. (2003). Tetraspanin CD151 regulates alpha6beta1 integrin adhesion strengthening. *Proc. Natl. Acad. Sci. USA* **100**, 7616-7621.

Latysheva, N., Muratov, G., Rajesh, S., Padgett, M., Hotchin, N. A., Overduin, M. and Berditchevski, F. (2006). Syntenin-1 is a new component of tetraspanin-enriched microdomains: mechanisms and consequences of the interaction of syntenin-1 with CD63. *Mol. Cell. Biol.* **26**, 7707-7718.

Le Naour, F., Rubinstein, E., Jasmin, C., Prenant, M. and Boucheix, C. (2000). Severely reduced female fertility in CD9-deficient mice. *Science* **287**, 319-321.

Le Naour, F., Andre, M., Greco, C., Billard, M., Sordat, B., Emile, J. F., Lanza, F., Boucheix, C. and Rubinstein, E. (2006). Profiling of the tetraspanin web of human colon cancer cells. *Mol. Cell. Proteomics* **5**, 845-857.

Letarte, M., Seehafer, J. G., Greaves, A., Masellis-Smith, A. and Shaw, A. R. (1993). Homotypic aggregation of pre-B leukemic cell lines by antibodies to VLA integrins correlates with their expression of CD9. *Leukemia* **7**, 93-103.

Levy, S. and Shoham, T. (2005). The tetraspanin web modulates immune-signalling complexes. *Nat. Rev. Immunol.* **5**, 136-148.

Liu, L., He, B., Liu, W. M., Zhou, D., Cox, J. V. and Zhang, X. A. (2007). Tetraspanin CD151 promotes cell migration by regulating integrin trafficking. *J. Biol. Chem.* **282**, 31631-31642.

Masellis-Smith, A. and Shaw, A. R. E. (1994). CD9-regulated adhesion: anti-CD9 monoclonal antibody induce pre-B cell adhesion to bone marrow fibroblasts through de novo recognition of fibronectin. *J. Immunol.* **152**, 2768-2777.

Masellis-Smith, A., Jensen, G. S., Seehafer, J. G., Slupsky, J. R. and Shaw, A. R. E. (1990). CD9-regulated adhesion: anti-CD9 monoclonal antibodies induce homotypic adhesion of pre-B cell lines by a novel mechanism. *J. Immunol.* **144**, 1607-1613.

Miranti, C. K. (2009). Controlling cell surface dynamics and signaling: how CD82/KAI1 suppresses metastasis. *Cell. Signal.* **21**, 196-211.

Miyado, K., Yamada, G., Yamada, S., Hasuwa, H., Nakamura, Y., Ryu, F., Suzuki, K., Kosai, K., Inoue, K., Ogura, A. et al. (2000). Requirement of CD9 on the egg plasma membrane for fertilization. *Science* **287**, 321-324.

Miyake, M., Nakano, K., Ieki, Y., Adachi, M., Huang, C.-L., Itoi, S., Koh, T. and Taki, T. (1995). Motility related protein 1 (MRP-1/CD9) expression: inverse correlation with metastases in breast cancer. *Cancer Res.* **55**, 4127-4131.

Murayama, Y., Miyagawa, J., Oritani, K., Yoshida, H., Yamamoto, K., Kishida, O., Miyazaki, T., Tsutsui, S., Kiyohara, T., Miyazaki, Y. et al. (2004). CD9-mediated activation of the p46 Shc isoform leads to apoptosis in cancer cells. *J. Cell Sci.* **117**, 3379-3388.

Nydegger, S., Khurana, S., Krementsov, D. N., Foti, M. and Thali, M. (2006). Mapping of tetraspanin-enriched microdomains that can function as gateways for HIV-1. *J. Cell Biol.* **173**, 795-807.

Ong, S. E., Blagoev, B., Kratchmarova, I., Kristensen, D. B., Steen, H., Pandey, A. and Mann, M. (2002). Stable isotope labeling by amino acids in cell culture, SILAC, as a simple and accurate approach to expression proteomics. *Mol. Cell. Proteomics* **1**, 376-386.

Ono, M., Handa, K., Withers, D. A. and Hakomori, S. (1999). Motility inhibition and apoptosis are induced by metastasis-suppressing gene product CD82 and its analogue CD9, with concurrent glycosylation. *Cancer Res.* **59**, 2335-2339.

Rous, B. A., Reaves, B. J., Ihrke, G., Briggs, J. A., Gray, S. R., Stephens, D. J., Banting, G. and Luzio, J. P. (2002). Role of adaptor complex AP-3 in targeting wild-type and mutated CD63 to lysosomes. *Mol. Biol. Cell* **13**, 1071-1082.

Rubinstein, E., Le Naour, F., Lagaudrière-Gesbert, C., Billard, M., Conjeaud, H. and Boucheix, C. (1996). CD9, CD63, CD81, and CD82 are components of a surface tetraspan network connected to HLA-DR and VLA antigens. *Eur. J. Immunol.* **26**, 2657-2665.

Runge, K. E., Evans, J. E., He, Z. Y., Gupta, S., McDonald, K. L., Stahlberg, H., Primakoff, P. and Myles, D. G. (2007). Oocyte CD9 is enriched on the microvillar membrane and required for normal microvillar shape and distribution. *Dev. Biol.* **304**, 317-325.

Ryu, F., Takahashi, T., Nakamura, K., Takahashi, Y., Kobayashi, T., Shida, S., Kameyama, T. and Mekada, E. (2000). Domain analysis of the tetraspanins: studies of CD9/CD63 chimeric molecules on subcellular localization and upregulation activity for diphtheria toxin binding. *Cell Struct. Funct.* **25**, 317-327.

Sala-Valdes, M., Ursa, A., Charrin, S., Rubinstein, E., Hemler, M. E., Sanchez-Madrid, F. and Yanez-Mo, M. (2006). EWI-2 and EWI-F link the tetraspanin web to the actin cytoskeleton through their direct association with ezrin-radixin-moesin proteins. *J. Biol. Chem.* **281**, 19665-19675.

Seigneuret, M., Delaguillaumie, A., Lagaudriere-Gesbert, C. and Conjeaud, H. (2001). Structure of the tetraspanin main extracellular domain. A partially conserved fold with a structurally variable domain insertion. *J. Biol. Chem.* **276**, 40055-40064.

Shaw, A. R. E., Domanska, A., Mak, A., Gilchrist, A., Dobler, K., Visser, L., Poppema, S., Fliegel, L., Letarte, M. and Willett, B. J. (1995). Ectopic expression of human and feline CD9 in a human B cell line confers β1 integrin-dependent motility on fibronectin and laminin substrates and enhanced tyrosine phosphorylation. *J. Biol. Chem.* **270**, 24092-24099.

Shi, W., Fan, H., Shum, L. and Derynck, R. (2000). The tetraspanin CD9 associates with transmembrane TGF-alpha and regulates TGF-alpha-induced EGF receptor activation and cell proliferation. *J. Cell Biol.* **148**, 591-602.

Singethan, K., Muller, N., Schubert, S., Luttge, D., Krementsov, D. N., Khurana, S. R., Krohne, G., Schneider-Schaulies, S., Thali, M. and Schneider-Schaulies, J. (2008). CD9 clustering and formation of microvilli zippers between contacting cells regulates virus-induced cell fusion. *Traffic* **9**, 924-935.

Stipp, C. S., Kolesnikova, T. V. and Hemler, M. E. (2001a). EWI-2 is a major CD9 and CD81 partner, and member of a novel Ig protein subfamily. *J. Biol. Chem.* **276**, 40545-40554.

Stipp, C. S., Orlicky, D. and Hemler, M. E. (2001b). FPRP: a major, highly stoichiometric, highly specific CD81 and CD9-associated protein. *J. Biol. Chem.* **276**, 4853-4862.

Stipp, C. S., Kolesnikova, T. V. and Hemler, M. E. (2003). EWI-2 regulates {alpha}3{beta}1 integrin-dependent cell functions on laminin-5. *J. Cell Biol.* **163**, 1167-1177.

Tachibana, I. and Hemler, M. E. (1999). Role of transmembrane-4 superfamily (TM4SF) proteins CD9 and CD81 in muscle cell fusion and myotube maintenance. *J. Cell Biol.* **146**, 893-904.

Takeda, Y., Tachibana, I., Miyado, K., Kobayashi, M., Miyazaki, T., Funakoshi, T., Kimura, H., Yamane, H., Saito, Y., Goto, H. et al. (2003). Tetraspanins CD9 and CD81 function to prevent the fusion of mononuclear phagocytes. *J. Cell Biol.* **161**, 945-956.

Tonikian, R., Zhang, Y., Sazinsky, S. L., Currell, B., Yeh, J. H., Reva, B., Held, H. A., Appleton, B. A., Evangelista, M., Wu, Y. et al. (2008). A specificity map for the PDZ domain family. *PLoS Biol.* **6**, e239.

Toyo-Oka, K., Yashiro-Ohtani, Y., Park, C. S., Tai, X. G., Miyake, K., Hamaoka, T. and Fujiwara, H. (1999). Association of a tetraspanin CD9 with CD5 on the T cell surface: role of particular transmembrane domains in the association. *Int. Immunol.* **11**, 2043-2052.

Unternaehrer, J. J., Chow, A., Pypaert, M., Inaba, K. and Mellman, I. (2007). The tetraspanin CD9 mediates lateral association of MHC class II molecules on the dendritic cell surface. *Proc. Natl. Acad. Sci. USA* **104**, 234-239.

Yanez-Mo, M., Barreiro, O., Gordon-Alonso, M., Sala-Valdes, M. and Sanchez-Madrid, F. (2009). Tetraspanin-enriched microdomains: a functional unit in cell plasma membranes. *Trends Cell Biol.* **19**, 434-446.

Yang, X., Claas, C., Kraeft, S. K., Chen, L. B., Wang, Z., Kreidberg, J. A. and Hemler, M. E. (2002). Palmitoylation of tetraspanin proteins: modulation of CD151 lateral interactions, subcellular distribution, and integrin-dependent cell morphology. *Mol. Biol. Cell* **13**, 767-781.

Yang, X. H., Kovalenko, O. V., Kolesnikova, T. V., Andzelm, M. M., Rubinstein, E., Strominger, J. L. and Hemler, M. E. (2006). Contrasting effects of EWI proteins, integrins, and protein palmitoylation on cell surface CD9 organization. *J. Biol. Chem.* **281**, 12976-12985.

Zhang, X. A., Bontrager, A. L., Stipp, C. S., Kraeft, S.-K., Bazzoni, G., Chen, L. B. and Hemler, M. E. (2001). Phosphorylation of a conserved integrin α3 chain QPSXXE motifs regulates signaling, motility, and cytoskeletal engagement. *Mol. Biol. Cell* **12**, 351-365.

Zhang, X. A., Kazarov, A. R., Yang, X., Bontrager, A. L., Stipp, C. S. and Hemler, M. E. (2002). Function of the tetraspanin CD151-a6b1 integrin complex during cellular morphogenesis. *Mol. Biol. Cell* **13**, 1-11.

Zhu, G. Z., Miller, B. J., Boucheix, C., Rubinstein, E., Liu, C. C., Hynes, R. O., Myles, D. G. and Primakoff, P. (2002). Residues SFQ (173-175) in the large extracellular loop of CD9 are required for gamete fusion. *Development* **129**, 1995-2002.

Ziyyat, A., Rubinstein, E., Monier-Gavelle, F., Barraud, V., Kulski, O., Prenant, M., Boucheix, C., Bomsel, M. and Wolf, J. P. (2006). CD9 controls the formation of clusters that contain tetraspanins and the integrin {alpha}6{beta}1, which are involved in human and mouse gamete fusion. *J. Cell Sci.* **119**, 416-424.

Zoller, M. (2009). Tetraspanins: push and pull in suppressing and promoting metastasis. *Nat. Rev. Cancer* **9**, 40-55.